The Astrophysical Journal, 838:73 (31pp), 2017 March 20 https://doi.org/10.3847/1538-4357/aa6338

Surface Gravities for 228 M, L, and T Dwarfs in the NIRSPEC Brown Dwarf Spectroscopic Survey*

Emily C. Martin[1], Gregory N. Mace[1,2], Ian S. McLean[1], Sarah E. Logsdon[1], Emily L. Rice[3,4,5], J. Davy Kirkpatrick[6], Adam J. Burgasser[7], Mark R. McGovern[8], and Lisa Prato[9]

[1] Department of Physics & Astronomy, University of California Los Angeles, 430 Portola Plaza, Box 951547, Los Angeles, CA 90095-1547, USA; emartin@astro.ucla.edu
[2] Department of Astronomy, UT Austin, 2515 Speedway, Stop C1400, Austin, TX 78712-1205, USA
[3] Department of Engineering Science & Physics, College of Staten Island, 2800 Victory Boulevard, Staten Island, NY 10301, USA
[4] Department of Astrophysics, American Museum of Natural History, Central Park West at 79th Street, New York, NY 10034, USA
[5] Physics Program, The Graduate Center, City University of New York, 365 Fifth Avenue, New York, NY 10016, USA
[6] Infrared Processing and Analysis Center, MS 100-22, California Institute of Technology, Pasadena, CA 91125, USA
[7] Center for Astrophysics and Space Science, University of California San Diego, La Jolla, CA 92093, USA
[8] Math & Sciences Division, Antelope Valley College, 3041 West Avenue K, Lancaster, CA 93536, USA
[9] Lowell Observatory, 1400 West Mars Hill Road, Flagstaff, AZ 86001, USA

Received 2016 August 12; revised 2017 February 22; accepted 2017 February 23; published 2017 March 27

Abstract

We combine 131 new medium-resolution ($R \sim 2000$) *J*-band spectra of M, L, and T dwarfs from the Keck NIRSPEC Brown Dwarf Spectroscopic Survey (BDSS) with 97 previously published BDSS spectra to study surface-gravity-sensitive indices for 228 low-mass stars and brown dwarfs spanning spectral types M5–T9. Specifically, we use an established set of spectral indices to determine surface gravity classifications for all of the M6–L7 objects in our sample by measuring the equivalent widths (EW) of the K I lines at 1.1692, 1.1778, and 1.2529 μm, and the 1.2 μm FeH_J absorption index. Our results are consistent with previous surface gravity measurements, showing a distinct double peak—at ∼L5 and T5—in K I EW as a function of spectral type. We analyze the K I EWs of 73 objects of known ages and find a linear trend between log(Age) and EW. From this relationship, we assign age ranges to the very low gravity, intermediate gravity, and field gravity designations for spectral types M6–L0. Interestingly, the ages probed by these designations remain broad, change with spectral type, and depend on the gravity-sensitive index used. Gravity designations are useful indicators of the possibility of youth, but current data sets cannot be used to provide a precise age estimate.

Key words: brown dwarfs – infrared: stars – stars: atmospheres – stars: low-mass – surveys

1. Introduction

Brown dwarfs are the lowest-mass products of star formation, with masses so low that they will never achieve stable hydrogen fusion in their cores (Kumar 1962, 1963; Hayashi & Nakano 1963). Substellar objects are classified by their spectral morphology as types M, L, T, and Y, a sequence which represents both a decrease in effective temperature and changes in chemical abundances. Since their discovery 20 years ago (Nakajima et al. 1995; Rebolo et al. 1995), most brown dwarfs have been found through infrared large area surveys such as the Two Micron All Sky Survey (2MASS; Skrutskie et al. 2006), the Sloan Digital Sky Survey (SDSS; York et al. 2000), the United Kingdom Infrared Deep Sky Survey (Lawrence et al. 2007), and the *Wide-field Infrared Survey Explorer* (*WISE*; Wright et al. 2010), among others. See, for example, Kirkpatrick et al. (1991), Kirkpatrick et al. (1999), Hawley et al. (2002), Burgasser et al. (2006), Chiu et al. (2006), Burningham et al. (2010), and Cushing et al. (2011) for details on brown dwarf discoveries made by the various surveys.

Extensive follow up using both optical and infrared imaging and spectroscopy has enabled astronomers to begin characterizing the physical properties of brown dwarfs, primarily through comparisons to atmospheric and evolutionary models, like those of Burrows et al. (2001), Saumon & Marley (2008), Allard et al. (2012), and Baraffe et al. (2015). It is possible to constrain the effective temperatures, surface gravities, and metallicities of brown dwarfs within the limits of current models, e.g., Cushing et al. (2008) and Rice et al. (2010). As the number of confirmed brown dwarfs has increased, the properties typical of field brown dwarfs have been constrained, outliers have been recognized, and methods of identifying extremely young or old objects have emerged (see Kirkpatrick et al. 2010; Allers & Liu 2013 and references therein).

1.1. Surface Gravity as an Age Indicator

Unlike stars, brown dwarfs contract and cool as they age, producing a degeneracy between the mass, age, and temperature such that temperature alone cannot reveal the mass or age of a given brown dwarf. For example, an L dwarf could be a young, planetary-mass brown dwarf, a moderately aged high-mass brown dwarf, or an old low-mass star. Brown dwarfs contract considerably in their first ∼300 Myr and significantly increase their surface gravity ($g = GM/R^2$) from $\log g \sim 3.5$ to $\log g \sim 5$ in units of $\mathrm{cm\,s^{-2}}$ (Burrows et al. 2001). Obtaining a surface gravity estimate is an important step toward disentangling the mass and age of a brown dwarf.

* The data presented herein were obtained at the W.M. Keck Observatory, which is operated as a scientific partnership among the California Institute of Technology, the University of California, and the National Aeronautics and Space Administration. The Observatory was made possible by the generous financial support of the W.M. Keck Foundation.

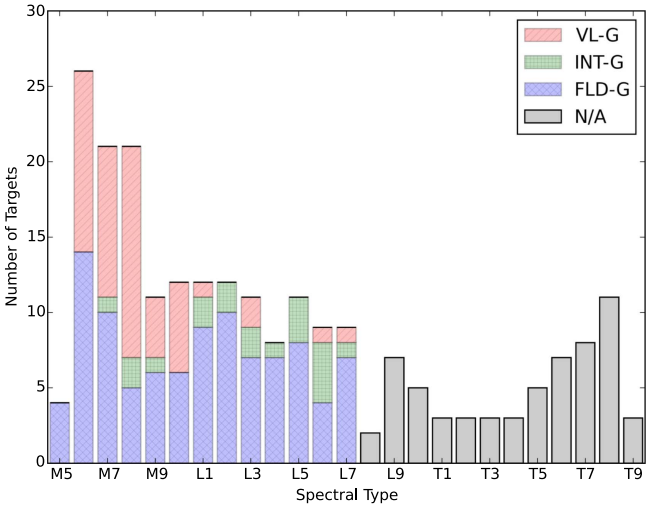

Figure 1. Number of targets vs. spectral type for all 228 objects in the BDSS. Shading represents gravity classifications, as defined by A13 and as determined in this paper. Red shading represents targets with a gravity classification of VL-G. These objects are likely very young. Green shaded regions denote targets with INT-G classification, indicating youth (∼30–200 Myr). Blue targets have FLD-G gravity classifications and are generally older than ∼200 Myr. Objects cooler than type L7 cannot be gravity typed by A13's methods and are shown in gray.

Surface gravity affects several features in the optical and near-infrared (NIR) spectra of brown dwarfs. Photospheric pressure, which is proportional to surface gravity assuming hydrostatic equilibrium, broadens atomic features and influences the chemical pathways of both atomic and molecular species (Lodders 1999). Neutral alkali lines such as K I and Na I are weaker in low-gravity objects compared to higher-gravity objects at similar spectral types because lower photospheric pressure decreases the column densities of the absorbing species above the photosphere, causing the absorption features to appear weaker in low-gravity dwarfs. FeH absorption also appears weaker in lower-gravity objects, while VO shows stronger absorption at lower gravity, as noted by McGovern et al. (2004) and Allers & Liu (2013). Additionally, the overall shape of the *H*-band spectral energy distribution is much "peakier" at lower gravities (Lucas et al. 2001; Allers et al. 2007; Looper et al. 2008; Rice et al. 2011), likely due to lower H_2 collision induced absorption, which is a result of the lower photospheric pressure at lower gravities (Kirkpatrick et al. 2006; Saumon & Marley 2008).

Kirkpatrick (2005) proposed a scheme in which a gravity classification (i.e., α, β, γ, δ) is appended to the spectral type of a brown dwarf as a means of distinguishing between field, intermediate, low, and very low-gravity objects with similar temperatures. For each spectral type, the gravity sequence acts as a proxy for an age sequence, and low-gravity objects of a particular spectral type are younger than their field counterparts at the same spectral type. Cruz et al. (2009) explored this gravity classification scheme using red-optical spectroscopy of 23 L dwarfs, primarily distinguishing the young objects from field-age objects by the weakness of their alkali lines, while also using the FeH, CrH, TiO and VO absorption bands as diagnostics.

Allers & Liu (2013, hereafter A13) were the first to present a systematic technique using NIR spectroscopy to determine the surface gravities of low-mass stars and brown dwarfs. A13 define spectral indices and pseudo-equivalent widths (EWs) of various gravity-sensitive features in lower-resolution NIR spectra to classify the spectra into three groups: low (VL-G), intermediate (INT-G), and high (FLD-G) gravity objects, roughly corresponding to young ($\lesssim$30 Myr), intermediate (∼30–200 Myr), and field-age ($\gtrsim$200 Myr) objects. Because brown dwarfs are significantly brighter in the NIR than the optical, an NIR gravity classification scheme is applicable to more targets. A13 determined gravity classifications for 73 low-mass stars and brown dwarfs showing signs of youth. Gagné et al. (2015b) applied the method prescribed in A13 to 182 objects of spectral types M4–L7 in their search for low-mass members of young moving groups.

In this paper, we follow up on prior NIR spectroscopy by our group and use a modified A13 method to determine surface gravities for 228 M, L, and T dwarfs. Twenty of these targets overlap with the A13 sample, and 5 objects overlap with the Gagné et al. (2015b) sample. Many previously unpublished NIR spectra from the Near-Infrared Spectrometer (NIRSPEC) Brown Dwarf Spectroscopic Survey (BDSS) are reported and analyzed.

1.2. The NIRSPEC BDSS

In 1999, NIRSPEC (McLean et al. 1998) was commissioned for the W.M. Keck II 10 m telescope on MaunaKea in Hawaii. NIRSPEC was built at the University of California, Los Angeles (UCLA), and designed for both medium-resolution ($R = \lambda/\Delta\lambda \sim 2000$) and high-resolution ($R \sim 20{,}000$) spectroscopy in the 1–5 μm regime. The BDSS was one of the key science drivers for NIRSPEC. The primary goal of the BDSS as outlined in McLean et al. (2003) is to gather a large suite of NIR spectra of low-mass stars and brown dwarfs in order to examine their spectral properties and make comparisons to evolutionary and atmospheric models. The low temperatures ($T \lesssim 2500$ K) of brown dwarfs make them excellent targets for NIR studies. Over the past 15 years, the BDSS team has gathered a large spectroscopic database of brown dwarfs and low-mass stars (see Section 2, Appendix), much of which is presented in McLean et al. (2001, 2003), McGovern et al. (2004), McLean et al. (2007), Rice et al. (2010), and Prato et al. (2015).

McGovern et al. (2004) presented the first comprehensive infrared observations to reveal gravity-sensitive spectral signatures in young, low-mass stars and brown dwarfs. The infrared and optical spectra of late-type giant stars and old field dwarfs were compared with the spectra of several young brown dwarfs to identify gravity-sensitive features, such as the K I lines in the *J* band, as well as TiO, VO, and FeH absorption systems. The paper also reported on the use of these spectral features to test the membership of potential very low-mass brown dwarfs in young clusters. McGovern et al. (2004) therefore forms the basis of the surface gravity analysis presented in this paper.

In this paper, we measure the EWs of K I lines in the *J* band and FeH absorption at 1.2 μm for all targets in the BDSS, and use the A13 method to determine surface gravities for all objects for which the method is viable (spectral types M5–L7). We expand upon previous surface gravity studies by calibrating the surface gravity classifications against objects of known ages from the literature, and discuss the extension of the gravity classifications beyond type L7. In Section 2, we discuss our observations and data reduction methods. Section 3 describes

Table 1
Observations and Designations

Designation	Disc. Ref	Short Name	SpT	SpT Ref	UT Date of Observation	A0V Calibrator	Slit Width (arcsec)	Exp. Time (s)
2MASS J06195260-2903592	29	2MASS 0619-2903	M5	1	2004 Nov 21	HD 41473	0.38	1200
2MASS J00433134+2054316	68	LHS 1135	d/sdM5	54	2003 Dec 4	HD 7215	0.38	600
GJ 577 BC	64	Gl 577 BC	M5.5+M5.5	88	2003 Mar 24	HD 132072	0.38	600
2MASS J16262152-2426009	40	ρ Oph GY 5	M5.5	81	2003 May 14	HD 151736	0.38	600
WDS J04325+1732Ba	27	GG Tau Ba	M6	103	2004 Nov 7	HD 28354	0.38	1200
2MASS J14594626+0004427	54	2MASS 1459+0004	M6	54	2005 Jul 19	HD 123233	0.38	1200
2MASS J22344161+4041387	29	2MASS 2234+4041AB	M6+M6	2	2003 Dec 4	BD +39 4890	0.38	600
2MASS J16051403-2406524	78	DENIS-P 1605-2406	M6	78	2004 May 2	HD 147384	0.38	1200
2MASS J04262939+2624137	11	KPNO Tau 3	M6	11	2004 Nov 7	24 Tau	0.38	600
2MASS J04312405+1800215	10	MHO Tau 4	M6	11	2003 Dec 4	HD 27761	0.38	600
2MASS J16262780-2426418	102	ρ Oph GY 37	M6	104	2003 May 12	HD 151736	0.38	1200
2MASS J05375745-0238444	8	S Ori 12	M6	8	2003 Dec 4	HD 37887	0.38	1200
2MASS J05390449-0238353	8	S Ori 17	M6	8	2004 Feb 9	HD 294285 (A1V)	0.38	1200
2MASS J16014955-2351082	3	USco CTIO 66AB	M6+M6	3	2003 May 12	HD 151736	0.38	600
2MASS J02535980+3206373	29	2MASS 0253+3206	M6	1	2003 Dec 4	BD+3i 500 (A3)	0.38	600
2MASS J08402975+1824091	42	2MASS 0840+1824	M6	48	2003 Dec 4	HD 89239	0.38	480
2MASS J10494146+2538535	36	2MASS 1049+2538	M6	36	2003 Dec 4	HD 89239	0.38	600
2MASS J03230483+4816111	97	AP 310	M6	97	2003 Jul 20	HD 22401	0.38	1200
Cl* Melotte 20 AP 316	97	AP 316	M6	97	2004 Nov 22	HD 20842	0.38	1200
2MASS J14121215-0035165	68	GJ 3828B	M6	45	2004 Apr 30	HD 123233	0.38	1200
2MASS J03473900+2436226	108	Roque 16	M6	108	2004 Nov 22	24 Tau	0.38	1200
2MASS J03520670+2416008	73	Teide 2	M6	73	2003 Dec 4	HD 23512	0.38	1200
2MASS J15514732-2623477	3	USco CTIO 121	M6	3	2003 Jul 19	HD 141442	0.38	1200
UScoCTIO 85	3	UScoCTIO 85	M6	3	2003 Mar 25	HD 142703	0.38	1200
2MASS J10562886+0700527	107	Wolf 359	M6	47	2000 Dec 6	HD 93346	0.38	120
2MASS J04321606+1812464	10	MHO Tau 5	M6.5	10	2003 Feb 8	HD 25175	0.38	480
2MASS J16262226-2424070	89	ρ Oph GY 11	M6.5	104	2004 Jul 22	HD 151736	0.38	1800
2MASS J16121185-2047267	94	SCH 1612-2047	M6.5	94	2009 Apr 7	HD 144925	0.38	1200
2MASS J03180906+4925189	97	AP 301	M6.5	97	2003 Jul 20	HD 22401	0.38	1200
2MASS J07401922-1724449	82	Gl 283B	M6.5	48	2001 Dec 31	HD 61486	0.38	400
2MASS J03454126+2354099	95	PPL 1	M6.5	72	2001 Dec 29	HD 34317	0.38	600
2MASS J04351455-1414468	29	2MASS 0435-1414	M7	1	2003 Dec 4	HD 31743	0.38	600
2MASS J03204346+5059396	83	AP 270	M7	6	2003 Dec 4	HD 20842	0.38	2400
2MASS J05382088-0246132	8	S Ori 31	M7	5	2004 Feb 9	HD 294285 (A1V)	0.38	1200
2MASS J05373648-0241567	8	S Ori 40	M7	8	2003 Dec 4	HD 37887	0.38	1200
2MASS J16020429-2050425	3	USco CTIO 100	M7	3	2003 May 13	HD 151736	0.38	600
2MASS J15591135-2338002	3	USco CTIO 128	M7	3	2003 Mar 25	HD 142703	0.38	1200
2MASS J03354735+4917430	97	AP 325	M7	97	2003 Dec 4	HD 20842	0.38	1800
2MASSI J0952219-192431	36	2MASS 0952-1924	M7	36	2003 Dec 4	HD 90606	0.38	600
2MASS J03551257+2317378	9	CFHT PL 15	M7	96	2003 Feb 8	HD 25175	0.38	1200
2MASS J11571691+2755489	47	CTI 115638.4+28	M7	47	2004 Apr 30	HD 105388	0.38	1200
2MASS J11061897+0428327	68	LHS 2351	M7	54	2000 Dec 14	HD 75159	0.38	600
2MASS J03464298+2424506	108	Roque 14	M7	108	2003 Dec 4	HD 7215	0.38	600
2MASS J15593777-2254136	3	USco CTIO 132	M7	3	2003 May 14	HD 151736	0.38	400
2MASS J16553529-0823401	101	VB 8	M7	44	2001 Jun 10	HD 152515 (A2V)	0.38	600
2MASS J18355309-3217129	54	2MASS 1835-3217	M7p	54	2005 Jul 19	HD 168086	0.38	1200
2MASS J04361038+2259560	77	CFHT BD-Tau 2	M7.5	11	2002 Dec 23	HD 40686	0.38	600
2MASS J16261882-2426105	28	*ISO*-Oph 23	M7.5	104	2004 May 2	HD 147384	0.38	1800
2MASS J15594366-2014396	3	USco CTIO 130	M7.5	3	2004 Apr 30	HD 147013	0.38	1200
Cl* Melotte 20 AP 326	97	AP 326	M7.5	97	2004 Nov 6	HD 23860	0.38	2400
2MASS J03455065+2409037	108	Roque 13	M7.5	108	2004 Nov 21	24 Tau	0.38	1200
WDS J04325+1732Bb	27	GG Tau Bb	M7.5	103	2004 Nov 7	HD 28354	0.38	1200
2MASS J12073346-3932539	35	2MASS 1207-3932	M8	53	2001 Dec 30	HD 112832 (A3V)	0.38	1200

Table 1
(Continued)

Designation	Disc. Ref	Short Name	SpT	SpT Ref	UT Date of Observation	A0V Calibrator	Slit Width (arcsec)	Exp. Time (s)
2MASS J04363893+2258119	77	CFHT BD-Tau 3	M8	11	2004 Nov 21	HD 105388	0.38	1200
2MASS J16191646-2347235	78	DENIS 1619-2347	M8	78	2005 Jul 18	HD 151736	0.38	1200
2MASS J16192988-2440469	78	DENIS 1619-2440	M8	78	2004 Jul 22	HD 151736	0.38	1200
2MASS J04305718+2556394	11	KPNO Tau 7	M8	11	2004 Nov 21	HD 28354	0.38	600
2MASS J16262189-2444397	40	ρ Oph GY 3	M8	105	2004 May 2	HD 147384	0.38	1200
2MASS J16224385-1951057	94	SCH 1622-1951	M8	94	2009 Apr 7	HD 144254	0.38	600
2MASS J16235155-2317270	94	SCH 1623-2317	M8	94	2009 Apr 7	HD 144925	0.38	600
2MASS J03471792+2422317	84	Teide 1	M8	72	2004 Nov 7	24 Tau	0.38	1200
2MASS J10471265+4026437	69	LP 213-67	M8+L0	26	2003 Dec 4	HD 98152	0.38	480
2MASS J03194133+5030451	97	AP 306	M8	97	2003 Feb 8	HD 21038	0.38	1200
2MASSI J2349489+122438	69	LP 523-55	M8	36	2004 Nov 6	HD 222749	0.38	600
2MASS J03471208+2428320	108	Roque 11	M8	33	2004 Nov 22	25 Tau	0.38	1200
2MASS J19165762+0509021	100	VB 10	M8	44	2001 Jun 10	HD 180759	0.38	600
2MASS J04151471+2800096	11	KPNO Tau 1	M8.5	11	2004 Nov 22	HD 28354	0.38	1200
2MASS J04300724+2608207	11	KPNO Tau 6	M8.5	11	2004 Nov 7	HD 28354	0.38	1200
2MASS J04355143+2249119	11	KPNO Tau 9	M8.5	11	2003 Dec 4	HD 27761	0.38	1200
2MASS J16265128-2432419	89	ρ Oph GY 141	M8.5	66	2003 May 13	HD 151736	0.38	960
2MASS J16273863-2438391	40	ρ Oph GY 310	M8.5	104	2004 Apr 30	HD 147013	0.38	960
2MASS J03434028+2430113	9	Roque 7	M8.5	76	2004 Nov 21	24 Tau	0.38	1200
2MASS J21402931+1625183	36	2MASS 2140+1625	M8.5+L2	26	2009 Nov 8	HD 210501	0.38	600
BD+16 2708B	75	Gl 569 BC	M8.5+M9	59	2002 Apr 23	HD131714 (A3V)	0.38	480
2MASS J11395113-3159214	35	2MASS 1139-3159	M9	87	2001 Dec 30	HD 102412 (A2V)	0.38	1200
2MASS J16110360-2426429	78	DENIS 1611-2426	M9	78	2004 May 2	HD 147384	0.38	1200
2MASS J16145258-2017133	78	DENIS 1614-2017	M9	78	2005 Jul 18	HD 151736	0.38	1200
2MASS J04190126+2802487	67	KPNO Tau 12	M9	67	2004 Nov 7	HD 28354	0.38	1200
2MASS J03435353+2431115	108	Roque 4	M9	108	2002 Dec 24	HD 23489 (A2V)	0.38	1200
2MASS J01400263+2701505	36	2MASS 0140+2701	M9	80	2009 Nov 8	HD 7215	0.38	600
2MASS J12391934+2029519	49	2MASS 1239+2029	M9	49	2002 Dec 24	HD 109055	0.38	600
2MASS J22085600-1227448	54	2MASS 2208-1227	M9	54	2005 Jul 18	HD 213030	0.38	1200
2MASS J08533619-0329321	68	LHS 2065	M9	47	2002 Apr 22	CCDM J08581+0132AB (A2V)	0.38	480
2MASS J22373255+3922398	51	G 216-7B	M9.5	51	2002 Dec 24	BD+394890	0.38	600
2MASS J01415823-4633574	52	2MASS 0141-4633	L0	52	2004 Nov 6	HD 8977	0.38	1200
2MASSI J0443376+000205	43	2MASS 0443+0002	L0	1	2004 Nov 21	24 Tau	0.38	1200
2MASS J06085283-2753583	29	2MASS 0608-2753	L0	1	2003 Dec 4	HD 31743	0.38	600
2MASS J04272799+2612052	11	KPNO Tau 4	L0	23	2002 Dec 24	HD 23489 (A2V)	0.38	1200
2MASS J00274197+0503417	91	PC0025+0447	L0	1	2002 Dec 24	BD+0345	0.38	1200
UGCS J053903.20-023019.9	110	S Ori 51	L0	23	2002 Dec 24	HD 40686	0.38	1200
2MASS J17312974+2721233	87	2MASS 1731+2721	L0	87	2014 Apr 14	HD 165029	0.38	1200
2MASS J21073169-0307337	29	2MASS 2107-0307	L0	29	2004 Nov 7	HD 202990	0.38	1200
2MASS J10221489+4114266	106	HD 89744B	L0	106	2001 Mar 6	HD 90470 (A2V)	0.38	1200
2MASS J03393521-3525440	68	LP 944-20	L0	1	2003 Dec 4	HD 23536	0.38	600
WISEA J043535.82+211508.9	56	WISE 0435+2115	sdL0	56	2013 Dec 14	HD 35036	0.38	2400
2MASS J14413716-0945590	74	DENIS 1441-0945	L0.5	53	2003 Mar 24	HD 132072	0.38	1200
2MASS J04062677-3812102	54	2MASS 0406-3812	L1	54	2014 Nov 12	HD 30397	0.38	2400
2MASS J00332386-1521309	38	2MASS 0033-1521	L1	1	2004 Nov 7	HD 218639	0.38	1200
2MASS J02081833+2542533	50	2MASS 0208+2542	L1	50	2000 Dec 5	BD +18 337A	0.38	1200
2MASS J03454316+2540233	57	2MASS 0345+2540	L1	54	2000 Dec 4	NSV 1280	0.38	2400
2MASS J10352455+2507450	50	2MASS 1035+2507	L1	50	2001 Dec 31	HD 98154 (A3V)	0.38	1200
2MASS J14532582+1420410	54	2MASS 1453+1420	L1	54	2005 Jul 19	HD 123233	0.38	1200
2MASS J21304464-0845205	53	2MASS 2130-0845	L1	54	2001 Jun 11	HD 205147 (A2)	0.38	1200
2MASS J02355993-2331205	37	GJ 1048B	L1	37	2001 Dec 31	HR 8569 (A2V)	0.38	1200
2MASS J13313310+3407583	54	2MASS 1331+3407	L1p	54	2011 Jun 9	10 Boo	0.38	1800

Table 1
(Continued)

Designation	Disc. Ref	Short Name	SpT	SpT Ref	UT Date of Observation	A0V Calibrator	Slit Width (arcsec)	Exp. Time (s)
2MASS J14403186-1303263	54	2MASS 1440-1303	L1p	54	2011 Jun 9	HD 132072	0.38	1200
2MASS J17561080+2815238	54	2MASS 1756+2815	L1p	54	2012 Sep 3	HD 165029	0.38	1800
2MASS J05381462-0240154	109	S Ori 47	L1.5	79	2003 Mar 24	HD 63741	0.38	3600
WISEA J054318.95+642250.2	56	WISE 0543+6422	L2	56	2013 Dec 14	HD 33654	0.38	1440
2MASS J00154476+3516026	50	2MASS 0015+3516	L2	50	2000 Dec 5	BD +18 122A	0.38	1200
2MASS J00311925-3840356	55	2MASS 0031-3840	L2	55	2014 Dec 2	HD 224622	0.38	1200
2MASS J08472872-1532372	29	2MASS 0847-1532	L2	29	2003 Dec 4	HD 74284	0.38	600
2MASS J20575409-0252302	29	2MASS 2057-0252	L2	1	2009 Oct 6	HD 203769	0.38	1800
2MASS J13054019-2541059	90	Kelu-1	L2+L3.5	98	1999 Apr 29	HR 5146 (A1V)	0.38	1200
WISEA J065958.55+171710.9	56	WISE 0659+1717	L2	56	2013 Nov 20	HD 39953	0.38	960
WISEA J235459.79-185222.4	56	WISE 2354-1852	L2	56	2013 Dec 14	HD 219833	0.38	1800
2MASS J14313097+1436539	92	2MASS 1431+1436	L2p	92	2011 Jun 9	HD 131951	0.38	2400
2MASS J16202614-0416315	106	Gl 618.1B	L2.5	106	2003 May 12	SAO 160448	0.38	2400
2MASS J21041491-1037369	29	2MASS 2104-1037	L2.5	53	2011 Aug 9	HD 202990	0.38	1800
WISEA J060742.13+455037.0	56	WISE 0607+4550	L2.5	56	2013 Dec 14	HD 45105	0.38	1800
2MASS J22081363+2921215	50	2MASS 2208+2921	L3	30	2001 Dec 31	HR 8569 (A2V)	0.38	1200
2MASS J10042066+5022596	85	G 196-3B	L3	30	2001 Mar 6	HD 83869 (A1V)	0.38	1200
2MASS J17260007+1538190	50	2MASS 1726+1538	L3	30	2002 Sep 1	HD 160765 (A1V)	0.38	1200
2MASS J11463449+2230527	49	2MASS 1146+2230	L3	49	2004 Nov 21	HD 105388	0.38	1200
2MASS J13004255+1912354	36	2MASS 1300+1912	L3	20	2009 Apr 7	HD 116960	0.38	600
2MASS J15065441+1321060	36	2MASS 1506+1321	L3	54	2000 Apr 26	ups Ser (A3V)	0.38	1200
2MASS J14243909+0917104	7	GD 165B	L3	58	1999 Jun 3	HD 135775 (A2)	0.38	600
WISEA J053257.29+041842.5	56	WISE 0532+0418	L3	56	2013 Nov 20	HD 39953	0.38	720
2MASS J13023811+5650212	54	2MASS 1302+5650	L3p	54	2012 Apr 9	81 UMa	0.38	2400
2MASS J22244381-0158521	50	2MASS 2224-0158	L3.5	58	2011 Oct 7	HD 210501	0.38	2400
2MASS J12563716-0224522	93	SDSS 1256-0224	sdL3.5	21	2009 Apr 7	q Vir	0.38	1800
2MASS J00361617+1821104	86	2MASS 0036+1821	L4	58	2000 Jul 28	HD 216716	0.38	1200
2MASS J11550087+2307058	49	2MASS 1155+2307	L4	49	2004 Nov 22	HD 105389	0.38	1200
2MASS J21580457-1550098	53	2MASS 2158-1550	L4	54	2001 Oct 9	HD 211278	0.38	1200
2MASS J09211410-2104446	87	SIPS 0921-2104	L4	20	2009 Apr 7	HD 82724	0.38	600
2MASS J18410861+3117279	50	2MASS 1841+3117	L4p	50	2001 Oct 10	BD +27 3016A	0.38	1200
WISEA J071552.38-114532.9	56	WISE 0715-1145	L4p	56	2013 Nov 20	HD 43607	0.38	960
2MASS J08053189+4812330	43	SDSS 0805+4812	L4+T5.5	58	2009 Apr 7	HD 71906	0.38	1200
2MASS J11122567+3548131	50	Gl 417 BC	L4.5+L6	1	2001 Dec 29	HD 96951 (A1V)	0.38	1200
2MASS J08350622+1953050	25	2MASS 0835+1953	L5	54	2014 Nov 11	HD 74721	0.38	1800
2MASS J17430860+8526594	65	G 259-20 B	L5	65	2012 Jun 8	HD 172864 (A2)	0.57	1920
2MASS J14460061+0024519	34	SDSS 1446+0024	L5	58	2005 Jul 19	HD 123233	0.38	1200
2MASS J17210390+3344160	29	2MASS 1721+3344	L5p	20	2011 Jun 9	HD 165029	0.38	1800
2MASS J18212815+1414010	54	2MASS 1821+1414	L5p	54	2005 Jul 18	HD 165029	0.38	1200
2MASS J23512200+3010540	54	2MASS 2351+3010	L5p	54	2011 Oct 7	HD 210501	0.38	1200
2MASS J00043484-4044058	39	GJ 1001 B	L5+L5	58	2004 Nov 6	HD 2339	0.38	1200
2MASS J17281150+3948593	50	2MASS 1728+3948	L5+L6.5	50	2000 Apr 27	HR 6814 (A3V)	0.38	2400
2MASS J02052940-1159296	32	DENIS 0205-1159	L5+L8	58	1999 Aug 20	rho Cet	0.38	1200
2MASS J13153094-2649513	41	2MASS 1315-2649	L5+T7	53	2003 Mar 24	HD 132072	0.38	1200
2MASS J15532142+2109071	49	2MASS 1553+2109	L5.5	49	2005 Jul 19	HD 123233	0.38	1200
2MASS J15074769-1627386	86	2MASS 1507-1627	L5.5	58	1999 Jun 3	HR 6061	0.38	600
2MASS J22443167+2043433	31	2MASS 2244+2043	L6	1	2001 Oct 10	HD 210501	0.38	1200
2MASS J07400712+2009216	58	2MASS 0740+2009	L6	25	2014 Dec 2	HD 58296	0.38	2400
2MASS J10101480-0406499	29	2MASS 1010-0406	L6	29	2015 Mar 30	HD 79752	0.38	1200
2MASS J21522609+0937575	87	2MASS 2152+0937	L6+L6	87	2004 Nov 7	HD 210501	0.38	1200
2MASS J12281523-1547342	32	DENIS 1228-1547	L6+L6	58	1999 Jun 3	HR 4911	0.38	600
2MASS J08503593+1057156	49	2MASS 0850+1057	L6+L7	49	2000 Dec 6	HD 48481	0.38	2400

Table 1
(Continued)

Designation	Disc. Ref	Short Name	SpT	SpT Ref	UT Date of Observation	A0V Calibrator	Slit Width (arcsec)	Exp. Time (s)
2MASS J22521073-1730134	46	2MASS 2252-1730	L6+T2	46	2004 Nov 7	HD 218639	0.38	1200
2MASS J04234858-0414035	34	SDSS 0423-0414	L6+T2	19	2001 Dec 31	HD 34317	0.38	1200
2MASS J03001631+2130205	54	2MASS 0300+2130	L6p	54	2011 Oct 8	HD 232258	0.38	3000
2MASS J11181292-0856106	54	2MASS 1118-0856	L6p	54	2014 Apr 14	HD 93346	0.38	2400
2MASS J21481633+4003594	54	2MASS 2148+4003	L6.5p	54	2011 Aug 9	HD 209932	0.38	1200
2MASS J01033203+1935361	50	2MASS 0103+1935	L7	54	2000 Dec 4	HD 16694 (B9)	0.38	2400
2MASS J15261405+2043414	50	2MASS 1526+2043	L7	50	2005 Jun 4	26 Ser	0.38	1200
2MASS J21513979+3402444	54	2MASS 2151+3402	L7p	54	2011 Oct 7	HD 210501	0.38	2400
2MASS J05325346+8246465	17	2MASS 0532+8246	sdL7	22	2002 Dec 24	HD 34360	0.38	600
2MASS J09310955+0327331	58	SDSS 0931+0327	L7.5	58	2009 Apr 7	HD 79108	0.38	1800
2MASS J11211858+4332464	25	SDSS 1121+4332	L7.5	25	2014 Apr 12	HD 109615	0.38	2400
2MASS J00150206+2959323	54	2MASS 0015+2959	L7.5p	54	2011 Oct 8	HD 9711	0.38	2400
2MASS J16322911+1904407	49	2MASS 1632+1904	L8	54	2002 Aug 31	SAO 102579 (B9.5V)	0.38	1200
2MASS J13314894-0116500	43	SDSS 1331-0116	L8	58	2009 Apr 7	HD 116960	0.38	1800
2MASS J09121469+1459396	106	Gl 337CD	L8+T0	19	2001 Dec 29	HD 80613 (A1V)	0.38	1200
DENIS-P J025503.3-470049	74	2MASS 0255-4700	L9	19	2014 Dec 3	HD 28812	0.38	1200
2MASS J03105986+1648155	50	2MASS 0310+1648	L9+L9	19	2001 Oct 9	34 Ari	0.38	1200
2MASS J14053729+8350248	24	2MASS 1405+8350	L9	24	2012 Jun 8	HD 172864 (A2)	0.57	960
WISEA J082640.45-164031.8	56	WISE 0826-1640	L9	56	2013 Dec 14	HD 72282	0.38	2400
WISE J020625.27+264023.6	55	WISE 0206+2640	L9p	55	2014 Dec 2	HD 19600	0.38	2400
2MASS J16471580+5632057	55	WISE 1647+5632	L9p	55	2014 Apr 12	HD 143187	0.38	900
2MASS J03284265+2302051	50	2MASS 0328+2302	L9.5	58	2001 Dec 29	HD 23409 (A2V)	0.38	1200
2MASS J12074717+0244249	43	2MASS 1207+0244	T0	19	2013 Dec 14	HD 111744	0.38	1800
2MASS J15203974+3546210	25	SDSS 1520+3546	T0	25	2009 Apr 7	26 Ser	0.38	1800
2MASS J15164306+3053443	25	SDSS 1516+3053	T0.5	25	2014 Jun 20	26 Ser	0.38	1800
2MASS J01514155+1244300	34	SDSS 0151+1244	T1	19	2001 Oct 9	34 Ari	0.38	1200
SDSS J083717.21-000018.0	60	SDSS 0837-0000	T1	19	2000 Dec 5	69 Leo	0.38	2400
2MASS J10210969-0304197	60	SDSS 1021-0304	T1+T5	19	2001 Jun 11	HD 90212	0.38	2000
2MASS J09090085+6525275	25	SDSS 0909+6525	T1.5	25	2009 Apr 7	39 UMa	0.38	1800
2MASS J12545393-0122474	60	SDSS 1254-0122	T2	19	2001 Mar 7	k Vir (A3V)	0.38	1200
2MASS J12095613-1004008	14	2MASS 1209-1004	T2+T7.5	19	2012 Apr 9	Q Vir	0.38	2400
2MASS J11061197+2754225	63	2MASS 1106+2754	T2.5	63	2009 Apr 7	HD 105388	0.38	600
2MASS J01365662+0933473	4	SIMP 0136+0933	T2.5	4	2009 Nov 8	BD +18 337A	0.38	1800
2MASS J17503293+1759042	34	SDSS 1750+1759	T3.5	19	2001 Oct 9	HD 165029	0.38	1200
2MASS J22541892+3123498	15	2MASS 2254+3123	T4	19	2000 Jul 25	HD 216716	0.38	1200
2MASS J05591914-1404488	14	2MASS 0559-1404	T4.5	19	2000 Dec 4	NSV 1280	0.38	1200
2MASS J09261537+5847212	34	SDSS 0926+5847	T4.5	19	2002 Dec 23	HD 77692 (A2V)	0.38	1200
2MASS J07554795+2212169	15	2MASS 0755+2212	T5	15	2015 Mar 30	HD 71906	0.38	600
2MASS J15031961+2525196	16	2MASS 1503+2525	T5	19	2012 Apr 9	HD 140775	0.38	1200
WISE J133750.46+263648.6	70	WISE 1337+2636	T5	70	2012 Jun 8	HD 122945	0.57	1440
2MASS J23565477-1553111	15	2MASS 2356-1553	T5.5	19	1999 Aug 19	SAO 191988	0.38	1200
WISE J195436.15+691541.3	70	WISE 1954+6915	T5.5	70	2012 Jun 9	HD 172728	0.57	1440
2MASS J16241436+0029158	111	SDSS 1624+0029	T6	19	1999 Jun 2	HR 6255 (A2Vs)	0.38	1200
WISE J003830.54+840517.7	70	WISE 0038+8405	T6	70	2011 Aug 9	HD 33541	0.76	3600
WISE J184041.77+293229.2	70	WISE 1840+2932	T6	70	2012 Sep 3	HD 165029	0.38	1800
WISE J223720.39+722833.8	70	WISE 2237+7225	T6	70	2011 Sep 8	HD 207636	0.38	1200
2MASS J09373487+2931409	15	2MASS 0937+2931	T6p	19	2001 Mar 7	AG +27 1006	0.38	1200
2MASS J12255432-2739466	12	2MASS 1225-2739	T6+T8	19	2009 Apr 7	HD 119752	0.38	1800
WISE J125015.56+262846.9	70	WISE 1250+2628	T6.5	70	2012 Jun 8	HD 122945	0.57	1440
2MASS J07271824+1710012	15	2MASS 0727+1710	T7	19	2001 Dec 29	HD 74721	0.38	1200
WISE J113949.24-332425.1	99	WISE 1139-3324	T7	99	2013 Feb 21	HD 101169	0.57	2400
WISE J175929.37+544204.7	70	WISE 1759+5442	T7	70	2012 Jun 8	HD 172728	0.57	1440

Table 1
(Continued)

Designation	Disc. Ref	Short Name	SpT	SpT Ref	UT Date of Observation	A0V Calibrator	Slit Width (arcsec)	Exp. Time (s)
WISE J233543.79+422255.2	70	WISE 2335+4222	T7	70	2011 Sep 5	HD 222749	0.76	1800
2MASS J15530228+1532369	15	2MASS 1553+1532	T7+T7	19	2001 Jun 11	HD 147005	0.38	2400
2MASS J14571496-2121477	13	Gl 570 D	T7.5	19	2001 Mar 6	HD 133569	0.38	1000
WISE J042417.94+072744.1	70	WISE 0424+0727	T7.5	70	2012 Sep 24	HD 31411	0.57	2400
WISE J214706.78-102924.0	70	WISE 2147-1029	T7.5	70	2012 Jun 9	HD 203769	0.57	1440
2MASS J04151954-0935066	15	2MASS 0415-0935	T8	19	2000 Dec 6	HD 48481	0.38	2400
WISE J031624.35+430709.1	70	WISE 0316+4307	T8	70	2011 Sep 5	HD 21038	0.76	6000
WISE J043052.92+463331.6	70	WISE 0430+4633	T8	70	2012 Sep 24	HD 31069	0.57	2400
WISE J105047.9+505606.2	70	WISE 1050+5056	T8	70	2012 Jun 9	HD 99966	0.57	1800
WISE J144806.48-253420.3	99	WISE 1448-2534	T8	99	2013 Feb 21	HD 129544	0.57	2400
WISE J173623.03+605920.2	70	WISE 1736+6059	T8	70	2012 Sep 3	HD 172728	0.38	1800
WISE J181329.40+283533.3	70	WISE 1813+2835	T8	70	2012 Jun 8	HD 165029	0.57	1800
WISE J195500.42-254013.9	70	WISE 1955-2540	T8	70	2012 Jun 9	HD 190285	0.57	1440
WISE J200520.38+542433.9	71	WISE 2005+5424	sdT8	71	2012 Jun 8	HD 199217/HD 205314	0.57	6600
WISE J051208.66-300404.4	70	WISE 0512-3004	T8.5	70	2012 Sep 25	HD 36965	0.57	2400
WISE J054047.00+483232.4	70	WISE 0540+4832	T8.5	70	2012 Sep 25	HD 45105	0.57	2400
WISE J000517.48+373720.5	70	WISE 0005+3737	T9	70	2011 Oct 7	HD 9711	0.38	2400
WISE J003829.05+275852.1	70	WISE 0038+2758	T9	70	2011 Sep 8	HD 7215	0.38	4800
WISE J033515.01+431045.1	70	WISE 0335+4310	T9	70	2012 Sep 25	HD 21038	0.57	2400

References. (1) Allers & Liu (2013), (2) Allers et al. (2009), (3) Ardila et al. (2000), (4) Artigau et al. (2006), (5) Barrado y Navascués et al. (2003), (6) Basri & Martín (1999), (7) Becklin & Zuckerman (1988), (8) Béjar et al. (1999), (9) Bouvier et al. (1998), (10) Briceño et al. (1998), (11) Briceño et al. (2002), (12) Burgasser et al. (1999), (13) Burgasser et al. (2000a), (14) Burgasser et al. (2000b), (15) Burgasser et al. (2002a), (16) Burgasser et al. (2003c), (17) Burgasser et al. (2003a), (18) Burgasser (2004), (19) Burgasser et al. (2006), (20) Burgasser (2008), (21) Burgasser et al. (2009), (22) Burgasser et al. (2007), (23) Canty et al. (2013), (24) Castro et al. (2013), (25) Chiu et al. (2006), (26) Close et al. (2003), (27) Cohen & Kuhi (1979), (28) Comeron et al. (1993), (29) Cruz et al. (2003), (30) Cruz et al. (2009), (31) Dahn et al. (2002), (32) Delfosse et al. (1997), (33) Festin (1998), (34) Geballe et al. (2002), (35) Gizis (2002), (36) Gizis et al. (2000), (37) Gizis et al. (2001), (38) Gizis et al. (2003), (39) EROS Collaboration et al. (1999), (40) Greene & Young (1992), (41) Hall (2002), (42) Haro & Chavira (1966), (43) Hawley et al. (2002), (44) Henry & Kirkpatrick (1990), (45) Jenkins et al. (2009), (46) Kendall et al. (2004), (47) Kirkpatrick et al. (1991), (48) Kirkpatrick (1992), (49) Kirkpatrick et al. (1999), (50) Kirkpatrick et al. (2000), (51) Kirkpatrick et al. (2001), (52) Kirkpatrick et al. (2006), (53) Kirkpatrick et al. (2008), (54) Kirkpatrick et al. (2010), (55) Kirkpatrick et al. (2011), (56) Kirkpatrick et al. (2014), (57) Kirkpatrick et al. (1997), (58) Knapp et al. (2004), (59) Konopacky et al. (2010), (60) Leggett et al. (2000), (61) Lépine et al. (2002), (62) Lépine et al. (2003), (63) Looper et al. (2007), (64) Lowrance et al. (2005), (65) Luhman (2012), (66) Luhman et al. (1997), (67) Luhman et al. (2003), (68) Luyten (1979a), (69) Luyten (1979b), (70) Mace et al. (2013a), (71) Mace et al. (2013b), (72) Martin et al. (1996), (73) Martín et al. (1998), (74) Martín et al. (1999), (75) Martín et al. (2000b), (76) Martín et al. (2000a), (77) Martín et al. (2001), (78) Martín et al. (2004), (79) McGovern et al. (2004), (80) McLean et al. (2007), (81) Natta et al. (2002), (82) Probst (1983), (83) Prosser (1994), (84) Rebolo et al. (1995), (85) Rebolo et al. (1998), (86) Reid et al. (2000), (87) Reid et al. (2008), (88) Rice et al. (2010), (89) Rieke & Rieke (1990), (90) Ruiz et al. (1997), (91) Schneider et al. (1991), (92) Sheppard & Cushing (2009), (93) Sivarani et al. (2009), (94) Slesnick et al. (2006), (95) Stauffer et al. (1989), (96) Stauffer et al. (1998), (97) Stauffer et al. (1999), (98) Stumpf et al. (2008), (99) Thompson et al. (2013), (100) van Biesbroeck (1944), (101) van Biesbroeck (1961), (102) Vrba et al. (1975), (103) White et al. (1999), (104) Wilking et al. (1999), (105) Wilking et al. (2005), (106) Wilson et al. (2001), (107) Wolf (1919), (108) Zapatero Osorio et al. (1997), (109) Zapatero Osorio et al. (1999), (110) Zapatero Osorio et al. (2000), (111) Strauss et al. (1999).

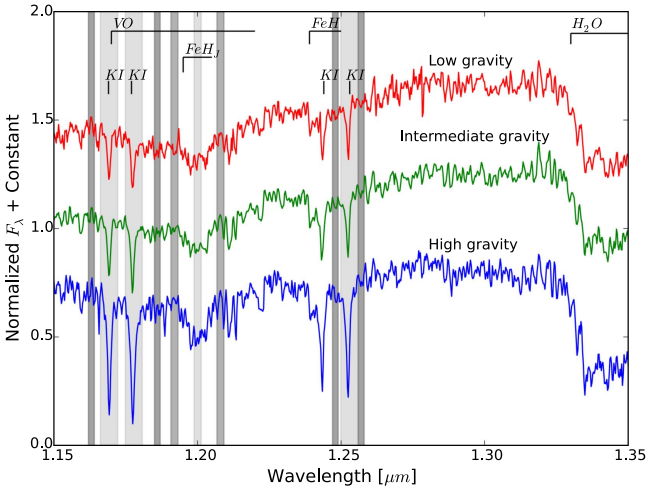

Figure 2. Three-example *J*-band spectra of spectral type L3 objects from the BDSS. Each spectrum represents a different gravity type: low gravity (2MASS 2208+2921), intermediate gravity (2MASS 1726+1538), and high gravity (2MASS 1300+1912). Major absorption features in the *J* band are also labeled. Light gray shaded regions denote the locations used to calculate K I EWs and the FeH_J index. Dark gray regions denote the locations of the pseudo-continua used in our calculations. The K I line at 1.2437 μm is marked but not shaded. This line was not used to determine gravity types because of contamination from FeH absorption at $\sim$1.24 μm.

our method of determining surface gravity, and Section 4 discusses general trends, interesting objects revealed by our analysis, and the ability of the gravity indices to distinguish the ages of objects. Section 5 summarizes our results.

2. Sample

We present medium-resolution *J*-band spectra of 85 M dwarfs, 92 L dwarfs, and 51 T dwarfs obtained as part of the BDSS. Ninety-seven spectra were published previously in McLean et al. (2003), Burgasser et al. (2003a), McGovern et al. (2004), Rice et al. (2010), Kirkpatrick et al. (2010), Luhman (2012), Thompson et al. (2013), Mace et al. (2013a), Mace et al. (2013b), and Kirkpatrick et al. (2014), and the remaining 131 are presented here for the first time. By design, our sample spans a large range of spectral types, ages, and distances. In addition to known standards and field objects, we have observed peculiar objects such as $J - K_s$ color outliers and known young and old objects. Sixty-four of our targets have age estimates based on their likely associations with clusters or moving groups, such as the Pleiades, Upper Scorpius, and Taurus regions, or from spectral analysis of stellar companions. However, the majority of the sample comprises field brown dwarfs and low-mass stars selected from the 2MASS and *WISE* surveys. As illustrated in Figure 1, our largest population of objects is late-type M dwarfs.

2.1. Observations

Targets were observed using the strategy described in McLean et al. (2003) for the NIRSPEC instrument on the Keck II telescope in non-echelle (medium-resolution) mode. For this mode, the slit used is typically 0.″38 wide (two pixels), although the 0.″57 slit was used for several fainter T dwarfs and for observing conditions with sub-optimal seeing. For most observations, 300 s exposures were taken in nod pairs of 20″ separation along the 42″ slit. These nods were generally done in ABBA format for a total observing time of 20 minutes per target. Fainter objects were observed for longer as needed. An A0V star at a similar airmass to each target was used for telluric corrections. If there were no nearby A0V stars, then calibrators as early as B9 or as late as A3 were used instead. In the N3 filter ($\sim$1.15–1.35 μm), the A0V stars typically only contain the Paβ absorption line at 1.282 μm which we interpolate over in the reduction process. In addition to telluric calibrators, flat field and dark frames were taken, as well as spectra of Ne and Ar lamps for wavelength calibration. Observation information for all of the targets in our sample is listed in Table 1, as well as spectral types taken from the literature.

2.2. Data Reduction

All spectroscopic reductions were made using the REDSPEC package[10], software produced at UCLA by S. Kim, L. Prato, and I. McLean specifically for the reduction of NIRSPEC data as described in McLean et al. (2003). The REDSPEC code first corrects for spatial and spectral distortion on the array using Ne and Ar lamp lines with wavelengths taken from the National Institute of Standards and Technology (NIST[11]; Kramida et al. 2015). Nod pairs of the target and calibrator are then background subtracted and divided by a flat field. Known bad pixels are removed as well. Spectra are obtained by summing over a range of $\sim$10 pixels (depending on seeing) and then dividing by the A0V calibrator spectrum to remove telluric features. Each pair of spectra was normalized and combined with other pairs (when available) to achieve a higher signal-to-noise ratio (S/N). This sample contains targets with S/N $\sim$ 10–200, although the majority of the spectra have an S/N of at least 20. Finally, heliocentric velocity corrections were applied to the normalized spectra. We also performed a quality check on all data to ensure that wavelength dispersion solutions differed by less than $\sim 10^{-5}$ Å/pixel. Plots and data files for all of our reduced spectra are available publicly through the BDSS archive[12] or by request.

3. Surface Gravity: Methods and Results

Below we describe our method for calculating the EWs and spectral indices used to determine the surface gravities of our objects. We then present surface gravity estimates for all M6–L7 objects in the BDSS, as well as EW and spectral index values for all BDSS objects.

3.1. Equivalent Widths

We compute pseudo-EWs for the four neutral potassium lines in the *J* band following the method described in A13. For accurate comparison, we use the same line and pseudo-continuum windows as defined in A13 (see Figure 2). The light gray shaded regions indicate the line windows used, while the dark gray shows the continuum windows. The K I doublet at 1.1692 and 1.1778 μm share the continuum windows on either side of the doublet, and the 1.2437 and 1.2529 μm lines share the continua surrounding the 1.2529 μm line. A13 chooses to exclude the 1.2437 μm line from their final analysis because of the FeH contamination on the blue side of the line. For

[10] http://www2.keck.hawaii.edu/inst/nirspec/redspec.html
[11] http://physics.nist.gov/asd
[12] http://bdssarchive.org

Table 2
Equivalent Widths and Spectral Index Values for the BDSS *J*-band Spectra

Name	SpT	K I EW (Å) 1.1692 μm	K I EW (Å) 1.1778 μm	K I EW (Å) 1.2437 μm	K I EW (Å) 1.2529 μm	FeH$_J$ 1.20 μm	Gravity Scores K1 K2 K4 FeH	Gravity Type This Paper	Gravity Type A13
2MASS 0619-2903	M5	0.08 ± 0.76	0.54 ± 0.67	0.52 ± 1.4	1.53 ± 0.62	1.021 ± 0.015	n n 0. n	N/A	N/A
LHS 1135	d/sdM5	2.17 ± 0.44	4.01 ± 0.34	1.92 ± 0.45	2.51 ± 0.17	1.045 ± 0.005	n n 0. n	N/A	···
Gl 577 BC	M5.5+M5.5	0.6 ± 0.04	1.81 ± 0.03	1.14 ± 0.1	1.44 ± 0.04	1.042 ± 0.001	n n 0. n	N/A	···
Rho Oph GY 5	M5.5	0.62 ± 0.87	0.5 ± 0.48	0.82 ± 0.68	0.65 ± 0.26	1.021 ± 0.012	n n 2. n	N/A	···
GG Tau Ba	M6	−1.57 ± 0.04	1.43 ± 0.04	1.23 ± 0.07	0.27 ± 0.04	1.019 ± 0.001	2. 2. 2. 2.	VL-G	···
2MASS 1459+0004	M6	0.76 ± 0.68	1.39 ± 0.63	1.54 ± 1.36	1.53 ± 0.65	1.022 ± 0.017	2. 2. 2. 2.	VL-G	···
2MASS 2234+4041AB	M6+M6	−0.05 ± 0.64	0.48 ± 0.52	1.02 ± 0.84	0.17 ± 0.32	1.027 ± 0.011	2. 2. 2. 2.	VL-G	···
DENIS-P 1605-2406	M6	0.09 ± 0.1	0.75 ± 0.09	0.8 ± 0.21	0.54 ± 0.1	1.039 ± 0.002	2. 2. 2. 2.	VL-G	···
KPNO Tau 3	M6	−0.71 ± 0.19	−0.81 ± 0.11	1.22 ± 0.21	0.71 ± 0.09	1.025 ± 0.003	2. 2. 2. 2.	VL-G	···
MHO Tau 4	M6	0.45 ± 0.11	0.95 ± 0.08	1.01 ± 0.13	0.91 ± 0.06	1.037 ± 0.002	2. 2. 2. 2.	VL-G	···
Rho Oph GY 37	M6	0.97 ± 0.19	1.04 ± 0.17	0.6 ± 0.36	1.1 ± 0.15	1.032 ± 0.004	2. 2. 2. 2.	VL-G	···
S Ori 12	M6	0.67 ± 0.19	1.25 ± 0.18	0.74 ± 0.41	0.41 ± 0.19	1.028 ± 0.005	2. 2. 2. 2.	VL-G	···
S Ori 17	M6	−0.93 ± 0.54	−0.08 ± 0.48	0.81 ± 1.05	1.41 ± 0.49	1.029 ± 0.011	2. 2. 2. 2.	VL-G	···
USco CTIO 66AB	M6+M6	0.87 ± 0.16	1.54 ± 0.16	1.36 ± 0.35	1.28 ± 0.16	1.038 ± 0.004	2. 2. 2. 2.	VL-G	···
2MASS 0253+3206	M6	2.77 ± 0.11	4.12 ± 0.1	2.41 ± 0.2	3.55 ± 0.09	1.067 ± 0.002	0. 0. 0. 0.	FLD-G	FLD-G
2MASS 0840+1824	M6	3.49 ± 0.06	5.29 ± 0.03	3.47 ± 0.04	4.01 ± 0.02	1.095 ± 0.002	0. 0. 0. 0.	FLD-G	···
2MASS 1049+2538	M6	2.48 ± 0.18	3.84 ± 0.17	3.1 ± 0.34	3.14 ± 0.15	1.072 ± 0.005	0. 0. 0. 0.	FLD-G	···
AP 310	M6	2.34 ± 0.42	3.49 ± 0.4	0.52 ± 1.0	2.39 ± 0.41	1.066 ± 0.011	0. 0. 0. 0.	FLD-G	···
AP 316	M6	1.6 ± 0.82	2.51 ± 0.73	2.61 ± 1.82	2.3 ± 0.8	1.069 ± 0.021	1. 2. 0. 0.	FLD-G	···
GJ 3828 B	M6	4.85 ± 0.11	7.21 ± 0.1	5.0 ± 0.23	5.43 ± 0.1	1.127 ± 0.003	0. 0. 0. 0.	FLD-G	···
Roque 16	M6	2.1 ± 1.08	3.38 ± 1.05	1.41 ± 2.35	3.41 ± 0.97	1.058 ± 0.026	0. 0. 0. 0.	FLD-G	···
Teide 2	M6	3.82 ± 0.53	4.21 ± 0.49	2.46 ± 1.06	3.06 ± 0.49	1.074 ± 0.013	0. 0. 0. 0.	FLD-G	···
USco CTIO 121	M6	3.45 ± 0.3	4.77 ± 0.26	3.25 ± 0.58	3.64 ± 0.27	1.091 ± 0.007	0. 0. 0. 0.	FLD-G	···
USco CTIO 85	M6	2.99 ± 0.15	4.13 ± 0.14	2.64 ± 0.32	3.45 ± 0.14	1.095 ± 0.004	0. 0. 0. 0.	FLD-G	···
Wolf 359	M6	3.16 ± 0.02	4.64 ± 0.03	2.93 ± 0.05	3.46 ± 0.02	1.078 ± 0.001	0. 0. 0. 0.	FLD-G	···
MHO Tau 5	M6.5	−2.17 ± 0.06	0.18 ± 0.06	0.87 ± 0.12	0.45 ± 0.06	1.036 ± 0.001	2. 2. 2. 2.	VL-G	···
Rho Oph GY 11	M6.5	−0.73 ± 1.21	1.04 ± 1.07	1.82 ± 1.82	1.03 ± 0.78	1.029 ± 0.024	2. 2. 2. 2.	VL-G	···
SCH 1612-2047	M6.5	−0.07 ± 0.11	0.67 ± 0.11	0.57 ± 0.21	0.68 ± 0.1	1.034 ± 0.002	2. 2. 2. 2.	VL-G	···
AP 301	M6.5	1.99 ± 0.32	3.77 ± 0.3	2.25 ± 0.7	1.77 ± 0.33	1.083 ± 0.009	0. 0. 1. 0.	FLD-G	···
Gl 283 B	M6.5	3.21 ± 0.06	4.88 ± 0.06	2.78 ± 0.14	3.29 ± 0.06	1.06 ± 0.002	0. 0. 0. 0.	FLD-G	···
PPL 1	M6.5	2.48 ± 2.36	3.53 ± 1.76	4.97 ± 1.79	4.52 ± 0.72	1.119 ± 0.043	0. 0. 0. 0.	FLD-G	···
2MASS 0435-1414	M7	0.09 ± 0.09	0.22 ± 0.06	0.47 ± 0.12	0.42 ± 0.05	1.023 ± 0.001	2. 2. 2. 2.	VL-G	VL-G
AP 270	M7	0.99 ± 0.17	3.1 ± 0.16	1.65 ± 0.36	2.16 ± 0.16	1.047 ± 0.004	2. 2. 2. 2.	VL-G	···
S Ori 31	M7	−0.01 ± 0.39	1.37 ± 0.36	0.44 ± 0.72	0.77 ± 0.35	1.03 ± 0.009	2. 2. 2. 2.	VL-G	···
S Ori 40	M7	0.33 ± 0.54	1.65 ± 0.51	1.79 ± 1.13	0.32 ± 0.55	1.047 ± 0.014	2. 2. 2. 2.	VL-G	···
USco CTIO 100	M7	0.75 ± 0.16	1.31 ± 0.16	1.31 ± 0.35	1.21 ± 0.14	1.053 ± 0.004	2. 2. 2. 2.	VL-G	···
USco CTIO 128	M7	0.96 ± 0.26	1.26 ± 0.23	2.11 ± 0.51	1.13 ± 0.24	1.065 ± 0.006	2. 2. 2. 1.	VL-G	···
AP 325	M7	2.54 ± 0.18	4.57 ± 0.17	2.54 ± 0.37	2.84 ± 0.16	1.1 ± 0.005	1. 1. 1. 0.	INT-G	···
2MASS 0952-1924	M7	3.58 ± 0.02	5.21 ± 0.03	3.4 ± 0.04	3.78 ± 0.02	1.092 ± 0.0	0. 0. 0. 0.	FLD-G	···
CFHT PL 15	M7	3.04 ± 0.74	6.37 ± 0.64	3.24 ± 1.55	4.46 ± 0.64	1.153 ± 0.02	0. 0. 0. 0.	FLD-G	···
CTI 115638.4+28	M7	5.19 ± 0.31	7.29 ± 0.26	4.03 ± 0.64	4.68 ± 0.28	1.115 ± 0.008	0. 0. 0. 0.	FLD-G	···
LHS 2351	M7	4.34 ± 0.25	5.78 ± 0.22	3.78 ± 0.57	3.84 ± 0.24	1.114 ± 0.008	0. 0. 0. 0.	FLD-G	···
Roque 14	M7	4.88 ± 2.3	6.2 ± 1.13	3.84 ± 1.35	4.3 ± 0.48	1.13 ± 0.008	0. 0. 0. 0.	FLD-G	···
USco CTIO 132	M7	8.16 ± 1.25	7.55 ± 1.04	4.99 ± 1.54	5.64 ± 0.65	1.149 ± 0.024	0. 0. 0. 0.	FLD-G	···
VB 8	M7	4.62 ± 0.45	6.65 ± 0.28	3.8 ± 0.58	4.93 ± 0.3	1.097 ± 0.009	0. 0. 0. 0.	FLD-G	···
2MASS 1835-3217	M7p	4.06 ± 0.52	5.42 ± 0.47	2.72 ± 1.04	3.86 ± 0.48	1.056 ± 0.013	0. 0. 0. 1.	FLD-G	···
CFHT BD Tau 2	M7.5	0.38 ± 3.21	0.63 ± 1.47	0.99 ± 0.59	0.8 ± 0.27	1.027 ± 0.023	2. 2. 2. 2.	VL-G	···

Table 2
(Continued)

Name	SpT	K I EW (Å) 1.1692 μm	K I EW (Å) 1.1778 μm	K I EW (Å) 1.2437 μm	K I EW (Å) 1.2529 μm	FeH$_J$ 1.20 μm	Gravity Scores K1 K2 K4 FeH	Gravity Type This Paper	Gravity Type A13
ISO-Oph 23	M7.5	0.69 ± 0.56	1.8 ± 0.57	0.22 ± 0.99	−0.2 ± 0.44	1.022 ± 0.013	2. 2. 2. 2.	VL-G	···
USco CTIO 130	M7.5	0.89 ± 0.24	1.68 ± 0.23	1.09 ± 0.47	1.32 ± 0.21	1.061 ± 0.006	2. 2. 2. 1.	VL-G	···
AP 326	M7.5	4.7 ± 0.43	2.67 ± 0.42	4.38 ± 0.93	4.12 ± 0.42	1.107 ± 0.012	0. 2. 0. 0.	FLD-G	···
Roque 13	M7.5	3.5 ± 0.8	4.56 ± 0.7	3.86 ± 1.71	4.39 ± 0.76	1.125 ± 0.023	0. 1. 0. 0.	FLD-G	···
GG Tau Bb	M7.5	−0.06 ± 0.08	2.03 ± 0.08	1.4 ± 0.15	0.07 ± 0.07	1.036 ± 0.002	2. 2. 2. 2.	VL-G	···
2MASS 1207-3932	M8	1.45 ± 0.31	1.24 ± 0.28	1.1 ± 0.64	1.34 ± 0.28	1.078 ± 0.008	2. 2. 2. 1.	VL-G	VL-G
CFHT BD Tau 3	M8	0.8 ± 0.22	1.05 ± 0.2	1.27 ± 0.4	0.94 ± 0.18	1.066 ± 0.005	2. 2. 2. 2.	VL-G	···
DENIS 1619-2347	M8	−0.42 ± 0.24	0.67 ± 0.23	0.88 ± 0.45	1.97 ± 0.19	1.055 ± 0.006	2. 2. 2. 2.	VL-G	···
DENIS 1619-2440	M8	0.11 ± 0.24	0.15 ± 0.24	1.48 ± 0.48	0.85 ± 0.21	1.04 ± 0.006	2. 2. 2. 2.	VL-G	···
KPNO Tau 7	M8	0.42 ± 3.24	1.87 ± 1.65	1.12 ± 3.13	0.86 ± 1.25	1.05 ± 0.048	2. 2. 2. 2.	VL-G	···
Rho Oph GY 3	M8	0.14 ± 0.08	0.81 ± 0.08	1.09 ± 0.17	0.43 ± 0.08	1.043 ± 0.002	2. 2. 2. 2.	VL-G	···
SCH 1622-1951	M8	0.7 ± 0.1	1.58 ± 0.1	1.02 ± 0.22	1.0 ± 0.1	1.063 ± 0.002	2. 2. 2. 2.	VL-G	···
SCH 1623-2317	M8	0.52 ± 0.08	1.02 ± 0.05	0.65 ± 0.09	1.05 ± 0.04	1.079 ± 0.004	2. 2. 2. 1.	VL-G	···
Teide 1	M8	2.24 ± 0.91	2.94 ± 0.81	4.74 ± 1.79	3.79 ± 0.79	1.13 ± 0.027	2. 2. 1. 0.	VL-G	···
LP 213-67	M8+L0	2.74 ± 0.14	4.34 ± 0.08	2.98 ± 0.1	3.26 ± 0.05	1.085 ± 0.002	1. 1. 1. 1.	INT-G	···
AP 306	M8	4.27 ± 0.48	6.0 ± 0.44	0.86 ± 1.1	4.5 ± 0.46	1.13 ± 0.013	0. 1. 0. 0.	FLD-G	···
LP 523-55	M8	4.76 ± 0.56	6.31 ± 0.28	4.55 ± 0.75	5.22 ± 0.26	1.127 ± 0.012	0. 0. 0. 0.	FLD-G	···
Roque 11	M8	4.92 ± 1.07	6.97 ± 1.08	2.43 ± 2.5	4.31 ± 1.1	1.134 ± 0.034	0. 0. 0. 0.	FLD-G	···
VB 10	M8	4.92 ± 0.08	6.88 ± 0.05	4.33 ± 0.14	4.87 ± 0.06	1.141 ± 0.002	0. 0. 0. 0.	FLD-G	···
KPNO Tau 1	M8.5	1.08 ± 0.76	2.48 ± 0.71	2.5 ± 1.53	0.93 ± 0.69	1.065 ± 0.02	2. 2. 2. 2.	VL-G	···
KPNO Tau 6	M8.5	1.03 ± 0.39	2.09 ± 0.37	1.84 ± 0.72	0.86 ± 0.33	1.068 ± 0.009	2. 2. 2. 2.	VL-G	···
KPNO Tau 9	M8.5	1.88 ± 0.49	2.25 ± 0.52	1.62 ± 1.01	1.39 ± 0.46	1.062 ± 0.013	2. 2. 2. 2.	VL-G	···
Rho Oph GY 141	M8.5	2.56 ± 0.42	4.35 ± 0.37	3.71 ± 0.77	1.44 ± 0.36	1.097 ± 0.01	2. 1. 2. 1.	VL-G	···
Rho Oph GY 310	M8.5	0.53 ± 0.23	0.93 ± 0.22	1.2 ± 0.38	1.18 ± 0.18	1.048 ± 0.005	2. 2. 2. 2.	VL-G	···
Roque 7	M8.5	3.45 ± 1.29	4.63 ± 1.16	3.08 ± 2.63	3.54 ± 1.18	1.13 ± 0.037	1. 1. 1. 0.	INT-G	···
2MASS 2140+1625	M8.5+L2	5.99 ± 0.21	8.18 ± 0.13	3.46 ± 0.21	5.48 ± 0.1	1.207 ± 0.004	0. 0. 0. 0.	FLD-G	···
Gl 569 BC	M8.5+M9	7.45 ± 0.04	9.63 ± 0.04	4.71 ± 0.08	6.02 ± 0.04	1.16 ± 0.001	0. 0. 0. 0.	FLD-G	···
2MASS 1139-3159	M9	1.87 ± 0.16	1.69 ± 0.16	1.79 ± 0.29	1.75 ± 0.13	1.064 ± 0.004	2. 2. 2. 2.	VL-G	VL-G
DENIS 1611-2426	M9	−0.18 ± 0.33	0.95 ± 0.36	1.01 ± 0.76	1.59 ± 0.33	1.073 ± 0.009	2. 2. 2. 2.	VL-G	···
DENIS 1614-2017	M9	−0.34 ± 0.3	1.14 ± 0.31	1.33 ± 0.6	1.66 ± 0.27	1.045 ± 0.008	2. 2. 2. 2.	VL-G	···
KPNO Tau 12	M9	2.19 ± 1.52	3.75 ± 1.62	1.92 ± 2.77	1.09 ± 1.34	1.132 ± 0.042	2. 2. 2. 1.	VL-G	···
Roque 4	M9	4.64 ± 1.15	5.75 ± 1.03	3.03 ± 2.35	3.78 ± 1.0	1.181 ± 0.035	1. 1. 1. 0.	INT-G	···
2MASS 0140+2701	M9	5.94 ± 0.17	8.1 ± 0.13	4.84 ± 0.27	5.74 ± 0.12	1.139 ± 0.004	0. 0. 0. 1.	FLD-G	···
2MASS 1239+2029	M9	5.92 ± 2.64	9.12 ± 1.11	5.45 ± 1.68	5.64 ± 0.57	1.137 ± 0.047	0. 0. 0. 1.	FLD-G	···
2MASS 2208-1227	M9	5.08 ± 1.04	6.05 ± 0.99	3.65 ± 2.34	5.41 ± 0.95	1.151 ± 0.035	0. 1. 0. 1.	FLD-G	···
LHS 2065	M9	6.31 ± 0.06	7.85 ± 0.05	4.92 ± 0.12	5.81 ± 0.05	1.19 ± 0.002	0. 0. 0. 0.	FLD-G	···
G 216-7B	M9.5	5.29 ± 0.25	7.35 ± 0.39	5.85 ± 0.72	5.34 ± 0.5	1.197 ± 0.009	0. 0. 0. 0.	FLD-G	···
2MASS 0141-4633	L0	3.32 ± 0.97	2.86 ± 0.96	3.21 ± 1.87	1.87 ± 0.8	1.107 ± 0.026	2. 2. 2. 2.	VL-G	VL-G
2MASS 0443+0002	L0	3.7 ± 0.06	4.6 ± 0.06	2.06 ± 0.14	3.18 ± 0.06	1.13 ± 0.002	2. 2. 2. 1.	VL-G	VL-G
2MASS 0608-2753	L0	2.31 ± 0.86	3.06 ± 0.66	2.48 ± 1.04	2.42 ± 0.44	1.096 ± 0.017	2. 2. 2. 2.	VL-G	VL-G
KPNO Tau 4	L0	−1.97 ± 0.33	−0.11 ± 0.29	0.31 ± 0.51	−1.15 ± 0.24	1.048 ± 0.007	2. 2. 2. 2.	VL-G	···
PC0025+0447	L0	2.96 ± 0.69	6.13 ± 0.63	3.38 ± 1.55	3.27 ± 0.67	1.149 ± 0.021	2. 1. 2. 1.	VL-G	INT-G
S Ori 51	L0	2.64 ± 1.83	3.77 ± 1.8	2.96 ± 3.36	1.54 ± 1.58	1.088 ± 0.054	2. 2. 2. 2.	VL-G	···
2MASS 1731+2721	L0	7.4 ± 0.15	9.36 ± 0.13	6.08 ± 0.31	6.95 ± 0.14	1.229 ± 0.005	0. 0. 0. 0.	FLD-G	FLD-G
2MASS 2107-0307	L0	7.64 ± 0.28	9.73 ± 0.27	5.84 ± 0.6	7.59 ± 0.25	1.233 ± 0.01	0. 0. 0. 0.	FLD-G	···
HD 89744 B	L0	7.86 ± 0.89	9.88 ± 0.46	4.89 ± 0.45	6.55 ± 0.24	1.23 ± 0.015	0. 0. 0. 0.	FLD-G	···
LP 944-20	L0	6.18 ± 0.02	7.72 ± 0.02	5.08 ± 0.04	5.94 ± 0.02	1.197 ± 0.001	0. 1. 0. 1.	FLD-G	INT-G/ FLD-G

Table 2
(Continued)

Name	SpT	K I EW (Å) 1.1692 μm	K I EW (Å) 1.1778 μm	K I EW (Å) 1.2437 μm	K I EW (Å) 1.2529 μm	FeH_J 1.20 μm	Gravity Scores K1 K2 K4 FeH	Gravity Type This Paper	Gravity Type A13
WISE 0435+2115	sdL0	8.17 ± 0.21	11.3 ± 0.19	4.64 ± 0.48	6.21 ± 0.2	1.118 ± 0.006	0. 0. 0. 2.	FLD-G	⋯
DENIS 1441-0945	L0.5	8.03 ± 0.12	10.11 ± 0.12	5.79 ± 0.26	7.03 ± 0.1	1.242 ± 0.004	0. 0. 0. 0.	FLD-G	⋯
2MASS 0406-3812	L1	4.29 ± 0.94	5.23 ± 1.04	4.81 ± 1.89	4.53 ± 0.85	1.116 ± 0.03	1. 2. 1. 2.	VL-G	VL-G
2MASS 0033-1521	L1	8.21 ± 0.5	10.31 ± 0.46	5.06 ± 1.01	6.86 ± 0.41	1.22 ± 0.017	0. 0. 0. 1.	FLD-G	FLD-G
2MASS 0208+2542	L1	8.25 ± 0.12	10.33 ± 0.11	5.7 ± 0.26	7.69 ± 0.11	1.26 ± 0.004	0. 0. 0. 0.	FLD-G	⋯
2MASS 0345+2540	L1	7.36 ± 0.08	8.77 ± 0.07	5.6 ± 0.17	7.07 ± 0.07	1.225 ± 0.003	0. 1. 0. 1.	FLD-G	⋯
2MASS 1035+2507	L1	8.22 ± 0.46	9.91 ± 0.41	4.16 ± 1.08	6.96 ± 0.42	1.251 ± 0.017	0. 0. 0. 1.	FLD-G	⋯
2MASS 1453+1420	L1	9.1 ± 0.45	13.56 ± 0.4	5.92 ± 1.03	9.46 ± 0.39	1.314 ± 0.02	0. 0. 0. 0.	FLD-G	⋯
2MASS 2130-0845	L1	8.59 ± 0.28	10.69 ± 0.25	5.75 ± 0.65	8.44 ± 0.27	1.263 ± 0.009	0. 0. 0. 0.	FLD-G	⋯
GJ 1048 B	L1	8.4 ± 0.29	10.35 ± 0.27	7.03 ± 0.69	8.0 ± 0.28	1.275 ± 0.012	0. 0. 0. 0.	FLD-G	⋯
2MASS 1331+3407	L1p	7.18 ± 0.24	9.46 ± 0.21	5.76 ± 0.49	6.58 ± 0.22	1.221 ± 0.008	1. 0. 1. 1.	INT-G	⋯
2MASS 1440-1303	L1p	7.63 ± 1.95	13.32 ± 1.69	6.92 ± 4.4	9.17 ± 1.79	1.343 ± 0.082	0. 0. 0. 0.	FLD-G	⋯
2MASS 1756+2815	L1p	11.86 ± 0.14	15.68 ± 0.13	4.95 ± 0.36	10.01 ± 0.14	1.215 ± 0.005	0. 0. 0. 1.	FLD-G	⋯
S Ori 47	L1.5	7.5 ± 0.25	8.96 ± 0.28	5.52 ± 0.65	4.7 ± 0.28	1.212 ± 0.011	0. 1. 1. 1.	INT-G	⋯
WISE 0543+6422	L2	8.25 ± 0.12	9.75 ± 0.13	6.02 ± 0.27	6.87 ± 0.12	1.244 ± 0.005	0. 1. 1. 1.	INT-G	⋯
2MASS 0015+3516	L2	8.27 ± 0.24	10.54 ± 0.14	5.15 ± 0.21	6.94 ± 0.06	1.249 ± 0.011	0. 0. 1. 1.	FLD-G	⋯
2MASS 0031-3840	L2	11.21 ± 0.25	13.05 ± 0.24	6.85 ± 0.6	9.79 ± 0.23	1.304 ± 0.011	0. 0. 0. 0.	FLD-G	⋯
2MASS 0847-1532	L2	8.62 ± 0.65	10.59 ± 0.3	6.64 ± 0.42	7.75 ± 0.16	1.274 ± 0.012	0. 0. 0. 1.	FLD-G	⋯
2MASS 2057-0252	L2	8.35 ± 0.08	9.58 ± 0.07	5.67 ± 0.17	7.44 ± 0.07	1.268 ± 0.003	0. 1. 0. 1.	FLD-G	INT-G/ FLD-G
Kelu 1	L2+L3.5	6.08 ± 0.09	11.47 ± 0.07	5.22 ± 0.17	7.73 ± 0.07	1.231 ± 0.003	1. 0. 0. 1.	FLD-G	⋯
WISE 0659+1717	L2	9.17 ± 0.61	11.78 ± 0.53	6.62 ± 1.4	7.12 ± 0.58	1.255 ± 0.024	0. 0. 1. 1.	FLD-G	⋯
WISE 2354-1852	L2	8.1 ± 0.47	10.46 ± 0.46	6.51 ± 0.97	8.61 ± 0.4	1.282 ± 0.017	1. 0. 0. 1.	FLD-G	⋯
2MASS 1431+1436	L2p	9.9 ± 0.47	12.48 ± 0.43	7.07 ± 0.84	9.4 ± 0.38	1.186 ± 0.015	0. 0. 0. 1.	FLD-G	⋯
GL 618.1 B	L2.5	8.05 ± 0.16	9.65 ± 0.15	4.67 ± 0.38	6.71 ± 0.15	1.244 ± 0.007	1. 1. 1. 1.	INT-G	⋯
2MASS 2104-1037	L2.5	8.5 ± 0.16	12.04 ± 0.15	6.32 ± 0.33	8.11 ± 0.14	1.283 ± 0.006	0. 0. 0. 1.	FLD-G	⋯
WISE 0607+4550	L2.5	9.63 ± 0.17	11.05 ± 0.16	6.98 ± 0.36	8.75 ± 0.14	1.257 ± 0.006	0. 0. 0. 1.	FLD-G	⋯
2MASS 2208+2921	L3	3.99 ± 0.76	4.34 ± 0.75	2.52 ± 1.44	2.47 ± 0.6	1.139 ± 0.024	2. 2. 2. 2.	VL-G	VL-G
G 196-3B	L3	5.4 ± 0.77	5.79 ± 0.73	4.21 ± 0.48	4.36 ± 0.19	1.157 ± 0.011	1. 2. 1. 2.	VL-G	VL-G
2MASS 1726+1538	L3	5.82 ± 0.81	6.77 ± 0.8	4.97 ± 1.45	4.57 ± 0.65	1.198 ± 0.026	1. 1. 1. 1.	INT-G	INT-G
2MASS 1146+2230	L3	9.24 ± 0.21	10.89 ± 0.21	6.55 ± 0.5	8.19 ± 0.2	1.296 ± 0.009	0. 1. 0. 0.	FLD-G	⋯
2MASS 1300+1912	L3	10.33 ± 0.1	13.08 ± 0.09	6.65 ± 0.17	9.07 ± 0.08	1.214 ± 0.002	0. 0. 0. 1.	FLD-G	⋯
2MASS 1506+1321	L3	10.55 ± 0.17	11.86 ± 0.12	7.15 ± 0.35	9.36 ± 0.15	1.256 ± 0.007	0. 0. 0. 1.	FLD-G	⋯
GD 165 B	L3	9.34 ± 0.34	11.13 ± 0.32	4.86 ± 0.67	8.3 ± 0.27	1.289 ± 0.016	0. 0. 0. 1.	FLD-G	⋯
WISE 0532+0418	L3	10.03 ± 1.62	13.33 ± 1.4	9.25 ± 3.31	10.9 ± 1.26	1.405 ± 0.075	0. 0. 0. 0.	FLD-G	⋯
2MASS 1302+5650	L3p	11.31 ± 0.72	12.04 ± 0.67	7.92 ± 1.71	9.94 ± 0.68	1.289 ± 0.033	0. 0. 0. 1.	FLD-G	⋯
2MASS 2224-0158	L3.5	11.02 ± 0.22	12.93 ± 0.19	7.19 ± 0.41	7.01 ± 0.18	1.175 ± 0.008	0. 0. 1. 1.	FLD-G	⋯
SDSS 1256-0224	sdL3.5	7.92 ± 0.34	12.3 ± 0.29	2.52 ± 0.78	5.06 ± 0.37	1.102 ± 0.01	1. 0. 1. 2.	INT-G	⋯
2MASS 0036+1821	L4	11.1 ± 0.24	13.76 ± 0.36	6.53 ± 0.45	10.23 ± 0.18	1.313 ± 0.015	0. 0. 0. 0.	FLD-G	⋯
2MASS 1155+2307	L4	4.74 ± 0.83	10.61 ± 0.67	6.4 ± 1.45	8.53 ± 0.57	1.304 ± 0.027	2. 1. 0. 0.	FLD-G	⋯
2MASS 2158-1550	L4	10.56 ± 0.87	11.37 ± 0.78	5.6 ± 1.77	8.71 ± 0.74	1.292 ± 0.034	0. 1. 0. 0.	FLD-G	⋯
SIPS 0921-2104	L4	11.13 ± 0.05	13.8 ± 0.05	7.2 ± 0.16	10.65 ± 0.07	1.231 ± 0.002	0. 0. 0. 1.	FLD-G	⋯
2MASS 1841+3117	L4p	9.24 ± 0.59	11.0 ± 0.51	5.48 ± 1.25	7.77 ± 0.49	1.245 ± 0.02	1. 1. 1. 1.	INT-G	⋯
WISE 0715-1145	L4p	11.34 ± 0.27	14.92 ± 0.23	6.89 ± 0.52	10.44 ± 0.22	1.234 ± 0.01	0. 0. 0. 1.	FLD-G	⋯
SDSS 0805+4812	L4+T5.5	12.38 ± 0.16	13.85 ± 0.15	5.92 ± 0.32	9.37 ± 0.12	1.285 ± 0.006	0. 0. 0. 0.	FLD-G	⋯
GL 417 BC	L4.5+L6	9.19 ± 0.25	10.1 ± 0.24	5.47 ± 0.51	7.57 ± 0.21	1.243 ± 0.009	1. 1. 1. 1.	INT-G	FLD-G
2MASS 0835+1953	L5	11.1 ± 0.36	12.21 ± 0.34	6.37 ± 0.77	8.62 ± 0.31	1.233 ± 0.014	0. 0. 0. 0.	FLD-G	⋯
G 259-20 B	L5	13.74 ± 0.35	16.67 ± 0.33	4.64 ± 0.86	11.11 ± 0.29	1.283 ± 0.014	0. 0. 0. 0.	FLD-G	⋯

Table 2
(Continued)

Name	SpT	K I EW (Å) 1.1692 μm	K I EW (Å) 1.1778 μm	K I EW (Å) 1.2437 μm	K I EW (Å) 1.2529 μm	FeH$_J$ 1.20 μm	Gravity Scores K1 K2 K4 FeH	Gravity Type This Paper	Gravity Type A13
SDSS 1446+0024	L5	10.53 ± 0.64	12.84 ± 0.58	4.98 ± 1.46	8.78 ± 0.58	1.212 ± 0.026	0. 0. 0. 0.	FLD-G	⋯
2MASS 1721+3344	L5p	11.64 ± 0.54	15.13 ± 0.49	5.8 ± 1.28	10.18 ± 0.49	1.242 ± 0.021	0. 0. 0. 0.	FLD-G	⋯
2MASS 1821+1414	L5p	9.22 ± 0.15	11.26 ± 0.14	5.32 ± 0.33	7.79 ± 0.13	1.229 ± 0.005	1. 1. 0. 0.	FLD-G	⋯
2MASS 2351+3010	L5p	11.15 ± 1.29	12.39 ± 1.13	6.27 ± 2.39	7.55 ± 1.02	1.18 ± 0.04	0. 0. 0. 1.	FLD-G	⋯
GJ 1001 B	L5+L5	11.49 ± 0.2	12.62 ± 0.19	5.75 ± 0.44	9.18 ± 0.17	1.254 ± 0.008	0. 0. 0. 0.	FLD-G	⋯
2MASS 1728+3948	L5+L6.5	9.85 ± 0.47	11.59 ± 0.44	4.62 ± 0.83	7.35 ± 0.34	1.102 ± 0.014	0. 1. 1. 2.	INT-G	⋯
DENIS 0205-1159	L5+L8	8.06 ± 1.12	10.9 ± 0.5	3.48 ± 0.98	6.41 ± 0.33	1.122 ± 0.023	1. 1. 1. 2.	INT-G	⋯
2MASS 1315-2649	L5+T7	7.92 ± 0.51	10.86 ± 0.44	5.01 ± 0.99	7.61 ± 0.4	1.171 ± 0.015	1. 1. 0. 1.	INT-G	⋯
2MASS 1553+2109	L5.5	9.3 ± 1.55	9.19 ± 1.5	3.81 ± 2.84	6.18 ± 1.02	1.13 ± 0.042	1. 1. 1. 1.	INT-G	⋯
2MASS 1507-1627	L5.5	11.2 ± 0.03	13.9 ± 0.04	5.64 ± 0.12	8.56 ± 0.04	1.252 ± 0.001	0. 0. 0. 0.	FLD-G	⋯
2MASS 2244+2043	L6	4.12 ± 1.69	5.25 ± 1.56	1.12 ± 2.29	3.06 ± 0.96	1.009 ± 0.032	2. 2. 2. 2.	VL-G	VL-G
2MASS 0740+2009	L6	7.36 ± 0.71	10.56 ± 0.62	3.82 ± 1.27	6.25 ± 0.54	1.079 ± 0.018	1. 0. 1. 2.	INT-G	⋯
2MASS 1010-0406	L6	10.12 ± 0.48	11.75 ± 0.45	5.65 ± 0.95	8.47 ± 0.39	1.174 ± 0.016	0. 0. 0. 0.	FLD-G	⋯
2MASS 2152+0937	L6+L6	6.86 ± 1.24	9.29 ± 1.03	5.48 ± 1.98	6.17 ± 0.84	1.085 ± 0.03	1. 1. 1. 2.	INT-G	⋯
Denis 1228-1547	L6+L6	10.18 ± 0.38	11.93 ± 0.25	5.46 ± 0.33	7.91 ± 0.15	1.229 ± 0.009	0. 0. 0. 0.	FLD-G	⋯
2MASS 0850+1057	L6+L7	6.61 ± 0.49	8.76 ± 0.44	3.99 ± 0.85	5.85 ± 0.36	1.1 ± 0.013	1. 1. 1. 1.	INT-G	⋯
2MASS 2252-1730	L6+T2	11.5 ± 0.48	13.07 ± 0.43	3.96 ± 0.95	8.56 ± 0.36	1.162 ± 0.015	0. 0. 0. 0.	FLD-G	⋯
SDSS 0423-0414	L6+T2	8.16 ± 0.35	10.42 ± 0.31	3.57 ± 0.64	6.79 ± 0.23	1.074 ± 0.008	1. 1. 0. 2.	INT-G	⋯
2MASS 0300+2130	L6p	10.14 ± 0.72	12.86 ± 0.65	6.54 ± 1.58	8.85 ± 0.61	1.219 ± 0.028	0. 0. 0. 0.	FLD-G	⋯
2MASS 1118-0856	L6p	10.53 ± 0.53	13.34 ± 0.49	6.67 ± 1.02	8.86 ± 0.45	1.224 ± 0.02	0. 0. 0. 0.	FLD-G	⋯
2MASS 2148+4003	L6.5p	7.45 ± 0.33	10.33 ± 0.28	4.53 ± 0.59	5.14 ± 0.26	1.149 ± 0.01	1. 1. 1. 0.	INT-G	⋯
2MASS 0103+1935	L7	6.46 ± 0.54	6.45 ± 0.48	3.49 ± 0.89	5.8 ± 0.37	1.094 ± 0.013	1. 1. 0. n	INT-G	INT-G
2MASS 1526+2043	L7	9.13 ± 0.36	10.71 ± 0.34	4.2 ± 0.73	7.54 ± 0.31	1.153 ± 0.012	0. 0. 0. n	FLD-G	⋯
2MASS 2151+3402	L7p	2.23 ± 1.56	4.35 ± 1.47	3.75 ± 2.49	7.31 ± 1.05	1.159 ± 0.041	2. 2. 0. n	VL-G	⋯
2MASS 0532+8246	sdL7	12.58 ± 0.35	16.41 ± 0.18	0.77 ± 0.52	6.81 ± 0.15	1.239 ± 0.028	0. 0. 0. n	FLD-G	⋯
SDSS 0931+0327	L7.5	11.83 ± 0.38	14.56 ± 0.33	6.41 ± 0.81	11.02 ± 0.31	1.238 ± 0.014	0. 0. 0. n	FLD-G	⋯
SDSS 1121+4332	L7.5	15.39 ± 0.47	18.0 ± 0.48	6.89 ± 1.13	10.72 ± 0.46	1.271 ± 0.021	0. 0. 0. n	FLD-G	⋯
2MASS 0015+2959	L7.5p	9.41 ± 1.81	12.29 ± 1.6	5.59 ± 3.64	9.49 ± 1.49	1.158 ± 0.058	0. 0. 0. n	FLD-G	⋯
2MASS 1632+1904	L8	5.42 ± 0.68	7.24 ± 0.57	2.62 ± 1.09	3.69 ± 0.5	1.04 ± 0.015	N/A	N/A	⋯
SDSS 1331-0116	L8	12.82 ± 0.2	14.44 ± 0.19	5.73 ± 0.43	9.57 ± 0.16	1.184 ± 0.007	N/A	N/A	⋯
GL 337 CD	L8+T0	7.4 ± 0.94	8.69 ± 0.82	2.52 ± 1.75	5.32 ± 0.63	1.049 ± 0.021	N/A	N/A	⋯
2MASS 0255-4700	L9	6.44 ± 0.19	8.96 ± 0.18	2.63 ± 0.38	5.38 ± 0.15	1.039 ± 0.005	N/A	N/A	⋯
2MASS 0310+1648	L9+L9	6.51 ± 0.69	9.24 ± 0.6	3.14 ± 1.12	5.64 ± 0.48	1.017 ± 0.014	N/A	N/A	⋯
2MASS 1405+8350	L9	7.85 ± 0.33	9.71 ± 0.31	4.15 ± 0.58	7.14 ± 0.25	1.036 ± 0.007	N/A	N/A	⋯
WISE 0826-1640	L9	7.95 ± 0.31	9.35 ± 0.26	3.99 ± 0.53	5.29 ± 0.23	1.035 ± 0.007	N/A	N/A	⋯
WISE 0206+2640	L9p	6.31 ± 0.61	7.58 ± 0.52	2.76 ± 0.92	4.33 ± 0.4	1.015 ± 0.013	N/A	N/A	⋯
WISE 1647+5632	L9p	6.14 ± 1.53	4.97 ± 1.52	4.44 ± 2.38	6.73 ± 1.04	1.029 ± 0.037	N/A	N/A	⋯
2MASS 0328+2302	L9.5	8.79 ± 1.76	11.25 ± 1.65	2.82 ± 3.16	4.78 ± 1.27	1.001 ± 0.038	N/A	N/A	⋯
2MASS 1207+0244	T0	6.9 ± 0.34	8.77 ± 0.28	2.83 ± 0.52	6.11 ± 0.2	1.076 ± 0.008	N/A	N/A	⋯
SDSS 1520+3546	T0	8.24 ± 0.26	10.29 ± 0.26	3.97 ± 0.53	6.85 ± 0.22	1.047 ± 0.007	N/A	N/A	⋯
SDSS 1516+3053	T0.5	6.45 ± 1.35	4.13 ± 1.27	2.81 ± 1.51	5.19 ± 0.59	0.989 ± 0.022	N/A	N/A	⋯
SDSS 0151+1244	T1	8.68 ± 1.12	11.26 ± 0.95	2.1 ± 1.85	6.53 ± 0.76	1.034 ± 0.025	N/A	N/A	⋯
SDSS 0837-0000	T1	8.05 ± 1.16	12.14 ± 0.93	4.31 ± 1.62	8.64 ± 0.63	1.023 ± 0.022	N/A	N/A	⋯
SDSS 1021-0304	T1+T5	10.81 ± 1.48	7.59 ± 1.4	4.43 ± 1.71	9.02 ± 0.63	1.006 ± 0.027	N/A	N/A	⋯
SDSS 0909+6525	T1.5	9.26 ± 0.5	11.26 ± 0.4	2.92 ± 0.74	5.83 ± 0.3	1.031 ± 0.011	N/A	N/A	⋯
SDSS 1254-0122	T2	10.61 ± 3.38	11.57 ± 1.54	3.64 ± 0.33	8.54 ± 0.11	1.011 ± 0.023	N/A	N/A	⋯

Table 2
(Continued)

Name	SpT	K I EW (Å) 1.1692 μm	K I EW (Å) 1.1778 μm	K I EW (Å) 1.2437 μm	K I EW (Å) 1.2529 μm	FeH_J 1.20 μm	Gravity Scores K1 K2 K4 FeH	Gravity Type This Paper	Gravity Type A13
2MASS 1209-1004	T2+T7.5	10.51 ± 1.71	14.55 ± 1.25	4.53 ± 1.93	7.96 ± 0.72	0.993 ± 0.031	N/A	N/A	···
2MASS 1106+2754	T2.5	11.1 ± 0.86	13.39 ± 0.52	3.81 ± 0.56	7.88 ± 0.23	1.058 ± 0.013	N/A	N/A	···
SIMP 0136+0933	T2.5	12.04 ± 0.11	14.05 ± 0.09	4.68 ± 0.16	9.43 ± 0.06	1.053 ± 0.002	N/A	N/A	···
SDSS 1750+1759	T3.5	11.67 ± 1.2	13.63 ± 1.04	3.54 ± 1.47	8.35 ± 0.59	1.052 ± 0.024	N/A	N/A	···
2MASS 2254+3123	T4	11.18 ± 4.5	13.26 ± 3.21	2.4 ± 2.99	9.15 ± 0.93	1.077 ± 0.05	N/A	N/A	···
2MASS 0559-1404	T4.5	14.45 ± 0.36	15.82 ± 0.26	3.06 ± 0.26	9.72 ± 0.09	1.07 ± 0.006	N/A	N/A	···
SDSS 0926+5847	T4.5	14.42 ± 1.36	14.62 ± 1.17	3.47 ± 1.55	9.02 ± 0.52	1.038 ± 0.027	N/A	N/A	···
2MASS 0755+2212	T5	16.22 ± 0.28	15.06 ± 0.17	0.52 ± 0.26	8.01 ± 0.07	1.056 ± 0.003	N/A	N/A	···
2MASS 1503+2525	T5	14.51 ± 0.47	15.01 ± 0.38	1.18 ± 0.44	7.05 ± 0.15	1.053 ± 0.008	N/A	N/A	···
WISE 1337+2636	T5	20.43 ± 1.8	14.85 ± 1.61	1.35 ± 1.63	7.39 ± 0.57	1.104 ± 0.036	N/A	N/A	···
2MASS 2356-1553	T5.5	12.23 ± 4.92	14.99 ± 5.1	2.93 ± 7.08	10.18 ± 2.1	1.091 ± 0.137	N/A	N/A	···
WISE 1954+6915	T5.5	13.87 ± 3.79	10.86 ± 2.78	1.11 ± 2.31	3.45 ± 0.92	0.992 ± 0.051	N/A	N/A	···
SDSS 1624+0029	T6	N/A	N/A	−2.25 ± 0.88	5.88 ± 0.28	1.031 ± 0.014	N/A	N/A	···
WISE 0038+8405	T6	N/A	N/A	0.17 ± 1.6	6.41 ± 0.59	1.095 ± 0.038	N/A	N/A	···
WISE 1840+2932	T6	N/A	N/A	−2.45 ± 5.77	1.71 ± 2.0	1.029 ± 0.105	N/A	N/A	···
WISE 2237+7225	T6	N/A	N/A	2.38 ± 1.85	8.63 ± 0.61	1.007 ± 0.037	N/A	N/A	···
2MASS 0937+2931	T6p	N/A	N/A	−0.98 ± 1.2	2.05 ± 0.46	0.995 ± 0.053	N/A	N/A	···
2MASS 1225-2739	T6+T8	N/A	N/A	1.07 ± 0.31	8.92 ± 0.11	1.027 ± 0.006	N/A	N/A	···
WISE 1250+2628	T6.5	N/A	N/A	0.23 ± 1.23	10.29 ± 0.37	1.049 ± 0.028	N/A	N/A	···
2MASS 0727+1710	T7	N/A	N/A	−0.92 ± 1.02	6.15 ± 0.34	0.999 ± 0.024	N/A	N/A	···
WISE 1139-3324	T7	N/A	N/A	−0.5 ± 4.74	2.84 ± 1.77	0.987 ± 0.119	N/A	N/A	···
WISE 1759+5442	T7	N/A	N/A	−0.87 ± 3.83	2.38 ± 1.42	1.042 ± 0.092	N/A	N/A	···
WISE 2335+4222	T7	N/A	N/A	1.49 ± 4.36	8.21 ± 1.44	1.013 ± 0.116	N/A	N/A	···
2MASS 1553+1532	T7+T7	N/A	N/A	0.05 ± 0.68	6.41 ± 0.23	0.949 ± 0.014	N/A	N/A	···
GL 570 D	T7.5	N/A	N/A	0.02 ± 0.61	3.99 ± 0.25	1.019 ± 0.07	N/A	N/A	···
WISE 0424+0727	T7.5	N/A	N/A	−0.81 ± 2.7	1.86 ± 0.94	1.027 ± 0.073	N/A	N/A	···
WISE 2147-1029	T7.5	N/A	N/A	0.72 ± 2.33	4.8 ± 0.84	0.943 ± 0.063	N/A	N/A	···
2MASS 0415-0935	T8	N/A	N/A	N/A	N/A	0.991 ± 0.01	N/A	N/A	···
WISE 0316+4307	T8	N/A	N/A	N/A	N/A	1.188 ± 0.743	N/A	N/A	···
WISE 0430+4633	T8	N/A	N/A	N/A	N/A	0.821 ± 0.061	N/A	N/A	···
WISE 1050+5056	T8	N/A	N/A	N/A	N/A	0.86 ± 0.067	N/A	N/A	···
WISE 1448-2534	T8	N/A	N/A	N/A	N/A	0.993 ± 0.148	N/A	N/A	···
WISE 1736+6059	T8	N/A	N/A	N/A	N/A	1.055 ± 0.105	N/A	N/A	···
WISE 1813+2835	T8	N/A	N/A	N/A	N/A	0.97 ± 0.046	N/A	N/A	···
WISE 1955-2540	T8	N/A	N/A	N/A	N/A	0.967 ± 0.115	N/A	N/A	···
WISE 2005+5424	sdT8	N/A	N/A	N/A	N/A	0.892 ± 0.04	N/A	N/A	···
WISE 0512-3004	T8.5	N/A	N/A	N/A	N/A	1.404 ± 0.339	N/A	N/A	···
WISE 0540+4832	T8.5	N/A	N/A	N/A	N/A	1.02 ± 0.058	N/A	N/A	···
WISE 0005+3737	T9	N/A	N/A	N/A	N/A	0.896 ± 0.221	N/A	N/A	···
WISE 0038+2758	T9	N/A	N/A	N/A	N/A	1.152 ± 0.248	N/A	N/A	···
WISE 0335+4310	T9	N/A	N/A	N/A	N/A	0.659 ± 0.083	N/A	N/A	···

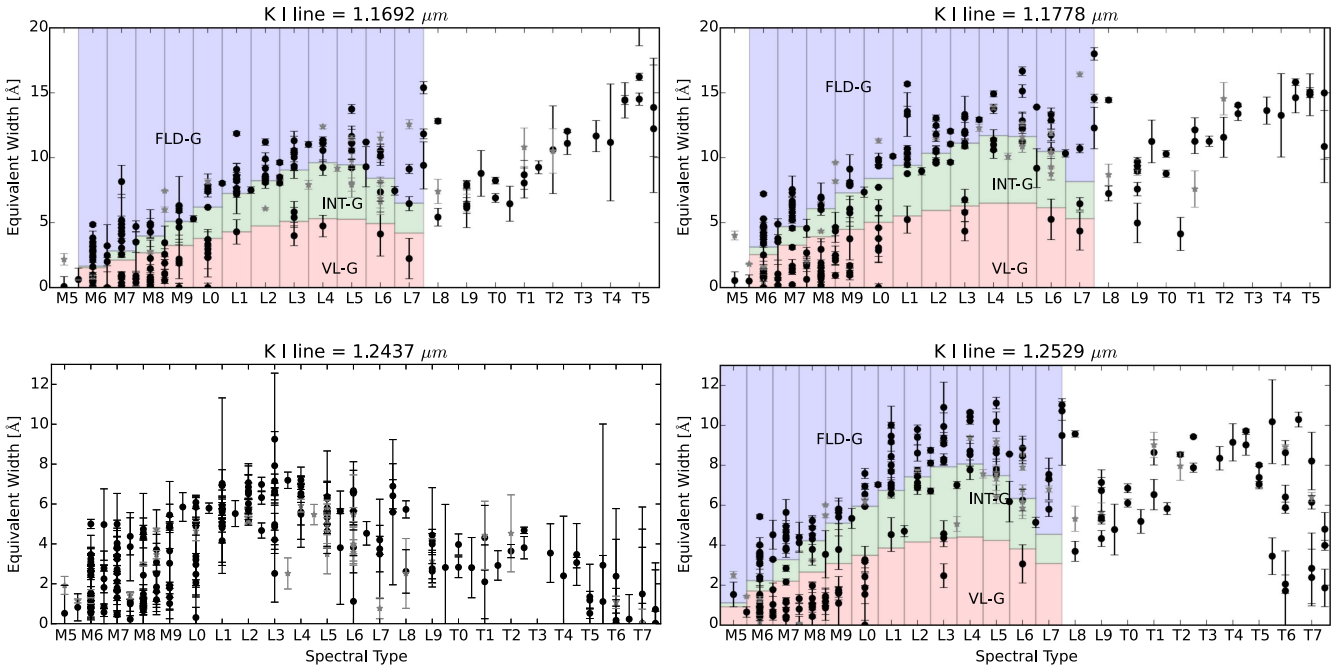

Figure 3. K I pseudo-equivalent width vs. spectral type for all M, L, and T dwarfs in the BDSS for which EWs can be measured. Field dwarfs are shown in black and binaries and subdwarfs are shown as gray stars. Uncertainties are calculated using a Monte Carlo technique with 1000 iterations of modulating the flux by the S/N and re-calculating the EW. The K I lines at 1.1692 μm and 1.1778 μm disappear from T dwarf spectra later than ∼T5 and the K I lines at 1.2437 μm and 1.2529 μm are not found in T dwarfs later than spectral type ∼T7. Shaded regions denote differing gravity types as defined by A13. Objects lying within the salmon shaded regions receive a score of "2" (indicating low gravity), objects in the green shaded regions receive a score of "1" (intermediate gravity), and objects within the blue shaded regions receive a score of "0" ("field" or high gravity). These scores are used along with the FeH$_J$ score to compute a median gravity type. VL-G and INT-G designations are not distinguishable for M5 dwarfs for the K I lines at 1.1692 and 1.1778 μm, and gravity types are not designated for dwarfs of spectral type L8 and later. FeH contamination of the 1.2437 μm line results in larger measurement uncertainties as well as a less-distinguishable low-gravity sequence. For this reason, A13 did not determine cutoff values for gravity types for this line.

completeness, we compute and report EWs for this line. Indeed, we find that the 1.2437 μm line exhibits more scatter and weaker correlation with surface gravity at this resolving power, and thus we also exclude it from our analysis.

Following a similar method as in A13, we estimate a continuum value using a linear regression fit to the flux in the continuum windows. The EW calculations are performed using a Monte Carlo technique of 1000 iterations to estimate our uncertainties. Unlike A13, we do not use the rms scatter about the continuum fit to estimate the flux uncertainty. Instead, for each iteration of the Monte Carlo calculation, we modulate the flux in each pixel by adding a noise factor calculated by multiplying a random number drawn from a Gaussian distribution ($\mu = 0$, $\sigma = 1$), multiplied by the estimated noise determined by the S/N of that pixel. The EW for each flux modulation is recorded, and we then compute the median and standard deviation of the EWs as the best estimate and 1σ uncertainties. This method is similar to that described in Aller et al. (2016), who found that the method in A13 tended to underestimate flux errors in modest S/N spectra (S/N $\lesssim$ 200).

We tested this technique using a range of number of iterations in our Monte Carlo calculations. We found that $\gtrsim$500 iterations were required to achieve stable results and that there is no significant difference between 10^3 and 10^6 iterations. In the interest of computational time, we opted for 10^3 iterations.

Table 2 lists our values for EW and uncertainties for the four K I lines in the J band for all objects in the BDSS. The first K I doublet at 1.17 μm disappears from the J-band spectra of dwarfs of spectral types ∼T5 and later. The K I doublet at 1.25 μm persists through ∼T7 (see spectral plots in Appendix). For this reason, objects later than T5 will have no K I EW measurements at 1.17 μm and objects later than T7 will have no K I EW measurements at 1.25 μm.

In Figure 3, we show results for the four K I EWs versus spectral type for all of the M, L, and T dwarfs in the sample. The spectral types are taken from the literature (see Table 1) and are measured in the NIR if available. Shaded regions in Figure 3 show the boundaries proposed by A13 to designate low, intermediate, and high surface gravity objects for objects of spectral type M6–L7.

It should be noted that for some objects with apparently very low K I absorption, the calculated EW can be less than zero. Visual inspection of these spectra shows that they do have very small or nonexistent K I lines. In these cases, we have plotted these targets with EW values of zero, but the values listed in Table 2 are as measured. We believe this effect is because the EW calculation windows were chosen for objects with much deeper absorption lines. Objects with very weak K I lines and a slightly higher continuum within the line-calculating region than the continuum region can thus have a negative EW. The negative EW does not affect the gravity classification of VL-G for these objects, and so we chose to stay consistent with the A13 line and continuum boundaries when computing EWs.

3.2. FeH$_J$ Index

In addition to the K I EW measurements, we studied the FeH$_J$ index from A13. This index measures the 1.2 μm FeH absorption feature for medium-resolution ($R \sim$ 750–2000) data

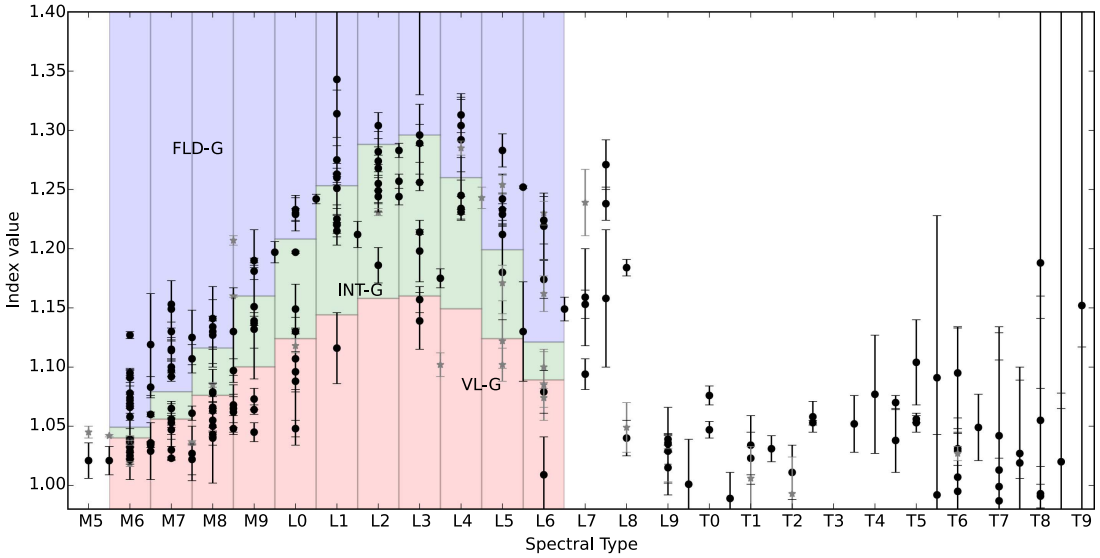

Figure 4. FeH$_J$ index vs. spectral type for all M, L, and T dwarfs in the BDSS. Normal dwarfs are shown in black and binaries and subdwarfs are shown as gray stars. Shading is the same as in Figure 3. This index measures the FeH absorption feature at 1.2 μm using the continuum and absorption bands shown in Figure 2. FeH is found in late-type M dwarfs and most L dwarfs. Spectral types later than ~L8 have atmospheres cool enough to condense this molecule. Index values of ~1.0 indicate the absorption feature is nearly absent in the spectra of L/T transition objects. This index re-emerges slightly in the mid-type T dwarfs.

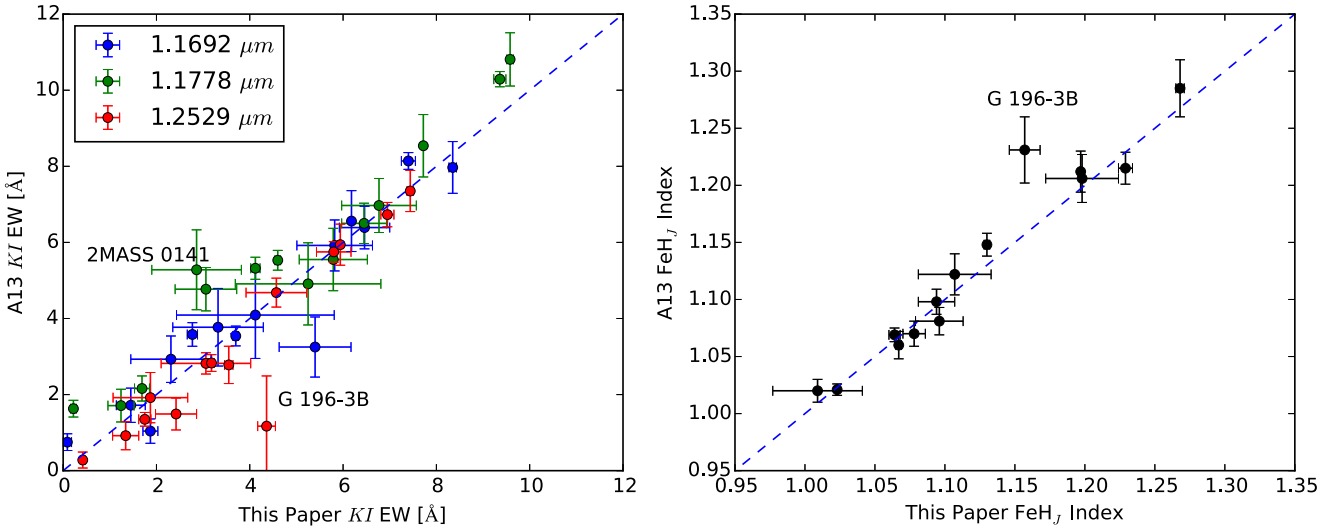

Figure 5. Left: comparison of K I EW values between A13 and this paper. Colors indicate the particular line at which the EWs were calculated. The one-to-one line is shown to aid comparison. Right: comparison of FeH$_J$ index values from A13 and this paper. Despite differing instruments and resolving powers, our values are consistent within the uncertainties.

for objects of spectral type M6–L6. Figure 2 shows the window used for computing the index in light gray and the windows used for estimating the continuum in dark gray. FeH absorption is found in late-type M dwarfs, most L dwarfs, and is seen weakly in some T dwarfs. FeH absorption depth is known to correlate with surface gravity (McGovern et al. 2004). Objects near the L/T transition do not show signs of FeH because the atmospheric conditions (i.e., cooler temperatures) have caused this molecule to precipitate (see, e.g., Marley & Robinson 2014). Spectral types later than ~T1 show a slight re-emergence of the molecule (Burgasser et al. 2002b), perhaps due to cloud clearing, allowing flux to emerge from deeper layers within the brown dwarf where some FeH remains in gaseous form (see also Tremblin et al. 2016 for an alternate interpretation).

We present our FeH$_J$ index values for all objects in the BDSS in Figure 4. An index value of ~1 is expected for the L/T transition dwarfs, indicating little to no absorption present in this spectral region. FeH$_J$ values for all BDSS targets are listed in Table 2.

3.3. Gravity Scores

A13 determined gravity score cutoff values for each K I EW for spectral types M5–L7 and for the FeH$_J$ index for spectral types M6–L6 using a sample of known young and field objects. They assigned final gravity types using a median value of scores from multiple spectral indices across the 0.9–2.5 μm range at both low and moderate resolutions. A13 gravity types for moderate-resolution spectra are calculated

Table 3
BDSS Objects with Known Ages

Designation	Short Name	R.A.	decl.	SpT	Age (Myr)	Gravity Type	Notes	% Membership	Membership Ref.
2MASS J22443167+2043433	2MASS 2244+2043	22 44 31.674	+20 43 43.30	L6	149^{+51}_{-19}	VL-G	AB Dor	99.6	7
2MASS J03230483+4816111	AP 310	03 23 04.83	+48 16 11.2	M6	90 ± 10	FLD-G	Alpha Persei	100	25
Cl* Melotte 20 AP 316	AP 316	03 27 01.3	+49 14 40	M6	90 ± 10	FLD-G	Alpha Persei	100	25
2MASS J03180906+4925189	AP 301	03 18 09.06	+49 25 19.0	M6.5	90 ± 10	FLD-G	Alpha Persei	100	25
2MASS J03204346+5059396	AP 270	03 20 43.47	+50 59 39.6	M7	90 ± 10	VL-G	Alpha Persei	54	12
2MASS J03354735+4917430	AP 325	03 35 47.36	+49 17 43.1	M7	90 ± 10	INT-G	Alpha Persei	62	12
Cl* Melotte 20 AP 326	AP 326	03 38 55.2	+48 57 31	M7.5	90 ± 10	FLD-G	Alpha Persei	100	25
2MASS J03194133+5030451	AP 306	03 19 41.334	+50 30 45.15	M8	90 ± 10	FLD-G	Alpha Persei	100	25
2MASSI J0443376+000205	2MASS 0443+0002	04 43 37.610	+00 02 05.18	L0	24 ± 3	VL-G	Beta Pic	99.8	7
-	…	…	…	…	<500	…	Lithium	…	34
2MASS J03393521-3525440	LP 944-20	03 39 35.220	−35 25 44.09	L0	400 ± 40	FLD-G	Castor	99.7	7,24
-	…	…	…	…	<500	…	Lithium	…	34
2MASS J06085283-2753583	2MASS 0608-2753	06 08 52.836	−27 53 58.35	L0	30 ± 20	VL-G	β Pic/Columba/ Cha-Near	Ambiguous	7, 35
GJ 577 BC	Gl 577 BC	15 05 50.07	+64 02 49.0	M5.5+M5.5	70^{+30}_{-40}	N/A	Companion	…	13
2MASS J22344161+4041387	2MASS 2234+4041	22 34 41.62	+40 41 38.8	M6	$1^{+1}_{-.5}$	VL-G	Companion	…	1
-	…	…	…	…	-	…	LkHα 233	…	1
BD+16 2708B	Gl 569 BC	14 54 29.36	+16 06 08.9	M8.5+M9	112.5 ± 12.5	FLD-G	Companion	-	30
2MASS J11122567+3548131	Gl 417 BC	11 12 25.674	+35 48 13.17	L4.5+L6	750^{+140}_{-120}	FLD-G	Gyrochronology	-	31
-	…	…	…	…	80-300	…	Companion	…	32
2MASS J03473900+2436226	Roque 16	03 47 39.01	+24 36 22.7	M6	125 ± 8	FLD-G	Pleiades	100	27
2MASS J03520670+2416008	Teide 2	03 52 06.71	+24 16 00.9	M6	125 ± 8	FLD-G	Pleiades	68	11
2MASS J03454126+2354099	PPL 1	03 45 41.265	+23 54 09.95	M6.5	125 ± 8	FLD-G	Pleiades	69	11
2MASS J03551257+2317378	CFHT PL 15	03 55 12.571	+23 17 37.82	M7	125 ± 8	FLD-G	Pleiades	100	3
2MASS J03464298+2424506	Roque 14	03 46 42.99	+24 24 50.6	M7	125 ± 8	FLD-G	Pleiades	100	26
2MASS J03455065+2409037	Roque 13	03 45 50.65	+24 09 03.8	M7.5	125 ± 8	FLD-G	Pleiades	65	11
2MASS J03471208+2428320	Roque 11	03 47 12.08	+24 28 32.0	M8	125 ± 8	FLD-G	Pleiades	100	26
2MASS J03471792+2422317	Teide 1	03 47 17.925	+24 22 31.71	M8	125 ± 8	VL-G	Pleiades	68	11
2MASS J03434028+2430113	Roque 7	03 43 40.289	+24 30 11.40	M8.5	125 ± 8	INT-G	Pleiades	100	3
2MASS J03435353+2431115	Roque 4	03 43 53.53	+24 31 11.5	M9	125 ± 8	INT-G	Pleiades	100	27
2MASS J16262152-2426009	Rho Oph GY 5	16 26 21.528	−24 26 00.96	M5.5	$0.3^{+2,7}_{-.2}$	N/A	Rho Oph	100	8
2MASS J16262780-2426418	Rho Oph GY 37	16 26 27.810	−24 26 41.82	M6	$0.3^{+2,7}_{-.2}$	VL-G	Rho Oph	100	8
2MASS J16262226-2424070	Rho Oph GY 11	16 26 22.269	−24 24 07.06	M6.5	$0.3^{+2,7}_{-.2}$	VL-G	Rho Oph	100	8
2MASS J16261882-2426105	*ISO*-Oph 23	16 26 18.821	−24 26 10.52	M7.5	$0.3^{+2,7}_{-.2}$	VL-G	Rho Oph	100	8
2MASS J16262189-2444397	Rho Oph GY 3	16 26 21.899	−24 44 39.76	M8	$0.3^{+2,7}_{-.2}$	VL-G	Rho Oph	100	8
2MASS J16265128-2432419	Rho Oph GY 141	16 26 51.284	−24 32 41.99	M8.5	$0.3^{+2,7}_{-.2}$	VL-G	Rho Oph	100	8
2MASS J16273863-2438391	Rho Oph GY 310	16 27 38.631	−24 38 39.19	M8.5	$0.3^{+2,7}_{-.2}$	VL-G	Rho Oph	100	22
2MASS J05375745-0238444	S Ori 12	05 37 57.457	−02 38 44.44	M6	3 ± 1	VL-G	Sigma Orionis	75	2
2MASS J05390449-0238353	S Ori 17	05 39 04.491	−02 38 35.37	M6	3 ± 1	VL-G	Sigma Orionis	75	2

Table 3
(Continued)

Designation	Short Name	R.A.	decl.	SpT	Age (Myr)	Gravity Type	Notes	% Membership	Membership Ref.
2MASS J05382088-0246132	S Ori 31	05 38 20.882	−02 46 13.27	M7	3 ± 1	VL-G	Sigma Orionis	75	2
2MASS J05373648-0241567	S Ori 40	05 37 36.485	−02 41 56.73	M7	3 ± 1	VL-G	Sigma Orionis	75	2
UGCS J053903.20-023019.9	S Ori 51	05 39 03.21	−02 30 19.9	L0	3 ± 1	VL-G	Sigma Orionis	75	2
2MASS J12073346-3932539	2MASS 1207-3932	12 07 33.467	−39 32 54.00	M8	10 ± 3	VL-G	TWA	100	18
2MASS J11395113-3159214	2MASS 1139-3159	11 39 51.140	−31 59 21.50	M9	10 ± 3	VL-G	TWA	100	18
WDS J04325+1732Ba	GG Tau Ba	04 32 30.25	+17 31 30.9	M6	1.5 ± .5	VL-G	Taurus	100	28
2MASS J04262939+2624137	KPNO Tau 3	04 26 29.392	+26 24 13.79	M6	1.5 ± .5	VL-G	Taurus	100	16
2MASS J04312405+1800215	MHO Tau 4	04 31 24.057	+18 00 21.53	M6	1.5 ± .5	VL-G	Taurus	100	5
2MASS J04321606+1812464	MHO Tau 5	04 32 16.067	+18 12 46.45	M6.5	1.5 ± .5	VL-G	Taurus	100	5
2MASS J04361038+2259560	CFHT BD Tau 2	04 36 10.387	+22 59 56.03	M7.5	1.5 ± .5	VL-G	Taurus	100	19
WDS J04325+1732Bb	GG Tau Bb	04 32 30.31	+17 31 29.9	M7.5	1.5 ± .5	VL-G	Taurus	100	28
2MASS J04363893+2258119	CFHT BD Tau 3	04 36 38.938	+22 58 11.90	M8	1.5 ± .5	VL-G	Taurus	100	19
2MASS J04305718+2556394	KPNO Tau 7	04 30 57.187	+25 56 39.48	M8	1.5 ± .5	VL-G	Taurus	100	4
2MASS J04151471+2800096	KPNO Tau 1	04 15 14.714	+28 00 09.61	M8.5	1.5 ± .5	VL-G	Taurus	100	4
2MASS J04300724+2608207	KPNO Tau 6	04 30 07.244	+26 08 20.79	M8.5	1.5 ± .5	VL-G	Taurus	100	4
2MASS J04355143+2249119	KPNO Tau 9	04 35 51.432	+22 49 11.95	M8.5	1.5 ± .5	VL-G	Taurus	100	4
2MASS J04190126+2802487	KPNO Tau 12	04 19 01.270	+28 02 48.70	M9	1.5 ± .5	VL-G	Taurus	100	15
2MASS J04272799+2612052	KPNO Tau 4	04 27 27.997	+26 12 05.27	L0	1.5 ± .5	VL-G	Taurus	100	16
2MASS J01415823-4633574	2MASS 0141-4633	01 41 58.233	−46 33 57.43	L0	45 ± 4	VL-G	Tucana Horlogium	99.5	33
2MASS J16051403-2406524	DENIS 1605-2406	16 05 14.033	−24 06 52.48	M6	11 ± 2	VL-G	U Sco	100	20
2MASS J16014955-2351082	U Sco CTIO 66AB	16 01 49.557	−23 51 08.20	M6+M6	11 ± 2	VL-G	U Sco	100	10
2MASS J16121185-2047267	SCH 1612-2047	16 12 11.860	−20 47 26.72	M6.5	11 ± 2	VL-G	U Sco	100	14
2MASS J16020429-2050425	U Sco CTIO 100	16 02 04.296	−20 50 42.57	M7	11 ± 2	VL-G	U Sco	100	14
2MASS J15591135-2338002	U Sco CTIO 128	15 59 11.359	−23 38 00.24	M7	11 ± 2	VL-G	U Sco	100	14
2MASS J15594366-2014396	U Sco CTIO 130	15 59 43.665	−20 14 39.61	M7.5	11 ± 2	VL-G	U Sco	100	14
2MASS J16191646-2347235	DENIS 1619-2347	16 19 16.463	−23 47 23.54	M8	11 ± 2	VL-G	U Sco	100	14
2MASS J16192988-2440469	DENIS 1619-2440	16 19 29.882	−24 40 46.97	M8	11 ± 2	VL-G	U Sco	100	14
2MASS J16224385-1951057	SCH 1622-1951	16 22 43.854	−19 51 05.77	M8	11 ± 2	VL-G	U Sco	100	14
2MASS J16235155-2317270	SCH 1623-2317	16 23 51.560	−23 17 27.03	M8	11 ± 2	VL-G	U Sco	100	14
2MASS J16110360-2426429	DENIS 1611-2426	16 11 03.609	−24 26 42.94	M9	11 ± 2	VL-G	U Sco	100	14
2MASS J16145258-2017133	DENIS 1614-2017	16 14 52.588	−20 17 13.32	M9	11 ± 2	VL-G	U Sco	100	14

References. Membership References: (1) Allers et al. (2009), (2) Béjar et al. (2011), (3) Bouvier et al. (1998), (4) Briceño et al. (2002), (5) Briceño et al. (1998), (6) Cruz et al. (2009), (7) Gagné et al. (2014), (8) Geers et al. (2011), (9) Kirkpatrick et al. (2010), (10) Kraus et al. (2005), (11) Lodieu et al. (2012a), (12) Lodieu et al. (2012b), (13) Lowrance et al. (2005), (14) Luhman & Mamajek (2012), (15) Luhman et al. (2003), (16) Luhman et al. (2006), (17) Luhman et al. (2008), (18) Mamajek (2005), (19) Martín et al. (2001), (20) Martín et al. (2004), (21) Muzerolle et al. (2003), (22) Mužić et al. (2012), (23) Pavlenko et al. (2006), (24) Ribas (2003), (25) Stauffer et al. (1999), (26) Stauffer et al. (2007), (27) Zapatero Osorio et al. (1997), (28) Cohen & Kuhi (1979), (29) Wilson et al. (2001), (30) Simon et al. (2006), (31) Allers et al. (2010), (32) Kirkpatrick et al. (2001), (33) Gagné et al. (2015c), (34) Reiners & Basri (2009), (35) Faherty et al. (2016).

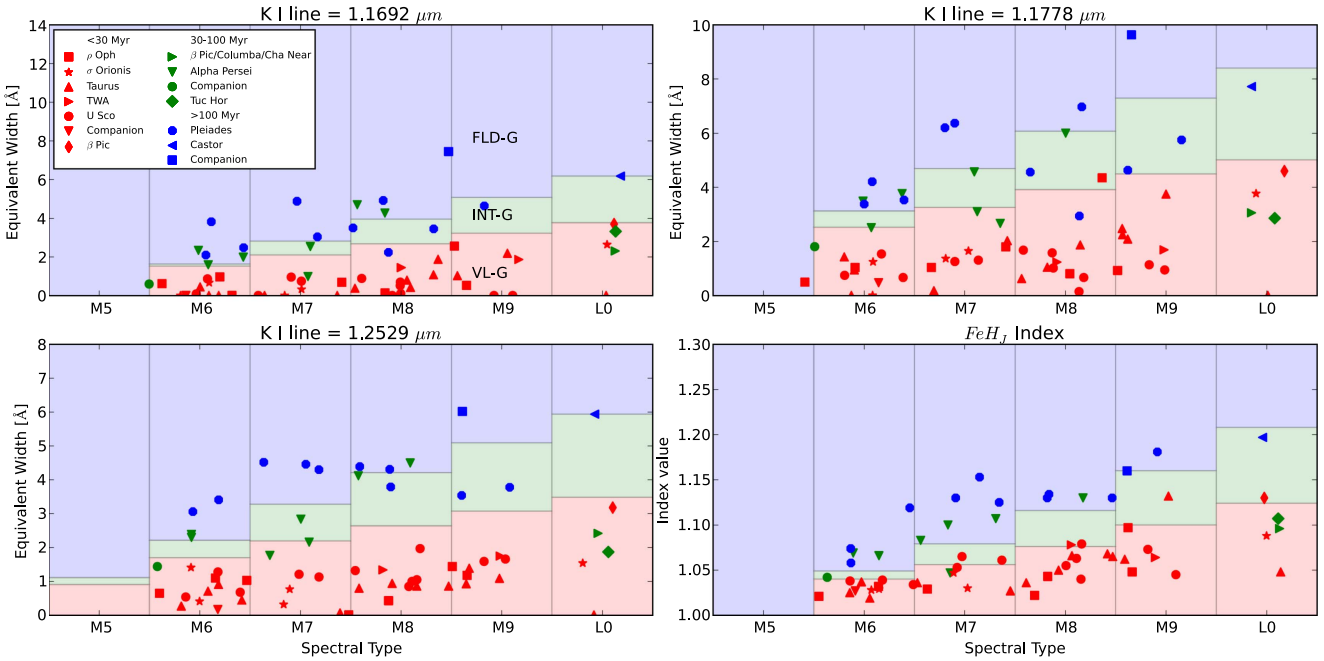

Figure 6. EW vs. SpT and FeH_J vs. SpT for dwarfs of spectral type M5.5-L0 with known ages. Different shaped symbols represent the methods used to estimate ages, i.e., group membership or an age estimate from a more massive stellar companion. For references, see Table 3. Symbols are colored by their known ages as follows: red symbols have ages <30 Myr, green symbols are ∼30–100 Myr, and blue symbols are >100 Myr. Binaries from Table 3 are not shown, nor is the only single object of spectral type later than L0 in our sample, 2MASS 2244+2043 (L6, VL-G, AB Dor). Spectral types have been distributed randomly in each spectral type bin for ease of viewing.

from four scores determined by the following indices: VO (z-band), H-band continuum, FeH (either z or J band), and the mean score of the Na I and K I EWs. As described above, we used similar methods and cutoff ranges to calculate our spectral indices and EWs. However, because we only had J-band spectra for most of our targets, we determined a gravity type using only the J-band medium-resolution indices from A13.

Gravity scores were computed for the K I EWs at 1.1692 μm, 1.1778 μm, and 1.2529 μm as well as for the FeH_J index. To determine gravity scores for our sample, we compared our computed EW and FeH_J values to the cutoffs tabulated in A13. If the index value was higher than the INT-G cutoff, then it received a score of "0," indicating field gravity. If the index value was between the INT-G and VL-G cutoffs, then it received a score of "1" and if the index value was smaller than the VL-G cutoff, then it received a value of "2," indicating low surface gravity. Similar to Aller et al. (2016), we opted not to use the "?" value, defined in A13, if the object receives a score that hints at intermediate gravity but has 1σ uncertainties that overlap with field gravity values. These objects received a score of "1." We computed the median score from these four indices to determine the final gravity designation for each target. Following the method from A13, median scores less than or equal to 0.5 are classified as "FLD-G," scores between 0.5 and 1.5 are classified as "INT-G," and scores greater than or equal to 1.5 receive "VL-G" classification. Table 2 lists gravity scores and the resultant gravity classification for objects of spectral type M5–L7. When available, the gravity score given by A13 is also listed.

Using multiple indices to characterize the surface gravity allows some objects to be seen as having borderline gravity classifications between VL-G and INT-G or INT-G and FLD-G. The combination of multiple indices is more robust against any particular index skewing the classification. Errors in an index might come from measurement errors or from physical effects causing the absorption in one index to be abnormal compared to the other indices calculated for a particular target. Sixty-two objects out of the 159 for which A13 gravity types were computed had more than one type of score. However, only seven targets received individual index scores spanning all three gravity types, and three of these objects are binaries or subdwarfs (see Section 3.5).

3.4. Radial Velocity (RV)

One consideration we made in our calculations was the effect of RV on the EW measurements, and therefore on the gravity estimations. One resolution element in the medium-resolution mode of NIRSPEC is equivalent to 150 km s^{-1}. Though rarely occurring, high RV targets could have their spectra shifted by a large enough amount that the calculation of a gravity estimate would be significantly altered. In order to understand the effect of RV on our EW and spectral index values, we examined 21 objects in our sample with known RVs from the literature, with RV magnitudes ranging from ∼5 to 195 km s^{-1}. First, we shifted their spectra to account for the known RV offset. Then, we recalculated their K I EWs and FeH_J indices and gravity types, and compared these values to our original calculations. Only two of our targets, the known L subdwarfs 2MASS 0532+8246 and SDSS 1256-0224, had RVs in excess of 100 km s^{-1} (Burgasser et al. 2003a, 2009, respectively). The other 19 targets had RVs $\lesssim$ 30 km s^{-1}.

None of our RV-shifted targets had differing gravity types from our original calculations. K I EW and FeH_J index values

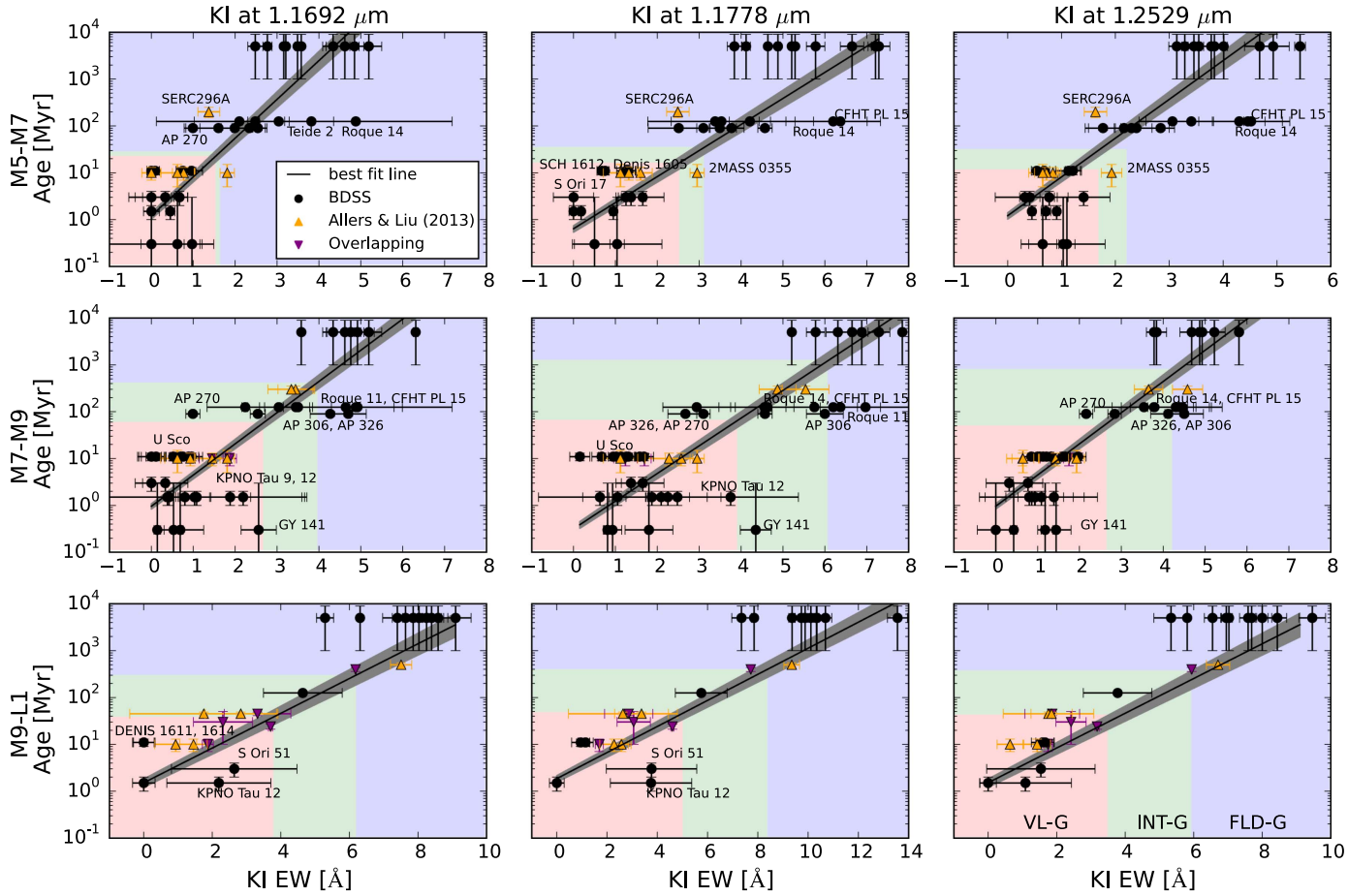

Figure 7. Age vs. K I EW at 1.1692, 1.1778, and 1.2529 μm, binned by spectral type. Blue, green, and red shaded regions are the same as in Figure 3. BDSS objects with known ages are shown as black circles, alongside a field sample selected from targets with "FLD-G" designations and given ages of 5 $\pm$ 4 Gyr to bound the upper limit of age as a function of EW. To increase our sample size, we include objects from A13 with moderate-resolution data and known ages (yellow upward-facing triangles). Objects with overlapping data between the A13 sample and our sample are marked by purple downward-facing triangles. Significant outliers are denoted in each panel as well. The black line represents the best-fit line as determined by a weighted orthogonal distance regression using the *scipy.odr* package in python. The gray shaded region represents the 1σ uncertainties in both slope and intercept.

differed by less than ~5% for all of the targets. Few dwarfs have measured RVs in excess of 200 km s^{-1} as the majority belong to the disk population and have similar space motions to the Sun. Because non-echelle NIRSPEC spectra can only resolve radial velocities greater than 150 km s^{-1} without cross-correlating to known RV targets, we estimate that this has a minimal impact on our measured gravity types.

We performed additional analysis to test the effect of RV on the EW measurements by performing a Monte Carlo simulation of 1000 iterations on high S/N spectra of both field-age and young targets, each time drawing a random RV from a normal distribution with σ_{RV} of 100 km s^{-1} and recalculating the EW. The resulting median and standard deviation of the distribution were entirely consistent with our original measurements. We therefore conclude that the RV of the target does not influence these calculations.

3.5. Excluded Objects

We present *J*-band spectra and measure the EWs and FeH absorption for all of the BDSS targets where relevant. However, two sub-populations of our sample were removed from the surface gravity analysis: known binaries and subdwarfs, whose spectral features are known to vary from the general field population for reasons other than their surface gravity.

3.5.1. Binaries

LP 213-67[13] (M8+L0; Close et al. 2003), 2MASS 0850 +1057 (L6+L7; Reid et al. 2001; Burgasser et al. 2011a), SDSS 0805+4812 (L4+T5; Burgasser 2007; Burgasser et al. 2016a), 2MASS 2140+1625 (M8.5+L2; Close et al. 2003), 2MASS 2152+0937 (L6+L6; Reid et al. 2006), and 2MASS 1315-2649 (L3.5+T7; Burgasser et al. 2011b) are known binaries in our sample. We caution against inferring a gravity type or age estimate for these objects, as their combined spectra could have an effect on the gravity-sensitive indices. For example, 2MASS 1315-2649 (L3.5+T7), which Burgasser et al. (2011b) finds to be at least 1 Gyr old given its kinematics, has an INT-G gravity type, which would imply an age of

[13] Post acceptance, we discovered that the object LP 213-67, also known as 2MASS J10471265+4026437, is in fact an M6.5 dwarf that is a possible binary (Dupuy & Liu 2017). The spectrum reported here is LP 213-67. LP 213-68, which is a common proper motion companion to LP 213-67, is an M8+L0 binary, although there is some confusion in the literature regarding these two objects.

Table 4
Best-fit Parameters for Age vs. K I Equivalent Width

SpT	A (Myr)	$3\sigma_A$	B ($Å^{-1}$)	$3\sigma_B$
K I at 1.1692 μm				
M6 ± 1	1.21397	0.18509	0.82751	0.03330
M7 ± 1	1.11259	0.13018	0.80449	0.02633
M8 ± 1	0.96102	0.12268	0.66583	0.02163
M9 ± 1	0.49177	0.08032	0.47582	0.01421
L0 ± 1	1.51591	0.29961	0.37076	0.01813
K I at 1.1778 μm				
M6 ± 1	0.64072	0.09984	0.55605	0.02238
M7 ± 1	0.49738	0.06485	0.58026	0.01879
M8 ± 1	0.31632	0.04927	0.59087	0.01819
M9 ± 1	0.23653	0.04466	0.42362	0.01261
L0 ± 1	1.85884	0.29051	0.27824	0.01156
K I at 1.2529 μm				
M6 ± 1	0.43282	0.07065	0.84337	0.03082
M7 ± 1	0.46584	0.06145	0.80843	0.02697
M8 ± 1	0.46064	0.06628	0.77101	0.02500
M9 ± 1	0.59026	0.07495	0.49215	0.01194
L0 ± 1	1.86551	0.29311	0.38854	0.01493

Note. The parameters in this table may be applied to determine an age estimate using the following equation: $\mathrm{Age[Myr]} = A \times 10^{B \times \mathrm{EW[Å]}}$.

$\lesssim$100 Myr. It is possible that this discrepancy in age estimate is caused by binarity.

3.5.2. Subdwarfs

Four targets in our sample are known subdwarfs: LHS 1135 (d/sd M5; Kirkpatrick et al. 2010), WISE 0435+2115 (sd L0; Kirkpatrick et al. 2014), SDSS 1256-0224 (sd L3.5; Burgasser et al. 2009), and 2MASS 0532+8246 (sd L7; Burgasser 2007). These objects tend to have large space motions, are typically found to be part of the Galactic halo population, and generally have sub-solar metallicity, although they exhibit stronger hydride features than similarly classified dwarfs. Because of their low metal content, we chose to exclude these objects from our analysis and do not determine gravity types for the subdwarfs in our sample. It should be noted that subdwarfs can exhibit small K I EWs due to their lower metal content. These smaller EWs can be misleading as it is thought that these objects are quite old and should not exhibit signs of low gravity. For example, the red K I doublet in the *J* band of SDSS 1256-0224 is weak enough to infer low gravity, although the strength of its FeH_J index implies high gravity and as a subdwarf it is likely older than ~5 Gyr.

4. Discussion

4.1. Comparison to Allers & Liu (2013)

In Figure 5, we plot our K I EW values (left) and FeH_J index values (right) versus those of A13, for the overlapping targets in our samples. We find that although the two data sets use different instruments with different resolving powers, our results are consistent within the uncertainties. The 1.1778 μm EW values appear to be slightly higher on average in A13 than in our own analysis, but our values are consistent within 2σ. The 1.2529 μm line appears to have the opposite result, with our values being slightly higher than those presented in A13. The major outlier is G 196-3B, which has a lower S/N spectrum in A13, as indicated by its larger error bar. A13's value is less than 2σ away from our result.

We find that the modified technique using only *J*-band indices with NIRSPEC $R \sim 2000$ spectra produces results consistent with the gravity classifications determined using spectral indices across the *z, J, H,* and *K* bands. Of the 20 matching targets between the two samples, all of the targets except one receive the same designation as found by A13, allowing for overlap in the borderline designations. For example, A13 finds that PC0025+0447 has intermediate gravity, while we classify it as borderline VL-G/INT-G. The exception is GL 417 BC (L4.5+L6), which we exclude because of its binary nature. When compared to the index value cutoffs for an L5 dwarf, we designate this object as FLD-G, as does A13.

4.2. Overall Trends

Before discussing the overall trends in our sample, we must clarify that all of the spectral types for our objects were compiled from the references listed in Table 1. Some objects were classified in the red-optical, while others were classified in the NIR, and objects can have a spectral type uncertainty as large as ±2 spectral types. Such discrepancies have been well documented in the literature and several methods have been presented in various papers for determining spectral types. For this reason, we can expect that the uncertainty in spectral type will cause larger uncertainty in the the overall trends.

As noted in Burgasser et al. (2002b) and McLean et al. (2003), potassium EWs in the *J* band tend to rise with increasing spectral type from M5 to ~L5 and at ~L5–L7 the EWs drop, rising again with increasing spectral type around L8. We see this same trend in the full sample (Figure 3), although it shows a large amount of scatter. Objects lying below the trend exhibited by the field dwarfs are primarily those exhibiting signs of youth (VL-G and INT-G). However, some objects show signs of low gravity in one absorption feature, while exhibiting field-like features elsewhere in their spectrum. For this reason, gravity types should be based on multiple gravity-sensitive indices, as A13 also cautions.

The behavior of the FeH_J index follows a similar trend to the K I EWs (Figure 4), although the FeH_J index peaks at ~L3, drops out almost entirely near the L/T transition, and then re-emerges at much lower levels of absorption in the mid-T spectral types, before again dropping out almost entirely in the late Ts. This trend is similar to results seen by Burgasser et al. (2003b) for the FeH feature at 0.9896 μm. They note a weakening in FeH-band strength in late-type L dwarfs, followed by a slight strengthening near spectral type ~T5.5, before disappearing again. Burgasser et al. (2003b) proposes that the re-emergence of this feature in the T dwarfs is an indication of cloud clearing. Holes in the cloud deck or a complete lack of clouds in the upper atmosphere allow the observer to detect light from deeper within the atmosphere of the brown dwarf where the temperatures are warm enough to sustain the presence of the FeH molecule. This interpretation has recently been challenged by Tremblin et al. (2016), who find that the FeH reversal can be reproduced by thermochemical instability effects, rather than cloud opacity

Table 5
Age Ranges for A13 Gravity Classifications for K I EWs

SpT	Age Ranges (Myr)								
	K I at 1.1692 μm			K I at 1.1778 μm			K I at 1.2529 μm		
	VL-G	INT-G	FLD-G	VL-G	INT-G	FLD-G	VL-G	INT-G	FLD-G
M6	0.3–22	22–27	27–10 Gyr	0.3–16	16–35	35–10 Gyr	0.3–12	12–32	32–10 Gyr
M7	0.3–55	55–205	205–10 Gyr	0.3–39	39–262	262–10 Gyr	0.3–27	27–208	208–10 Gyr
M8	0.3–57	57–413	413–10 Gyr	0.3–64	64–1.21 Gyr	1.21 Gyr–10 Gyr	0.3–50	50–817	817–10 Gyr
M9	0.3–17	17–128	128–10 Gyr	0.3–19	19–290	290–10 Gyr	0.3–19	19–190	190–10 Gyr
L0	0.3–38	38–296	296–10 Gyr	0.3–46	46–403	403–10 Gyr	0.3–42	42–378	378–10 Gyr

changes. Regardless of the interpretation, we verify the trend in the re-emergence of FeH absorption.

The A13 gravity classifications do not extend to spectral types cooler than L7. We are unable to extend these classifications to later spectral types, even with our larger sample. Establishing a low-gravity sequence requires a large enough sample of field dwarfs to determine the field sequence. Additionally, a large sample of known young objects are required to determine the location of the low-gravity objects. Currently, there are very few known young late-type L or early T dwarfs, none of which are in our sample. Searches for very low-mass objects in nearby young moving groups could yield a larger sample to carry out such a study, but this is not possible with the sample presented here.

Some of the VL-G and INT-G objects in our sample are known "red" L dwarfs because their $J - K_s$ colors are significantly redder than the $J - K_s$ colors of typical field dwarfs. Red $J - K_s$ color can be an indication of youth, although the term "red" should be reserved for those L dwarfs with red $J - K_s$ color that do not otherwise show signs of youth (see Kirkpatrick et al. 2010 for further discussion of the red and blue L dwarfs). Likewise, L dwarfs with significantly bluer $J - K_s$ colors compared to typical field dwarfs are called "blue," although this nomenclature should also be reserved for those L dwarfs with significantly bluer colors that do not exhibit signs of very low metallicity. In general, we find that the "red" and "blue" L dwarfs do not show consistent signs of low or high gravity, respectively.

4.3. Comparison of Objects of Known Age

To understand the age limits represented by the gravity classifications, we compare objects with known or predicted ages in the literature, determined by independent methods, such as kinematics or companionship to a well-characterized star. Table 3 lists age estimates and gravity types for 64 objects in the BDSS with previously determined ages. All BDSS targets that are candidate or suspected members of nearby young associations are included. Likelihood of membership (where available in the literature) is noted as well. Also included are several targets with age estimates from their more massive companions. Figure 6 shows the three adopted gravity-sensitive K I EWs and the FeH_J index versus spectral type for objects with known ages for dwarfs of spectral type M5.5-L0. Binaries from Table 3 are not shown, nor is the only single object of spectral type later than L0 in our sample of known-age objects, 2MASS 2244+2043 (L6, VL-G, AB Dor). Red symbols represent objects of ages <30 Myr, green symbols denote objects between ~30 and 100 Myr, and blue symbols represent objects >100 Myr. Varying shapes are used to distinguish between the different young associations (see figure legend for more details).

As seen in Figure 6 and Table 3, the members of various associations tend to have the gravity type corresponding to the estimated age of the association. A few targets have previously been found to be interlopers, and so we exclude these from our analysis. Additionally, several objects with known ages are also tight binaries with potentially contaminated spectra (see Section 3.5.1). Binaries of known ages are listed in Table 3, but are excluded from Figure 6 and any additional age calibration analysis (Section 4.5). Below, we discuss each of the associations in order of estimated age.

All 6 of the ρ Ophiuchi candidates (<1 Myr, Greene & Meyer 1995), all 13 Taurus (~1.5 Myr, Briceño et al. 2002) candidates, and 2MASS 2234+4041 (1 Myr; Companion to LkHα 233; Allers et al. 2009) have VL-G classifications, as expected. For targets with σ Orionis (3 Myr, Brown et al. 1994) designations, all but one of the six targets is classified as VL-G. Only S Ori 47 is classified as INT-G (not shown in Figure 6 or Table 3). Unlike the other σ Orionis candidates, this target's J-band spectrum shows very clear K I absorption features, more akin to a field dwarf, as noted in McGovern et al. (2004). McGovern et al. (2004) conclude that this object is likely a several Gyr old object located ~120 pc away, with a mass near the hydrogen burning limit, and is not associated with the σ Orionis cluster. Our analysis of S Ori 47 suggests that S Ori 47 is likely much younger than 1 Gyr, but is certainly older than ~30 Myr and very unlikely to be associated with σ Orionis. Based on the age versus EW values in Section 4.5, we estimate that S Ori 47 has an age closer to ~150 Myr and is likely an intermediate-aged field dwarf. For this reason, we have excluded S Ori 47 from the age-calibrated sample in Section 4.5.

Both TW Hya (~10 Myr, Bell et al. 2016) targets have VL-G classifications. Of the 15 objects with Upper Scorpius (11 ± 2 Myr, Pecaut et al. 2012) designations in our sample, all but 3 have VL-G classifications. U Sco 121, 85, and 132 each have FLD-G designations, and they are all previously suspected non-members (Muzerolle et al. 2003). Our analysis supports this conclusion. These three objects are not shown in Figure 6 or Table 3 and are excluded from the age-calibrated sample in Section 4.5. The β Pic (21–26 Myr; Bell et al. 2016) target, 2MASS 0443+0002, is classified as VL-G.

2MASS 0141-4633 in Tucana Horlogium (45 ± 4 Myr, Bell et al. 2016) is classified as VL-G. 2MASS 0608-2753 also receives a VL-G classification. Based on results from Gagné

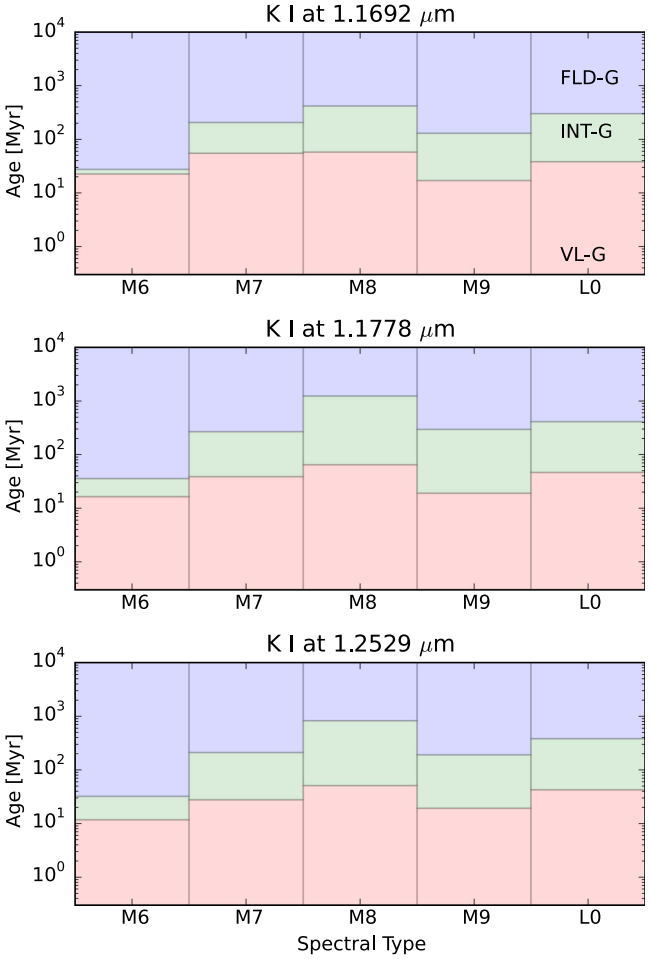

Figure 8. Age vs. Spectral Type for each gravity index in A13. Ages were estimated by applying the best-fit parameters for each spectral type bin and K I line in Table 4 to the A13 EW boundaries between each gravity classification. Red shaded regions represent VL-G classifications, green shading denotes INT-G classification, and blue shading represents FLD-G ages.

et al. (2014) and Faherty et al. (2016), we list this target as a candidate member of three groups: Cha-Near (∼10 Myr, Zuckerman & Song 2004), β Pic, and Columba (42^{+6}_{-4} Myr, Bell et al. 2016).

Of the Alpha Persei (80–100 Myr, Stauffer et al. 1999) members, one is classified VL-G, one is INT-G, and the other five are FLD-G. AP 270, which receives a VL-G classification, is less likely to be a member of Alpha Persei and could potentially be a young interloper. Gl 577 BC (70 Myr; companion) is classified as FLD-G.

The majority of the Pleiades (∼125 Myr) targets receive FLD-G classifications. Two Pleiades members (Roque 7 and Roque 4) are classified as INT-G, and Teide 1 is a borderline VL-G/INT-G object, but all three of these targets have much lower S/N spectra (S/N ∼ 10), and thus have much more uncertain gravity types. Simon et al. (2006) used a comparison to the Pleiades to date Gl 569 BC at ∼100 Myr. Gl 569 BC receives a FLD-G classification using our method, similar to the Pleiades objects studied here.

Surprisingly, the AB Doradus (149^{+51}_{-19} Myr, Bell et al. 2016) candidate 2MASS 2244+2043 is classified as VL-G in our analysis. Several other studies of the members of AB Doradus have determined a variety of gravity classifications for different members. A13 and Faherty et al. (2016) also present AB Doradus members with VL-G signatures, as well as members with INT-G and FLD-G classifications. Aller et al. (2016) presents new AB Doradus members with INT-G classifications.

LP 944-20 has been identified as a member of the Castor moving group (400 ± 40 Myr, Zuckerman et al. 2013), although the existence of the group is disputed and age estimates vary broadly for proposed members (see, e.g., Monnier et al. 2012 and Mamajek et al. 2013). However, LP 944-20 also has a Li measurement in Reiners & Basri (2009), suggesting an age <500 Myr and implying that this target is younger than the typical "old" field dwarf. This target receives a FLD-G designation.

The object in our sample with the oldest measured age is Gl 417BC, which Allers et al. (2010) estimate to be 750^{+140}_{-120} based on gyrochronology. Kirkpatrick et al. (2001) estimates an age of 80–300 Myr based on various dating methods for Gl 417A. This target is also a FLD-G object.

Our analysis suggests that the VL-G classification is only sensitive to ages as old as ∼20–30 Myr, as originally proposed in A13. The INT-G designation appears to probe only the ∼30–100 Myr range, while the FLD-G designation probes $\gtrsim$100 Myr, not $\gtrsim$200 Myr as suggested by A13. However we see that, similar to the results seen in Faherty et al. (2016), there is a spread in gravity classifications even among targets belonging to the same association, although they are assumed to be coeval. In Section 4.5, we further examine the age ranges probed by each gravity designation as a function of spectral type and K I line.

4.4. Potentially Young Objects

Here, we highlight targets with VL-G and INT-G designations that have not previously been discussed in A13 and are not known members of nearby young associations or young clusters. For each of the targets, we calculate the BANYAN II v1.4 likelihood of membership in various nearby young moving groups, as well as the likelihood of being a young (<1 Gyr) or old (>1 Gyr) field object (Malo et al. 2013; Gagné et al. 2014). The BANYAN II tool utilizes the 3D space motions and positions of many nearby young moving groups to determine via bayesian statistics the likelihood of a target being a member of a nearby young association. Not all associations are accounted for, and so a BANYAN II "young field" object could be a member of a young association not included in BANYAN II, or it could indeed be a young field dwarf, that is, a field dwarf exhibiting signs of youth. BANYAN II requires at least target coordinates and proper motion to estimate membership probability, but we input distance and RV information for the BANYAN II online tool when available from the literature. We used the priors developed by and outlined in Gagné et al. (2014) and did not use the uniform priors option.

2MASS 1459+0004 is an M6 dwarf with a VL-G designation. Kirkpatrick et al. (2010) present the discovery of this object as well as a proper motion of $\mu_\alpha = 308 \pm 248$ mas yr^{-1} and $\mu_\delta = -342 \pm 275$ mas yr^{-1}. BANYAN II results for this target suggest $\lesssim$1% likelihood of this object belonging to Argus or AB Dor, a 13.9% probability of being a young field object, and 85.85% likelihood of being an old field object, based solely on the target's coordinates and proper motion. If we assume that the target is <1 Gyr old, then it receives a 98.2% probability of being a young field object.

2MASS 1331+3407 is an L1pec object with an INT-G classification noted as being particularly red by Kirkpatrick et al. (2010). Gagné et al. (2014) found that this object has no likelihood of belonging to a nearby young moving group, and so this is most likely an intermediate-aged field dwarf. Having particularly red spectroscopic or photometric features can be an indication of youth, although Kirkpatrick et al. (2010) emphasizes that the term "red" should be reserved for objects with significantly red $J - K_s$ colors or spectra that do not show signs of youth.

2MASS 0543+6422 is an L2 dwarf with an INT-G classification. Gagné et al. (2015b) also gave this object an INT-G classification based on an IRTF SpeX spectrum and do not find any probability of this object belonging to currently known young moving groups.

2MASS 1841+3117 is an L4pec dwarf with an INT-G designation. The optical spectrum for this object in Kirkpatrick et al. (2000) is noticeably blue, which can imply higher gravity, however, the K I lines in the J band exhibit signs of lower gravity. It is possible that the peculiar nature of its spectrum is implying that a physical mechanism other than low gravity could be the cause of the smaller K I EWs, or that its blueness could be caused by some reason other than high surface gravity. BANYAN II results using coordinates, proper motion, and parallax for this object (Faherty et al. 2009) suggest a 54% probability that this object is a young field object.

2MASS 1553+2109 is an L5.5 dwarf with an INT-G classification. This object is known to have red NIR colors and strong Li absorption (Kirkpatrick et al. 1999), further indication that it is a young field dwarf. Based on the BANYAN II results using the kinematics from Schmidt et al. (2010), this object has 30.5% likelihood of being a young field dwarf, and a 69.5% likelihood of being an old field dwarf.

2MASS 0740+2009 is an INT-G classified L6 dwarf, previously found to have unusually red $J - K_s$ colors (Thompson et al. 2013). Its red colors could be attributed to lower surface gravity, in this case, and is likely younger than ~100 Myr. Using the kinematics and distance from Faherty et al. (2009) and the the BANYAN II predictions, we find only a 2.4% likelihood that this object belongs to the young field population and a 97.6% likelihood of being an old field dwarf.

2MASS 2151+3402 is an L7pec dwarf with a VL-G classification. However, Kirkpatrick et al. (2010) find that it has slightly blue NIR colors. This particular object has a low S/N spectrum and it is likely that the noise contaminated the estimation of the K I EWs. We smoothed the spectrum using a Gaussian 1D Kernel with a width of 3 pixels and recalculated the K I EWs using the methods described above. After smoothing, the gravity scores this object receives are "1," "1," and "0." Additionally, if FeH_J were defined for L7 dwarfs, then this would likely receive a FLD-G designation for that index, making it more likely to be a FLD-G object overall. Schneider et al. (2014) publish a measurement of the $H_2(K)$ index for this object, which they measure to be larger than the median $H_2(K)$ value for L7 dwarfs. The $H_2(K)$ index (Canty et al. 2013) is an index designed to measure the slope of the K-band continuum, which is known to be "peakier" in low-gravity objects. A high $H_2(K)$ for this object is further indication that this is likely to be a field-gravity object. However, BANYAN II predictions based on the proper motion from Kirkpatrick et al. (2010) and the sky coordinates suggest a slight (<1%) probability that this object could be a member of β Pic or Columba, a ~1%–2% probability of belonging to Argus or AB Dor, and a 34.4% likelihood of being a young field object.

4.5. Determining Ages

To further investigate the ability of the gravity indices to determine ages, we study the dependence of object age, taken from the literature, with K I EW for the lines at 1.1692 μm, 1.1778 μm, and 1.2529 μm binned by spectral type (Figure 7). There are a total of 73 objects used in this analysis, which are not known to be binaries and are assumed to be reliable age calibrators. Of these, 51 objects are BDSS targets, 15 objects come from A13, and 7 objects overlap both the BDSS and A13 samples. An additional 24 BDSS targets without known associations to young moving groups that received FLD-G designations in all four indices are also plotted, with age estimates of 5 ± 4 Gyr. Each panel plots age versus K I EW for a bin of three spectral types, because of the need to remove the previously shown trend of EW with spectral type. In general, spectral types are only known to ±1 type, so this coarser grouping of spectral types is analogous to the inherent spread in spectral features seen by objects of the same given spectral type. There is a clear linear trend between the K I EWs and log (Age) as displayed in Figure 7. Thus, for each graph, we perform a weighted orthogonal distance regression to determine a best-fit function of the form in Equation (1) using the *scipy.odr* package[14] in python.

$$\mathrm{Age} = A \times 10^{B \times \mathrm{EW}} \quad (1)$$

Parameters and 3σ uncertainties for the best-fit lines for each spectral type bin from M6 to L0 and each K I line are listed in Table 4. For ages in units of Myr and EWs measured in Å, the coefficient A is in units of Myr and B is Å^{-1}.

Figure 7 shows only three of the spectral type bins. The figures for spectral types M7 ± 1 and M9 ± 1 show similar trends and are not shown, however, the best-fit parameters for these spectral type bins are listed in Table 4. We were unable to achieve satisfactory fits to the function of log(Age) versus FeH_J index, likely because the range of values for the FeH_J index is much smaller. Additionally, we were unable to extend the age versus EW relationship beyond ~L0 because of the lack of later-type, age-calibrated objects in our sample.

The red, green, and blue shaded regions in Figure 7 are taken from the A13 boundaries for VL-G, INT-G, and FLD-G for the average spectral type at each wavelength. These aid in demonstrating the large and varying age ranges probed by each of the gravity types. From this figure, one can see that the large inherent spread in EW value makes it difficult to draw firm conclusions about the age of an object solely based on the measurement of its K I EWs. Coeval objects of similar spectral types can have widely varying EWs, as mentioned previously in regards to the AB Doradus moving group.

Although it is tempting to assign ages to each of the targets based on the relationships shown in Figure 7 and Table 4, we discourage against this because of the inability to significantly determine an age by combining the age estimates from each of the K I EWs. Instead, we have determined broad age limits for each of the gravity classifications at each spectral type and for each K I line. These are provided in Table 5 and shown in Figure 8. We determine the age at which each of the gravity classifications intersects the best-fit lines from Figure 7 for each

[14] https://docs.scipy.org/doc/scipy/reference/odr.html

spectral type bin and each K I line. The lower age limits are set by ρ Oph at 0.3 Myr and the upper age limits are set by age estimates of the field population at ~10 Gyr. The results in Table 5 and Figure 8 show how large of a spread in age estimates there can be for objects of similar spectral types with varying gravity types. For example, an M8 target with an INT-G classification would be estimated to have an age ranging from 50 Myr–1.21 Gyr depending on the K I line used. An M9 INT-G target, on the other hand, has age estimates ranging from 17 to 290 Myr. Additionally, the bounds of the intermediate-age range for a single K I index across all five spectral types show large variation. The most extreme example of the range in age estimates for a single K I line is seen for the upper age limit probed by INT-G for the K I line at 1.1778 μm, which ranges from 35 Myr to 1.21 Gyr depending on spectral type. We find that assigning a specific age range to the A13 gravity classifications is beyond the scope of this paper.

Uncertainty in age determination and gravity classification was also discussed in Aller et al. (2016). The authors of that paper determined uncertainties on the gravity types using a Monte Carlo approach in order to distinguish borderline objects that might otherwise be classified as FLD-G objects but show hints of youth. The broad range of ages associated with each gravity classification indicates the importance of further age analysis using other techniques. For example, kinematic information, potential young moving group membership, or stellar/substellar benchmark companions could further distinguish the age of a particular object. Low-mass stars and brown dwarfs exhibiting signs of low gravity merit follow-up observations to confirm or refute their potential youth status.

4.6. The Future for Surface Gravity Analysis

With the aforementioned limitations of gravity classification as a method for establishing the age of a young brown dwarf, we can make significant advances in this field in several ways. First, a larger sample of young L and T dwarfs of known ages is needed to extend the A13 classifications to later spectral types. In this paper, we do not have a large enough sample of young objects with spectral types later than ~L6 to expand these classifications into the L/T transition. The unshaded regions of Figures 3 and 4 display the regime in which significant progress can be made in furthering our understanding of gravity and age at varying masses and temperatures for these substellar objects.

Several recent works have highlighted discoveries in this area. Examples include the new bonafide T5.5 member of AB Doradus (Gagné et al. 2015a), the young L7 TW Hya interloper presented in Gagné et al. (2016), the two new candidate L7 members of TW Hya presented in Kellogg et al. (2016) and Schneider et al. (2016), and the 10 candidate YMG members of spectral type L7-T4.5 found with Pan-STARRS and *WISE* in Best et al. (2015). Additionally, discoveries of Jovian exoplanets around young stars present a method for studying objects that appear very similar to young field L and T dwarfs. Some examples of these exciting discoveries include 51 Eri b (Macintosh et al. 2015) and GU Psc b (Naud et al. 2014). Progress in extending the sample of known-age late-M and early-L dwarfs will also further our understanding of observational signatures of brown dwarf evolution. To this end, Burgasser et al. (2016b) presented the first planetary-mass member of 32 Ori (L1). Kinematic information of M and L dwarfs with Gaia (Gaia Collaboration et al. 2016a, 2016b) will confirm or refute the membership of young moving group candidates and allow for discoveries of new members.

Second, high-resolution spectroscopy obtained with the next generation of 30 m class telescopes in conjunction with improved atmospheric models will allow us to better correlate surface gravity with age in these young brown dwarfs. The current atmospheric models have incomplete line lists and do not accurately represent the observed behavior of the K I lines. The diversity of spectral features present in low-mass stars and brown dwarfs likely stems from physical properties and atmospheric conditions that we cannot probe at these moderate resolving powers or using these particular diagnostics. If atmospheric models continue to improve in tandem with observational capabilities, then it may be possible to better isolate the effect that surface gravity has on brown dwarf spectral features.

5. Summary

We presented 228 *J*-band spectra of M, L, and T dwarfs in the BDSS, the largest set of publicly available NIR spectra at $R \sim 2000$. Using the same *J*-band gravity-sensitive indices as Allers & Liu (2013), we calculated K I EWs and FeH absorption to determine gravity classifications for objects of spectral type M6–L7. Our technique is verified with 20 overlapping targets from A13 for which we derive similar gravity classifications despite using fewer spectral indicators. A subset of 73 objects with known (or suspected) ages from the literature (after excluding binaries from the full sample of known-age objects) define the trend of K I EW with age. By assigning ages to the boundaries of each gravity designation for spectral types M6–L0, we find that the age ranges probed by each of the K I lines vary widely. With a larger sample of age-calibrated M, L, and T dwarfs it will be possible to estimate ages for the entire sample with much greater certainty. This level of precision will likely require high signal-to-noise, high-resolution spectra of benchmark systems and detailed model comparison. Until then, the gravity designations from A13 remain a useful tool for dividing the low-mass products of star formation by relative age.

The authors wish to recognize and acknowledge the very significant cultural role and reverence that the summit of Maunakea has always had within the indigenous Hawaiian community. We are most fortunate to have the opportunity to conduct observations from this mountain. This research has benefitted from the M, L, T, and Y dwarf compendium housed at DwarfArchives.org. This research has made use of the SIMBAD database, operated at CDS, Strasbourg, France. We thank the anonymous referee for their insightful comments which improved the paper.

Facility: Keck:II(NIRSPEC).

Appendix

Here, we present all of the *J*-band spectra for the BDSS, ordered by spectral type and then surface gravity (if applicable), in Figures 9–13. Many of these spectra were previously published in McLean et al. (2003), McGovern et al. (2004), Kirkpatrick et al. (2010), and Mace et al. (2013a), but the majority are published here for the first time. All spectra

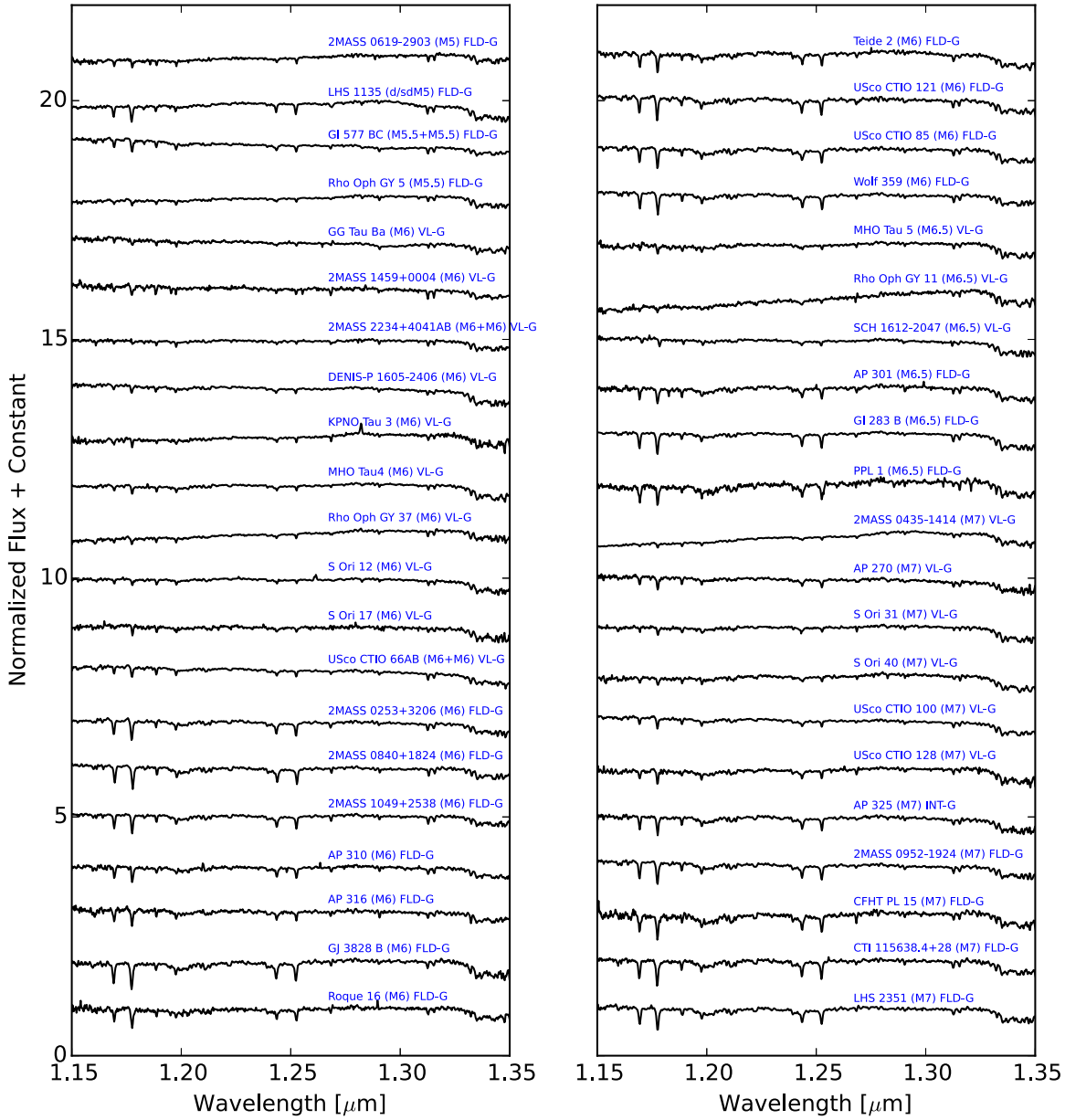

Figure 9. M5–M7 dwarfs, ordered by spectral type and then surface gravity type (if applicable).

will be available for download on bdssarchive.org. In addition to the K I, FeH, VO, and H_2O absorption features noted in Figure 2, some spectra have the Al doublet at 1.32 μm, the Paβ emission line at 1.28 μm, and some show significant reddening. The A13 indices were shown to be robust against reddening, and so this should not affect our results.

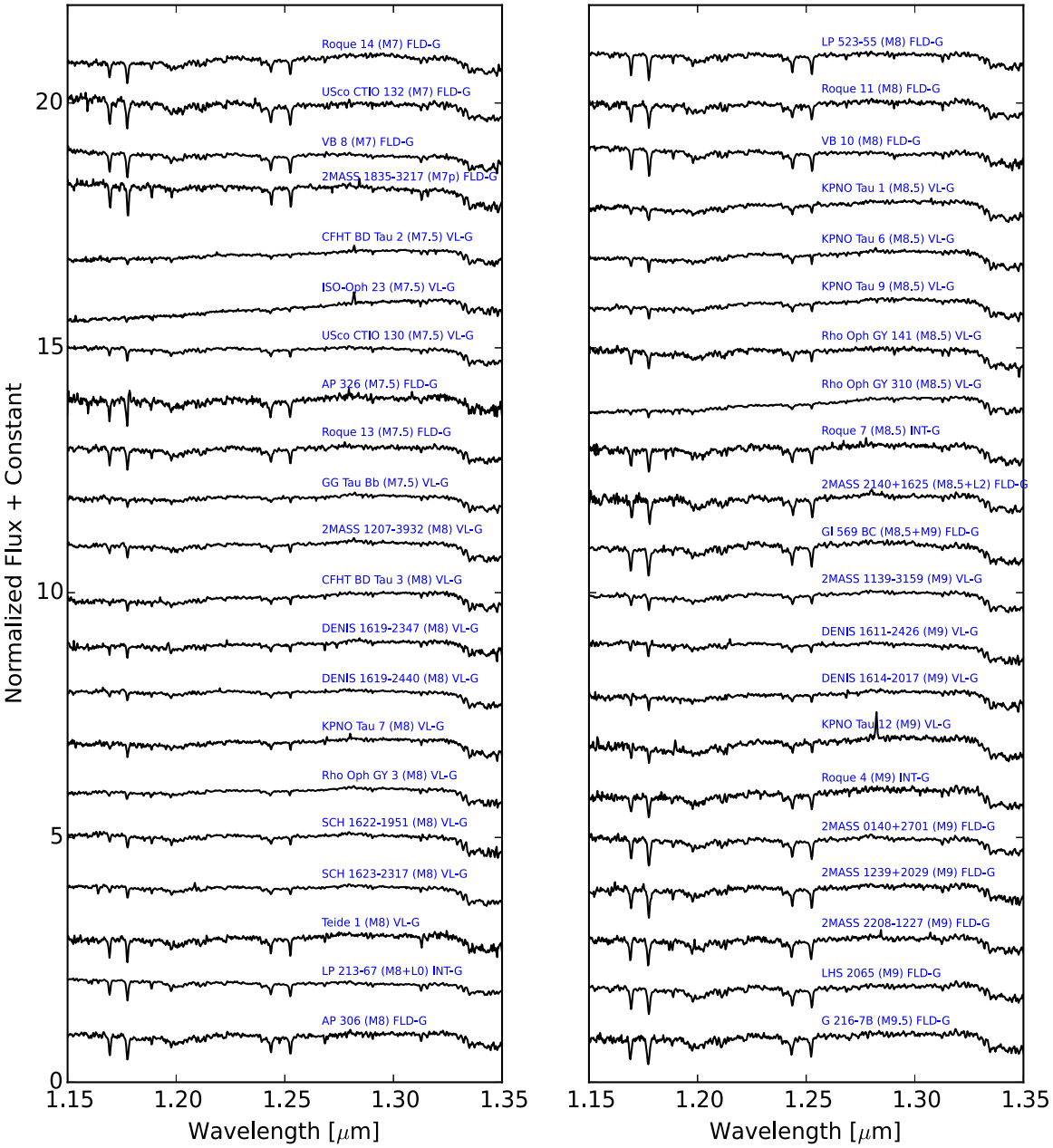

Figure 10. M7–M9.5 dwarfs, ordered by spectral type and then surface gravity type (if applicable).

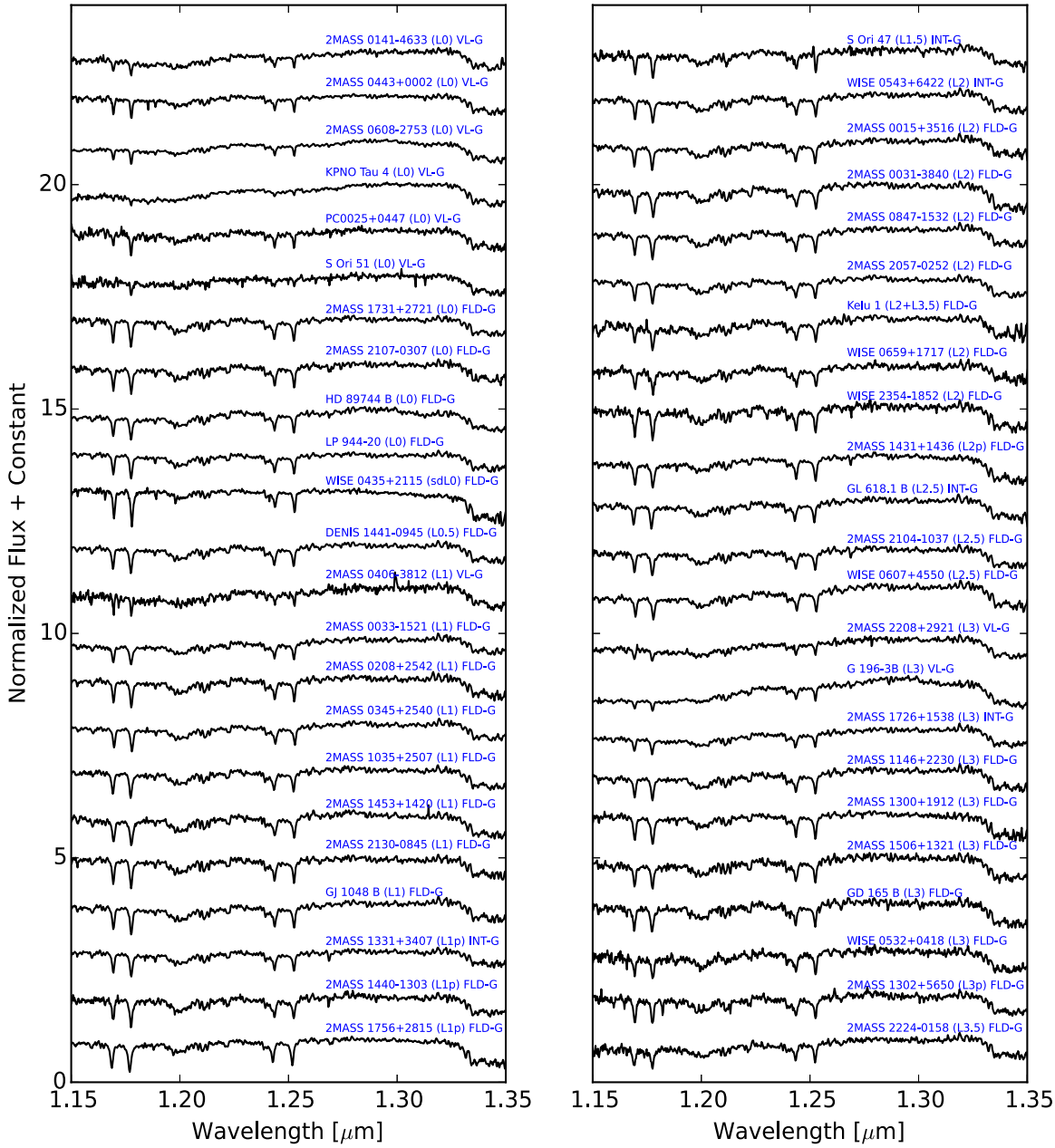

Figure 11. L0–L3.5 dwarfs, ordered by spectral type and then surface gravity type (if applicable).

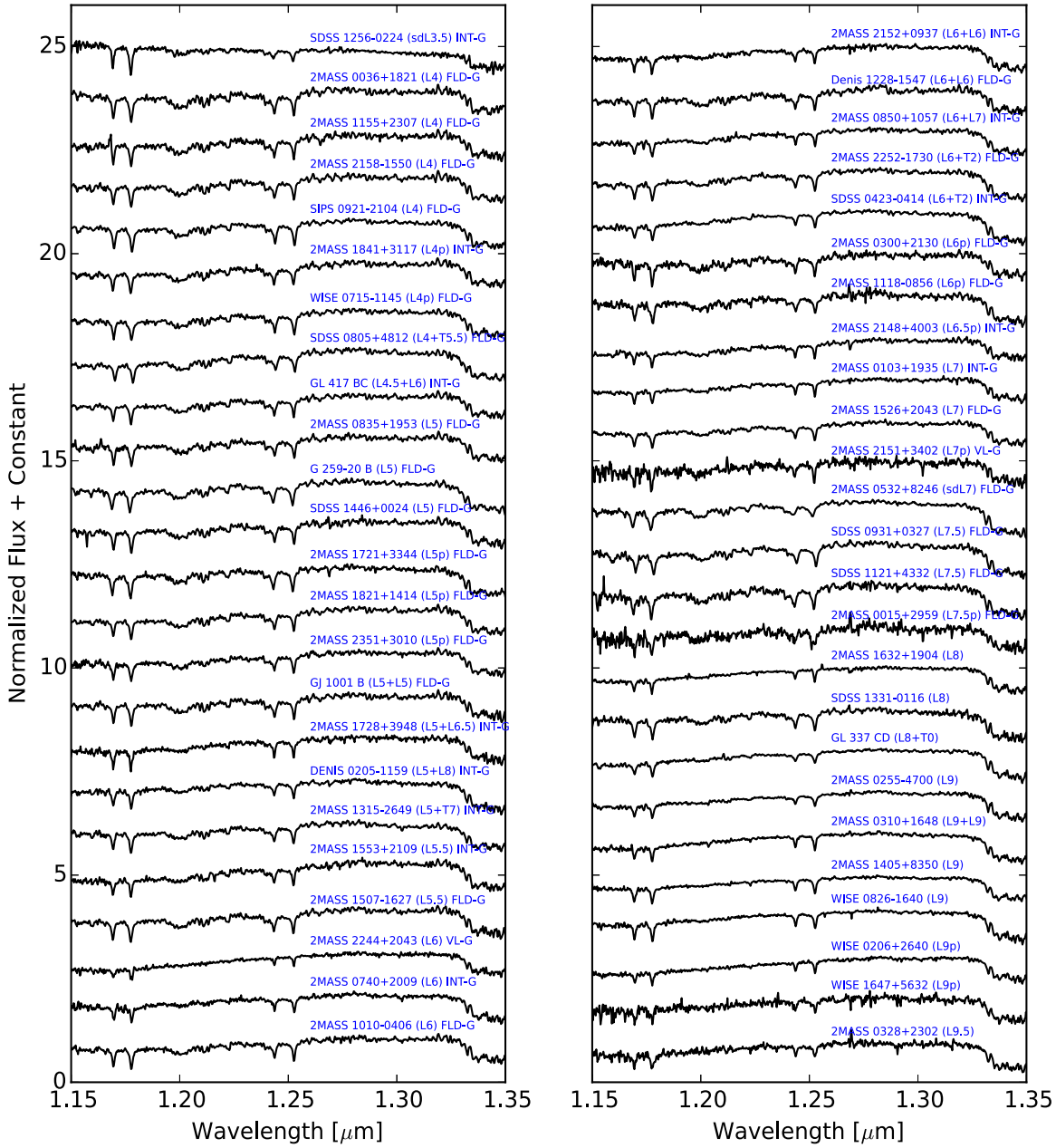

Figure 12. L3.5–L9.5 dwarfs, ordered by spectral type and then surface gravity type (if applicable).

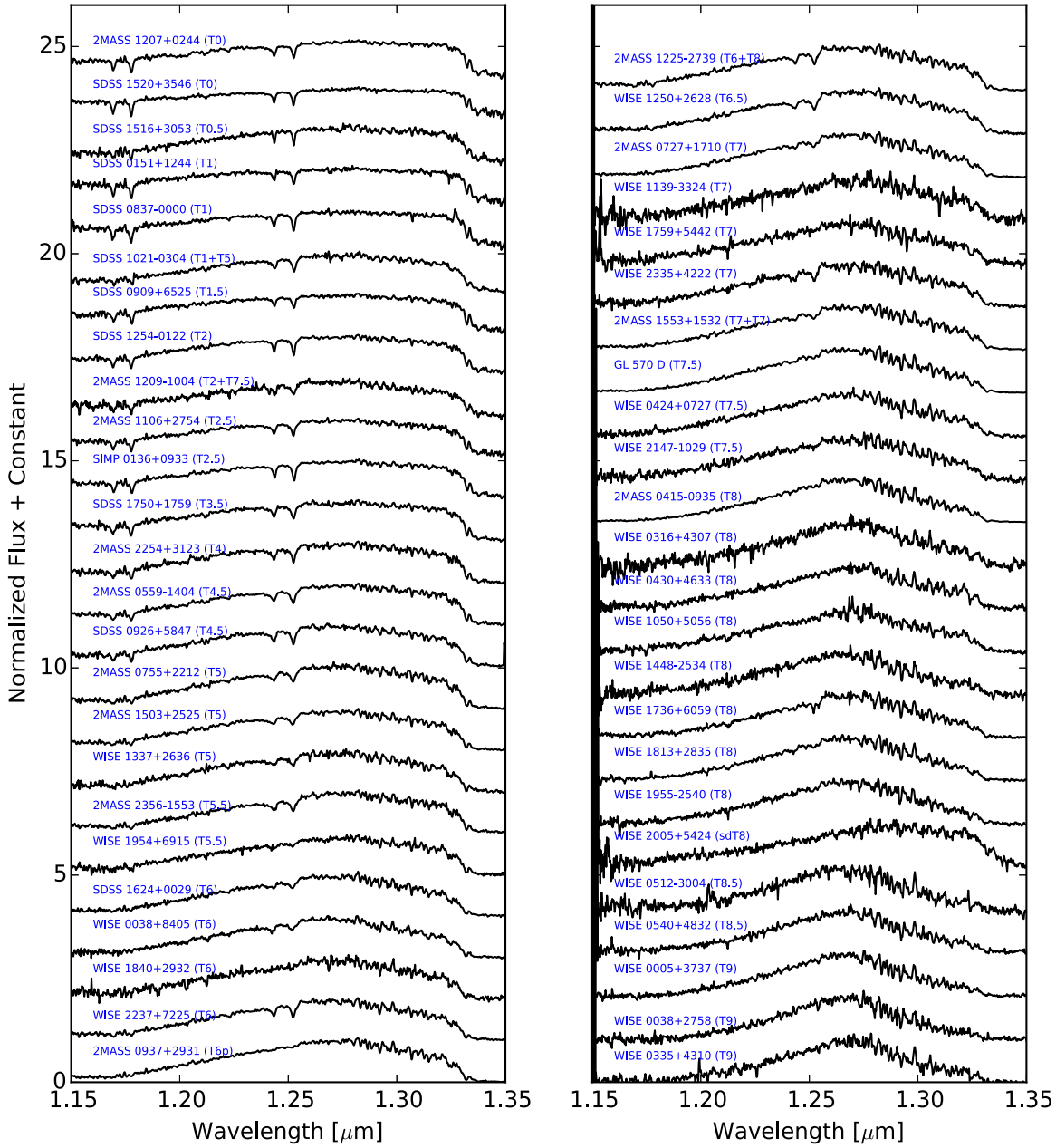

Figure 13. T0–T9 dwarfs, ordered by spectral type and then surface gravity type (if applicable).

References

Allard, F., Homeier, D., & Freytag, B. 2012, RSPTA, 370, 2765
Aller, K. M., Liu, M. C., Magnier, E. A., et al. 2016, ApJ, 821, 120
Allers, K. N., Jaffe, D. T., Luhman, K. L., et al. 2007, ApJ, 657, 511
Allers, K. N., & Liu, M. C. 2013, ApJ, 772, 79
Allers, K. N., Liu, M. C., Dupuy, T. J., & Cushing, M. C. 2010, ApJ, 715, 561
Allers, K. N., Liu, M. C., Shkolnik, E., et al. 2009, ApJ, 697, 824
Ardila, D., Martín, E., & Basri, G. 2000, AJ, 120, 479
Artigau, É., Doyon, R., Lafrenière, D., et al. 2006, ApJL, 651, L57
Baraffe, I., Homeier, D., Allard, F., & Chabrier, G. 2015, A&A, 577, A42
Barrado y Navascués, D., Béjar, V. J. S., Mundt, R., et al. 2003, A&A, 404, 171
Basri, G., & Martín, E. L. 1999, ApJ, 510, 266
Becklin, E. E., & Zuckerman, B. 1988, Natur, 336, 656
Béjar, V. J. S., Osorio, M. R. Z., & Rebolo, R. 1999, ApJ, 521, 671
Béjar, V. J. S., Zapatero Osorio, M. R., Rebolo, R., et al. 2011, ApJ, 743, 64
Bell, C. P. M., Mamajek, E. E., & Naylor, T. 2016, in IAU Symp. 314, Young Stars & Planets Near the Sun, ed. J. H. Kastner, B. Stelzer, & S. A. Metchev (Cambridge: Cambridge Univ. Press), 41
Best, W. M. J., Liu, M. C., Magnier, E. A., et al. 2015, ApJ, 814, 118
Bouvier, J., Stauffer, J. R., Martin, E. L., et al. 1998, A&A, 336, 490
Briceño, C., Hartmann, L., Stauffer, J., & Martín, E. 1998, AJ, 115, 2074
Briceño, C., Luhman, K. L., Hartmann, L., Stauffer, J. R., & Kirkpatrick, J. D. 2002, ApJ, 580, 317
Brown, A. G. A., de Geus, E. J., & de Zeeuw, P. T. 1994, A&A, 289, 101
Burgasser, A. J. 2004, ApJS, 155, 191
Burgasser, A. J. 2007, AJ, 134, 1330
Burgasser, A. J. 2008, in ASP Conf. Ser. 384, 14th Cambridge Workshop on Cool Stars, Stellar Systems, and the Sun, ed. G. van Belle (San Francisco, CA: ASP), 126
Burgasser, A. J., Bardalez-Gagliuffi, D. C., & Gizis, J. E. 2011a, AJ, 141, 70
Burgasser, A. J., Blake, C. H., Gelino, C. R., Sahlmann, J., & Bardalez Gagliuffi, D. 2016a, arXiv:1605.05390
Burgasser, A. J., Cruz, K. L., & Kirkpatrick, J. D. 2007, ApJ, 657, 494
Burgasser, A. J., Geballe, T. R., Leggett, S. K., Kirkpatrick, J. D., & Golimowski, D. A. 2006, ApJ, 637, 1067
Burgasser, A. J., Kirkpatrick, J. D., Brown, M. E., et al. 1999, ApJL, 522, L65
Burgasser, A. J., Kirkpatrick, J. D., Brown, M. E., et al. 2002a, ApJ, 564, 421

Burgasser, A. J., Kirkpatrick, J. D., Burrows, A., et al. 2003a, ApJ, 592, 1186
Burgasser, A. J., Kirkpatrick, J. D., Cutri, R. M., et al. 2000a, ApJL, 531, L57
Burgasser, A. J., Kirkpatrick, J. D., Liebert, J., & Burrows, A. 2003b, ApJ, 594, 510
Burgasser, A. J., Kirkpatrick, J. D., McElwain, M. W., et al. 2003c, AJ, 125, 850
Burgasser, A. J., Lopez, M. A., Mamajek, E. E., et al. 2016b, ApJ, 820, 32
Burgasser, A. J., Marley, M. S., Ackerman, A. S., et al. 2002b, ApJL, 571, L151
Burgasser, A. J., Sitarski, B. N., Gelino, C. R., Logsdon, S. E., & Perrin, M. D. 2011b, ApJ, 739, 49
Burgasser, A. J., Wilson, J. C., Kirkpatrick, J. D., et al. 2000b, AJ, 120, 1100
Burgasser, A. J., Witte, S., Helling, C., et al. 2009, ApJ, 697, 148
Burningham, B., Pinfield, D. J., Lucas, P. W., et al. 2010, MNRAS, 406, 1885
Burrows, A., Hubbard, W. B., Lunine, J. I., & Liebert, J. 2001, RvMP, 73, 719
Canty, J. I., Lucas, P. W., Roche, P. F., & Pinfield, D. J. 2013, MNRAS, 435, 2650
Castro, P. J., Gizis, J. E., Harris, H. C., et al. 2013, ApJ, 776, 126
Chiu, K., Fan, X., Leggett, S. K., et al. 2006, AJ, 131, 2722
Close, L. M., Siegler, N., Freed, M., & Biller, B. 2003, ApJ, 587, 407
Cohen, M., & Kuhi, L. V. 1979, ApJS, 41, 743
Comeron, F., Rieke, G. H., Burrows, A., & Rieke, M. J. 1993, ApJ, 416, 185
Cruz, K. L., Kirkpatrick, J. D., & Burgasser, A. J. 2009, AJ, 137, 3345
Cruz, K. L., Reid, I. N., Liebert, J., Kirkpatrick, J. D., & Lowrance, P. J. 2003, AJ, 126, 2421
Cushing, M. C., Kirkpatrick, J. D., Gelino, C. R., et al. 2011, ApJ, 743, 50
Cushing, M. C., Marley, M. S., Saumon, D., et al. 2008, ApJ, 678, 1372
Dahn, C. C., Harris, H. C., Vrba, F. J., et al. 2002, AJ, 124, 1170
Delfosse, X., Tinney, C. G., Forveille, T., et al. 1997, A&A, 327, L25
Dupuy, T. J., & Liu, M. C. 2017, ApJS, submitted (arXiv:1703.05775)
EROS Collaboration, Goldman, B., Delfosse, X., et al. 1999, A&A, 351, L5
Faherty, J. K., Burgasser, A. J., Cruz, K. L., et al. 2009, AJ, 137, 1
Faherty, J. K., Riedel, A. R., Cruz, K. L., et al. 2016, ApJS, 225, 10
Festin, L. 1998, MNRAS, 298, L34
Gagné, J., Burgasser, A. J., Faherty, J. K., et al. 2015a, ApJL, 808, L20
Gagné, J., Faherty, J. K., Cruz, K. L., et al. 2015b, arXiv:1506.07712
Gagné, J., Faherty, J. K., Mamajek, E. E., et al. 2016, arXiv:1612.02881
Gagné, J., Lafrenière, D., Doyon, R., Malo, L., & Artigau, É. 2014, ApJ, 783, 121
Gagné, J., Lafrenière, D., Doyon, R., Malo, L., & Artigau, É. 2015c, ApJ, 798, 73
Gaia Collaboration, Brown, A. G. A., Vallenari, A., et al. 2016a, A&A, 595, A2
Gaia Collaboration, Prusti, T., de Bruijne, J. H. J., et al. 2016b, A&A, 595, A1
Geballe, T. R., Knapp, G. R., Leggett, S. K., et al. 2002, ApJ, 564, 466
Geers, V., Scholz, A., Jayawardhana, R., et al. 2011, ApJ, 726, 23
Gizis, J. E. 2002, ApJ, 575, 484
Gizis, J. E., Kirkpatrick, J. D., & Wilson, J. C. 2001, AJ, 121, 2185
Gizis, J. E., Monet, D. G., Reid, I. N., et al. 2000, AJ, 120, 1085
Gizis, J. E., Reid, I. N., Knapp, G. R., et al. 2003, AJ, 125, 3302
Greene, T. P., & Meyer, M. R. 1995, ApJ, 450, 233
Greene, T. P., & Young, E. T. 1992, ApJ, 395, 516
Hall, P. B. 2002, ApJL, 564, L89
Haro, G., & Chavira, E. 1966, VA, 8, 89
Hawley, S. L., Covey, K. R., Knapp, G. R., et al. 2002, AJ, 123, 3409
Hayashi, C., & Nakano, T. 1963, PThPh, 30, 460
Henry, T. J., & Kirkpatrick, J. D. 1990, ApJL, 354, L29
Jenkins, J. S., Ramsey, L. W., Jones, H. R. A., et al. 2009, ApJ, 704, 975
Kellogg, K., Metchev, S., Gagné, J., & Faherty, J. 2016, ApJL, 821, L15
Kendall, T. R., Delfosse, X., Martín, E. L., & Forveille, T. 2004, A&A, 416, L17
Kirkpatrick, J. D. 1992, PhD thesis, Arizona Univ.
Kirkpatrick, J. D. 2005, ARA&A, 43, 195
Kirkpatrick, J. D., Barman, T. S., Burgasser, A. J., et al. 2006, ApJ, 639, 1120
Kirkpatrick, J. D., Beichman, C. A., & Skrutskie, M. F. 1997, ApJ, 476, 311
Kirkpatrick, J. D., Cruz, K. L., Barman, T. S., et al. 2008, ApJ, 689, 1295
Kirkpatrick, J. D., Cushing, M. C., Gelino, C. R., et al. 2011, ApJS, 197, 19
Kirkpatrick, J. D., Dahn, C. C., Monet, D. G., et al. 2001, AJ, 121, 3235
Kirkpatrick, J. D., Henry, T. J., & McCarthy, D. W., Jr. 1991, ApJS, 77, 417
Kirkpatrick, J. D., Liebert, J., Cruz, K. L., Gizis, J. E., & Reid, I. N. 2001, PASP, 113, 814
Kirkpatrick, J. D., Looper, D. L., Burgasser, A. J., et al. 2010, ApJS, 190, 100
Kirkpatrick, J. D., Reid, I. N., Liebert, J., et al. 1999, ApJ, 519, 802
Kirkpatrick, J. D., Reid, I. N., Liebert, J., et al. 2000, AJ, 120, 447
Kirkpatrick, J. D., Schneider, A., Fajardo-Acosta, S., et al. 2014, ApJ, 783, 122
Knapp, G. R., Leggett, S. K., Fan, X., et al. 2004, AJ, 127, 3553
Konopacky, Q. M., Ghez, A. M., Barman, T. S., et al. 2010, ApJ, 711, 1087
Kramida, A., Ralchenko, Y., Reader, J., & Team, N. A. 2015, NIST Atomic Spectra Database, version 5.4 (Gaithersburg, MD: National Institute of Standards and Technology), http://physics.nist.gov/asd
Kraus, A. L., White, R. J., & Hillenbrand, L. A. 2005, ApJ, 633, 452
Kumar, S. S. 1962, AJ, 67, 579
Kumar, S. S. 1963, ApJ, 137, 1121
Lawrence, A., Warren, S. J., Almaini, O., et al. 2007, MNRAS, 379, 1599
Leggett, S. K., Geballe, T. R., Fan, X., et al. 2000, ApJL, 536, L35
Lépine, S., Rich, R. M., & Shara, M. M. 2003, AJ, 125, 1598
Lépine, S., Shara, M. M., & Rich, R. M. 2002, AJ, 124, 1190
Lodders, K. 1999, ApJ, 519, 793
Lodieu, N., Deacon, N. R., & Hambly, N. C. 2012a, MNRAS, 422, 1495
Lodieu, N., Deacon, N. R., Hambly, N. C., & Boudreault, S. 2012b, MNRAS, 426, 3403
Looper, D. L., Kirkpatrick, J. D., & Burgasser, A. J. 2007, AJ, 134, 1162
Looper, D. L., Kirkpatrick, J. D., Cutri, R. M., et al. 2008, ApJ, 686, 528
Lowrance, P. J., Becklin, E. E., Schneider, G., et al. 2005, AJ, 130, 1845
Lucas, P. W., Roche, P. F., Allard, F., & Hauschildt, P. H. 2001, MNRAS, 326, 695
Luhman, K. L. 2012, ARA&A, 50, 65
Luhman, K. L., Briceño, C., Stauffer, J. R., et al. 2003, ApJ, 590, 348
Luhman, K. L., Hernández, J., Downes, J. J., Hartmann, L., & Briceño, C. 2008, ApJ, 688, 362
Luhman, K. L., Liebert, J., & Rieke, G. H. 1997, ApJL, 489, L165
Luhman, K. L., & Mamajek, E. E. 2012, ApJ, 758, 31
Luhman, K. L., Whitney, B. A., Meade, M. R., et al. 2006, ApJ, 647, 1180
Luyten, W. J. 1979a, A Catalogue of Stars with Proper Motions Exceeding 0″5 Annually (2nd ed.; Minneapolis: Univ. Minnesota Press)
Luyten, W. J. 1979b, New Luyten Catalogue of Stars with Proper Motions Larger than Two Tenths of an Arcsecond; and First Supplement; NLTT (Minneapolis: Univ. Minnesota Press)
Mace, G. N., Kirkpatrick, J. D., Cushing, M. C., et al. 2013a, ApJS, 205, 6
Mace, G. N., Kirkpatrick, J. D., Cushing, M. C., et al. 2013b, ApJ, 777, 36
Macintosh, B., Graham, J. R., Barman, T., et al. 2015, Sci, 350, 64
Malo, L., Doyon, R., Lafrenière, D., et al. 2013, ApJ, 762, 88
Mamajek, E. E. 2005, ApJ, 634, 1385
Mamajek, E. E., Bartlett, J. L., Seifahrt, A., et al. 2013, AJ, 146, 154
Marley, M. S., & Robinson, T. D. 2014, arXiv:1410.6512
Martín, E. L., Basri, G., Gallegos, J. E., et al. 1998, ApJL, 499, L61
Martín, E. L., Brandner, W., Bouvier, J., et al. 2000a, ApJ, 543, 299
Martín, E. L., Delfosse, X., Basri, G., et al. 1999, AJ, 118, 2466
Martín, E. L., Delfosse, X., & Guieu, S. 2004, AJ, 127, 449
Martín, E. L., Dougados, C., Magnier, E., et al. 2001, ApJL, 561, L195
Martín, E. L., Koresko, C. D., Kulkarni, S. R., Lane, B. F., & Wizinowich, P. L. 2000b, ApJL, 529, L37
Martin, E. L., Rebolo, R., & Zapatero-Osorio, M. R. 1996, ApJ, 469, 706
McGovern, M. R., Kirkpatrick, J. D., McLean, I. S., et al. 2004, ApJ, 600, 1020
McLean, I. S., Becklin, E. E., Bendiksen, O., et al. 1998, Proc. SPIE, 3354, 566
McLean, I. S., McGovern, M. R., Burgasser, A. J., et al. 2003, ApJ, 596, 561
McLean, I. S., Prato, L., Kim, S. S., et al. 2001, ApJL, 561, L115
McLean, I. S., Prato, L., McGovern, M. R., et al. 2007, ApJ, 658, 1217
Monnier, J. D., Che, X., Zhao, M., et al. 2012, ApJL, 761, L3
Muzerolle, J., Hillenbrand, L., Calvet, N., Briceño, C., & Hartmann, L. 2003, ApJ, 592, 266
Mužić, K., Scholz, A., Geers, V., Jayawardhana, R., & Tamura, M. 2012, ApJ, 744, 134
Nakajima, T., Oppenheimer, B. R., Kulkarni, S. R., et al. 1995, Natur, 378, 463
Natta, A., Testi, L., Comerón, F., et al. 2002, A&A, 393, 597
Naud, M.-E., Artigau, É., Malo, L., et al. 2014, ApJ, 787, 5
Pavlenko, Y. V., Jones, H. R. A., Lyubchik, Y., Tennyson, J., & Pinfield, D. J. 2006, A&A, 447, 709
Pecaut, M. J., Mamajek, E. E., & Bubar, E. J. 2012, ApJ, 746, 154
Prato, L., Mace, G. N., Rice, E. L., et al. 2015, ApJ, 808, 12
Probst, R. G. 1983, ApJS, 53, 335
Prosser, C. F. 1994, AJ, 107, 1422
Rebolo, R., Zapatero Osorio, M. R., Madruga, S., et al. 1998, Sci, 282, 1309
Rebolo, R., Zapatero Osorio, M. R., & Martín, E. L. 1995, Natur, 377, 129
Reid, I. N., Cruz, K. L., Kirkpatrick, J. D., et al. 2008, AJ, 136, 1290
Reid, I. N., Gizis, J. E., Kirkpatrick, J. D., & Koerner, D. W. 2001, AJ, 121, 489
Reid, I. N., Kirkpatrick, J. D., Gizis, J. E., et al. 2000, AJ, 119, 369
Reid, I. N., Lewitus, E., Allen, P. R., Cruz, K. L., & Burgasser, A. J. 2006, AJ, 132, 891
Reiners, A., & Basri, G. 2009, ApJ, 705, 1416

Ribas, I. 2003, A&A, 400, 297
Rice, E. L., Barman, T., Mclean, I. S., Prato, L., & Kirkpatrick, J. D. 2010, ApJS, 186, 63
Rice, E. L., Faherty, J. K., Cruz, K., et al. 2011, in ASP Conf. Ser. 448, 16th Cambridge Workshop on Cool Stars, Stellar Systems, and the Sun, ed. C. Johns-Krull, M. K. Browning, & A. A. West (San Francisco, CA: ASP), 481
Rieke, G. H., & Rieke, M. J. 1990, ApJL, 362, L21
Ruiz, M. T., Leggett, S. K., & Allard, F. 1997, ApJL, 491, L107
Saumon, D., & Marley, M. S. 2008, ApJ, 689, 1327
Schmidt, S. J., West, A. A., Hawley, S. L., & Pineda, J. S. 2010, AJ, 139, 1808
Schneider, A. C., Cushing, M. C., Kirkpatrick, J. D., et al. 2014, AJ, 147, 34
Schneider, A. C., Windsor, J., Cushing, M. C., Kirkpatrick, J. D., & Wright, E. L. 2016, ApJL, 822, L1
Schneider, D. P., Greenstein, J. L., Schmidt, M., & Gunn, J. E. 1991, AJ, 102, 1180
Sheppard, S. S., & Cushing, M. C. 2009, AJ, 137, 304
Simon, M., Bender, C., & Prato, L. 2006, ApJ, 644, 1183
Sivarani, T., Lépine, S., Kembhavi, A. K., & Gupchup, J. 2009, ApJL, 694, L140
Skrutskie, M. F., Cutri, R. M., Stiening, R., et al. 2006, AJ, 131, 1163
Slesnick, C. L., Carpenter, J. M., & Hillenbrand, L. A. 2006, AJ, 131, 3016
Stauffer, J., Hamilton, D., Probst, R., Rieke, G., & Mateo, M. 1989, ApJL, 344, L21
Stauffer, J. R., Hartmann, L. W., Fazio, G. G., et al. 2007, ApJS, 172, 663
Stauffer, J. R., Navascués, D. B. y., Bouvier, J., et al. 1999, ApJ, 527, 219
Stauffer, J. R., Schultz, G., & Kirkpatrick, J. D. 1998, ApJL, 499, L199
Strauss, M. A., Fan, X., Gunn, J. E., et al. 1999, ApJL, 522, L61
Stumpf, M. B., Brandner, W., Henning, T., et al. 2008, arXiv: 0811.0556
Thompson, M. A., Kirkpatrick, J. D., Mace, G. N., et al. 2013, PASP, 125, 809
Tremblin, P., Amundsen, D. S., Chabrier, G., et al. 2016, ApJL, 817, L19
van Biesbroeck, G. 1944, AJ, 51, 61
van Biesbroeck, G. 1961, AJ, 66, 528
Vrba, F. J., Strom, K. M., Strom, S. E., & Grasdalen, G. L. 1975, ApJ, 197, 77
White, R. J., Ghez, A. M., Reid, I. N., & Schultz, G. 1999, ApJ, 520, 811
Wilking, B. A., Greene, T. P., & Meyer, M. R. 1999, AJ, 117, 469
Wilking, B. A., Meyer, M. R., Robinson, J. G., & Greene, T. P. 2005, AJ, 130, 1733
Wilson, J. C., Kirkpatrick, J. D., Gizis, J. E., et al. 2001, AJ, 122, 1989
Wolf, M. 1919, VeHei, 7, 195
Wright, E. L., Eisenhardt, P. R. M., Mainzer, A. K., et al. 2010, AJ, 140, 1868
York, D. G., Adelman, J., Anderson, J. E., Jr., et al. 2000, AJ, 120, 1579
Zapatero Osorio, M. R., Béjar, V. J. S., Martín, E. L., et al. 2000, Sci, 290, 103
Zapatero Osorio, M. R., Béjar, V. J. S., Rebolo, R., Martín, E. L., & Basri, G. 1999, ApJL, 524, L115
Zapatero Osorio, M. R., Rebolo, R., Martín, E. L., et al. 1997, ApJL, 491, L81
Zuckerman, B., & Song, I. 2004, ARA&A, 42, 685
Zuckerman, B., Vican, L., Song, I., & Schneider, A. 2013, ApJ, 778, 5